Year: 2024

# Low dose photodynamic therapy promotes vascular E-Selectin expression in malignant pleural mesothelioma which increases immune infiltration and improves tumor control

Chriqui Louis-Emmanuel

Chriqui Louis-Emmanuel, 2024, Low dose photodynamic therapy promotes vascular E-Selectin expression in malignant pleural mesothelioma which increases immune infiltration and improves tumor control

Originally published at : Thesis, University of Lausanne

Posted at the University of Lausanne Open Archive http://serval.unil.ch
Document URN : urn:nbn:ch:serval-BIB_03C69FDF199A4

UNIL | Université de Lausanne
Faculté de biologie et de médecine

**Département de Biologie et Médecine**

# Low dose photodynamic therapy promotes vascular E-Selectin expression in malignant pleural mesothelioma which increases immune infiltration and improves tumor control

**Thèse de doctorat en médecine et ès sciences (MD-PhD)**

présentée à la

Faculté de biologie et de médecine
de l'Université de Lausanne

par

**Louis-Emmanuel CHRIQUI**

Médecin diplômé de la Confédération Helvétique

**Jury**

Prof. Dela Golshayan, Présidente et répondante MD-PhD
Dr. Jean-Yannis Perentes, Directeur de thèse
Prof. Johanna Joyce, Co-directrice de thèse
Prof. Lucas Liaudet, Expert
Prof. Mikael Pittet, Expert

Lausanne
(2023)

UNIL | Université de Lausanne
Faculté de biologie et de médecine

**Département de Biologie et Médecine**

# Low dose photodynamic therapy promotes vascular E-Selectin expression in malignant pleural mesothelioma which increases immune infiltration and improves tumor control

**Thèse de doctorat en médecine et ès sciences (MD-PhD)**

présentée à la

Faculté de biologie et de médecine
de l'Université de Lausanne

par

**Louis-Emmanuel CHRIQUI**

Médecin diplômé de la Confédération Helvétique

**Jury**

Prof. Dela Golshayan, Présidente et répondante MD-PhD
Dr. Jean-Yannis Perentes, Directeur de thèse
Prof. Johanna Joyce, Co-directrice de thèse
Prof. Lucas Liaudet, Expert
Prof. Mikael Pittet, Expert

Lausanne
(2023)

UNIL | Université de Lausanne
Faculté de biologie
et de médecine

**Ecole Doctorale**
**Doctorat MD-PhD**

# Imprimatur

Vu le rapport présenté par le jury d'examen, composé de

| | | | | |
|---|---|---|---|---|
| **Président·e** | Madame | Prof. | Déla | **Golshayan** |
| **Directeur·trice de thèse** | Monsieur | Dr | Yannis | **Perentes** |
| **Co-Directeur·trice de thèse** | Madame | Prof. | Johanna | **Joyce** |
| **Répondant·e** | Madame | Prof. | Déla | **Golshayan** |
| **Expert·e·s** | Monsieur | Prof. | Lucas | **Liaudet** |
| | Monisieur | Prof. | Mikaël | **Pittet** |

le Conseil de Faculté autorise l'impression de la thèse de

## Monsieur Louis-Emmanuel CHRIQUI

Maîtrise universitaires en médecine Université de Lausanne

intitulée

**Low dose photodynamic therapy promotes vascular E-Selectin expression in malignant pleural mesothelioma which increases immune infiltration and improves tumor control**

Lausanne, le 7 juin 2024

pour Le Doyen
de la Faculté de Biologie et de Médecine

Prof. Déla Golshayan

## List of abbreviations

MPM – Malignant pleural mesothelioma

PDT – Photodynamic therapy

L-PDT – Low-dose photodynamic therapy

ICI – Immune checkpoint inhibitors

EPP – Extra pleural pneumonectomy

EPD - Extended pleural decortication

NF-κB – Nuclear factor Kappa B

ICAM-1 – Intercellular adhesion molecule 1

VCAM-1 – Vascular cell adhesion molecule 1

CTLA-4 - Cytotoxic T lymphocyte antigen-4

PD-L1 - Programmed death-ligand 1

TME – Tumor Microenvironment

TIL – Tumor infiltrating lymphocytes

ECM – Extracellular matrix

OS – Overall survival

PFS – Progression free survival

EC- Endothelial cell

CAM – Cellular adhesion molecule

ROS – Reactive oxygen species

IFP – Interstitial fluid pressure

NK – Natural killer

IVIS - Intravital imaging system

IKK – I Kappa B Kinase

NBD – NEMO Binding domain

TMA – Tumor microarray

IVM – Intravital imaging

GFP – Green fluorescent protein

# Table of content

# List of Figures

# 1. Acknowledgements

I precisely remember when I first discussed with my PI Jean Yannis Perentes about eventually applying for a MD-PhD in his lab: I was in my 4th year of medical school, during my rotation in thoracic surgery. 6 years later, I started as a resident in thoracic surgery, submitting my thesis manuscript to (almost) conclude this 3-years adventure.

I like to call it an adventure because my MD-PhD exactly fit this definition: Something surprising and unattended happening to someone. While I always known I wanted to do research, I was not sure about the direction to take. Through his contact, Yannis gave me the opportunity to pursue this passion in a great environment, surrounded by skilled and supportive people.

I would like to start by thanking my colleagues in the lab: Alex, Christophe, Damien, Olga, Sabrina, Severine and Yameng. You are great persons to work (and to party) with and I am happy to have spend my last years around you. I would like to thank Pr. Johanna Joyce and her lab for allowing me to join them for their weekly labmeeting and also their valuable input all along my project.

Of course, I also would like to thank my family: It would have never happened without you. You always gave me a fresh perspective during the journey allowing me to get back on track with new ideas. And thank you for letting me talk about failed experiments for the last 3 years without seeming bothered. This also apply to my friends: You were the best to change my mind and to keep me motivated!

Finally I would like to thank Yannis again. In addition to the opportunity he gave me, he also inspired me a lot and gave me a direction to follow. I believe we learn mostly by observing others and I am highly grateful to be able to learn at his contact. I highly value your way of thinking as a leader, at work but also as a person.

I would have loved to say more about you all but as I am limited to one page, I will conclude that as everything in life, a PhD is a team work and you are the best team.

# 2. Summary

Malignant pleural mesothelioma (MPM) is an aggressive disease arising from the pleural tissue which surrounds the lungs. Its prognosis remains limited even for patients able to benefit from multimodal approaches. Recent clinical trials in MPM patients led to the adoption of dual immunotherapy, instead of chemotherapy. However, the incremental survival remains poor and restricted to only a subset of patients responding to immunotherapy. MPM is known to be an immune altered tumor. Thus, a partial explanation to the limited effectiveness of immunotherapy could be the absence of immune cells infiltrating the tumor. To reverse this microenvironment phenotype, numerous approaches have been tried. In my thesis, I focus on the effects of vascular targeted low-dose photodynamic therapy (L-PDT). Photodynamic therapy is an approved treatment modality with pleiotropic effects on the vascular and immune compartments. The hypothesis of my thesis is that L-PDT can modulate the tumor vasculature and immune microenvironment which results in improved tumor control in a mouse model of MPM.

Building upon previous results from my host lab indicating that L-PDT could contribute to enhance the immune infiltration of MPM, I showed that L-PDT had the potential to induce adhesion molecules such as ICAM-1, VCAM-1 and E-Selectin on tumor endothelial cells. I then demonstrated that E-Selectin was essential to promote the infiltration of MPM with active GRZB+CD8+ T-cells and thus improve tumor control. Furthermore, by inhibiting selectively E-Selectin, NF-κB pathway and CD8+ T lymphocytes, I found that all components were necessary and sufficient to induce the MPM tumor control mediated by L-PDT. To determine the clinical relevance of the uncovered mechanism, I then validated in an MPM patient tissue microarray cohort of 82 patients the correlation between vascular E-Selectin expression and CD8+ infiltration. I also demonstrated that patients with MPM with higher levels of vascular E-Selectin expression had better survival compared to others.

In conclusion, the present thesis shows a potent role of low dose photodynamic therapy as an MPM immune priming method which can lead to improved tumor control. These findings suggest a favroable role for L-PDT alone or in combination with immunotherapies. Further validation of these findings in patients are warranted.

# 3. Résumé

Le mésothéliome pleural malin (MPM) est un cancer agressif émanant de la plèvre qui est un tissue séreux entourant les poumons et recouvrant la cavité intrathoracique. Son pronostic demeure limité même chez les patients pouvant bénéficier d'approches multimodales. Des essais cliniques récents incluant des patients avec MPM ont démontré la supériorité de l'immunothérapie (double inhibition des points de contrôle) par rapport à la chimiothérapie conventionnelle. Néanmoins, le gain en survie reste faible et se limite à une fraction des patients traités. L'infiltration et la réponse immunitaire dirigée contre le MPM reste alterée et pourrait expliquer l'efficacité limitée de l'immunothérapie. Afin d'améliorer le pronostic du MPM, de nombreuses approches centrées l'amélioration de la réponse immunitaire ont été tentées. Dans ma thèse, je m'intéresse à l'impact immunitaire et vasculaire de la thérapie photodynamique à faible dose (L-PDT) du mésothéliome. La thérapie photodynamique est une modalité de traitement qui a des effets pléiotropiques sur les compartiments vasculaire et immunitaire. L'hypothèse de ma thèse est que la L-PDT module la vascularisation tumorale et l'infiltration immunitaire et améliore le contrôle du mésothéliome malin dans un modèle murin orthotopique syngénique.

Dans la première partie de mon projet, je me base sur des résultats acquis de mon laboratoire d'accueil et démontre sur un modèle orthotopique de MPM que la L-PDT est capable d'induire l'expression de molécules vasculaires d'adhésion telles que ICAM-1, VCAM-1 et E-Selectin. Je démontre ensuite que l'expression de E-Selectin corrèle avec l'infiltration tumorale de lymphocytes CD8+ et avec un meilleur contrôle tumoral. En utilisant des inhibiteurs de la E-Selectin, du NF-κB et des lymphocytes CD8+, je découvre un mécanisme impliquant l'expression vasculaire d'E-Selectin via NF-κB qui est nécessaire et suffisante pour l'infiltration de lymphocytes CD8+ et le contrôle du MPM dans le modèle murin.

Dans un second temps, je valide l'importance de ce mécanisme sur des échantillons clinques de patients avec MPM. En effectuant des immunohistochimies et corrélations statistiques avec la survie des patients, j'ai pu trouver que l'expression vasculaire d'E-Selectin corrélait avec l'infiltration lymphocytaire (CD8+) du MPM. Par ailleurs, une

expression vasculaire élevée de l'E-Selectin corrélait avec une meilleure survie des patients.

Ces trouvailles et ce mécanisme prédisent un impact intéressant de la photothérapie dynamique dans le contexte du MPM et une potentielle combinaison de ce traitement avec l'immunothérapie pour améliorer le pronostic des patients.

# 4. Introduction

## 4.1 Malignant Pleural Mesothelioma

### *4.1.1 Lungs and pleura*

The respiratory system is responsible for two distinct functions: conduction and respiration. The conduction function consists in conveying air to the respiratory portion where respiration, meaning blood oxygenation through gas exchanges, can occur. Conduction is provided by the upper respiratory tract which include nasal cavities, nasopharynx, larynx, trachea and the lungs. In the lungs, the conduction spans from the trachea to the terminal bronchioles where gas exchanges happen downstream, (1). By providing the only respiratory unit of the body, lungs are the major organs implicated in respiration. They are composed of lobes; three for the right lung and two on the left lung. Trachea is dividing at the carina into two main bronchi, one right and one left. Each lobe is then defined following the lobar bronchi emerging from the main bronchus. Bronchi are further dividing in smaller anatomical structure from the segmental bronchi to the terminal bronchioles. Terminal bronchioles finally open on the respiratory bronchioles where blood oxygenation takes place, (1,2). Respiratory bronchioles are communicating with grouped alveoli through alveolar ducts, altogether constituting a respiratory unit, (3). Pulmonary capillaries bring deoxygenated blood from the right ventricle to the alveoli. Alveoli are covered by a thin, highly specialized epithelial layer composed of alveolar epithelial cells named pneumocytes. Type I pneumocytes accounts for 96% of the alveolar epithelium and are in contact with endothelial cells of the pulmonary capillaries. Type II pneumocytes are secretory cells producing surfactant. Surfactant is a lipidic solution that avoids collapsing the alveoli during expiration by lowering the surface tension produced at the blood air interface, (4). Indeed, during breathing, air is shifted from the outside into the lung by creating a depression inside the chest cavity.

An essential element to facilitate breathing is the pleural space. Two pleurae, one on the chest cage (the parietal pleura) and one on the lung (visceral pleura) delimits the serosal pleural cavity. This cavity is filled with pleural fluid produced by the pleura and negatively pressurized at approximately −3 to −5 cmH2O. Those characteristics are critical for

transmitting movements of the chest wall to the lungs, maintaining the lungs in a properly inflated state and for blood circulation within the thorax, (5,6). The pleura derives from the lateral mesoderm splitting into somatic and splanchnic mesoderm, giving rise to parietal and visceral pleura respectively, (7). A monolayer of mesothelial cells composes each pleura. By secreting surfactant, both pleural surfaces repulse each other creating the negative pressure. The extracellular matrix is richly composed of supportive elements such as blood vessels, lymphatic vessels, elastic fibers, and nerves endings, (8). Blood vessels vascularizing the pleural spaces either arise from the systemic circulation alone (for the parietal pleura) or from the systemic and pulmonary circulation (for the visceral pleura), (8). The lymphatic drainage of the pleura is responsible to clear excessive liquid found in the interstitium of the pulmonary parenchyma. Lymph vessels converge into the lobar and hilar lymph nodes stations, (9). The immune landscape of pleura is limited under physiologic conditions. Pleural inflammation mainly arises from pulmonary inflammation. A major player of pleural inflammation are resident macrophages. Their role remains poorly understood but it appears to contribute to clear apoptotic cell under physiologic conditions and participate to the neutrophil influx during inflammation, (10). Conversely, dysfunction of their cleaning function could lead to pleural diseases.

### *4.1.2 Development and classification of malignant pleural mesothelioma*

While its origin remains a matter of debate, an inefficient cleaning of inhaled mineral fibers by resident macrophages appears to be the cause for development of malignant pleural mesothelioma (MPM). Indeed, studies have shown a link between asbestos fiber exposure (chrysotile, crocidolite, and amosite) and development of MPM. This ability relies on their intrinsic properties: because of their length, alveolar and resident pleural macrophages are unable to phagocytose the fibers completely, leading to a state of "frustrated phagocytosis". The latter then causes the production of reactive oxygen species that cause DNA strand breaks and cell-cycle arrest, ultimately causing cancer development, (11). Asbestos fibers have been banned from construction material in the 90s and the incidence of MPM is expected to decrease. More recently, it was shown that other types of material containing nano-fibers could have properties similar to asbestos and have health hazard consequences (11, 12). In addition to the occupational exposure which explains 90% of MPMs, an estimated 4% are caused by ionizing radiation (for

diagnostic or therapeutic purposes) (13, 14). Finally, spontaneous MPM or MPM arising from genetic mutations subsequent to viruses such as simian polyomavirus SV40 exposure represent the last small proportion of MPM etiologies, (11, 15).

MPM is a deadly disease with an estimated median survival time from diagnosis of 11 months, (13). The histology of the tumor is a well-identified factor affecting survival and can be classified as epithelioid, sarcomatoïd or biphasic, (Fig. 1). The epithelioid subtype represents up to 80% of MPMs, (16). This subtype has the lowest histological invasiveness of the surrounding stroma with tumor cells harboring a solid, trabecular or tubulopapillary pattern. This subtype has the best 15 month median survival prognosis, (17). The sarcomatoïd subtype represents 5% to 10% of MPMs, (16). It is the most aggressive histology with spindle or mesenchymal cells that have high invasive potential. The prognosis of sarcomatoid MPM is the worst with 5 month median survival (17). Finally, biphasic MPMs are a mixture of epithelioid and sarcomatoid (17). The prognosis is linked to the predominant histology composing the biphasic MPM, e.g., a higher proportion of sarcomatoïd cells (> 80%) is associated with lower survival, (18). Alternative genetic criteria for MPM classification were described (17).

Genetic alterations identified in MPM concerned the tumor suppressor genes such as BAP1, NF2 and CDKN2A/CDKN2B genes that are frequently inactivated by deletion (11). BRCA-1 associated protein is a tumor suppressor protein encoded by the BAP1 gene. The functions of this protein are multiple from cell-cycle and transcription regulation by de-ubiquitination of histones to homologous recombination of the DNA through BARD1 interaction. BAP1 mutations are found in up to 65% of MPM, (19). BAP1 mutations were more frequent in epithelioid than sarcomatoid histologies. BAP1 mutation is also associated with improved overall patient survival (OS), (19, 20). NF2 or neurofibromatosis 2 gene, encodes merlin, a tumor suppressor protein. Merlin regulates diverse cellular events mediated through HER1/2, Hippo and mTOR signaling such as transcription or translation. NF2 mutations are the second most common mutation after BAP1 and concerns 35% of MPMs. NF2 mutations are more frequent in sarcomatoïd than epithelioid histologies and associated to lower patient survival (21, 22). Finally, the CDKN2A gene encodes for two proteins enhancing p53 activity: p14ARF and p16INK4a, (23). Loss of p16 from CDKN2A by homozygous deletion is found in up to 70% of MPMs. Studies have supported the use of p16 detection by immunohistochemistry in MPM

patients since it is a frequent mutation and its expression is associated with better survival and response to chemotherapy, (24, 25).

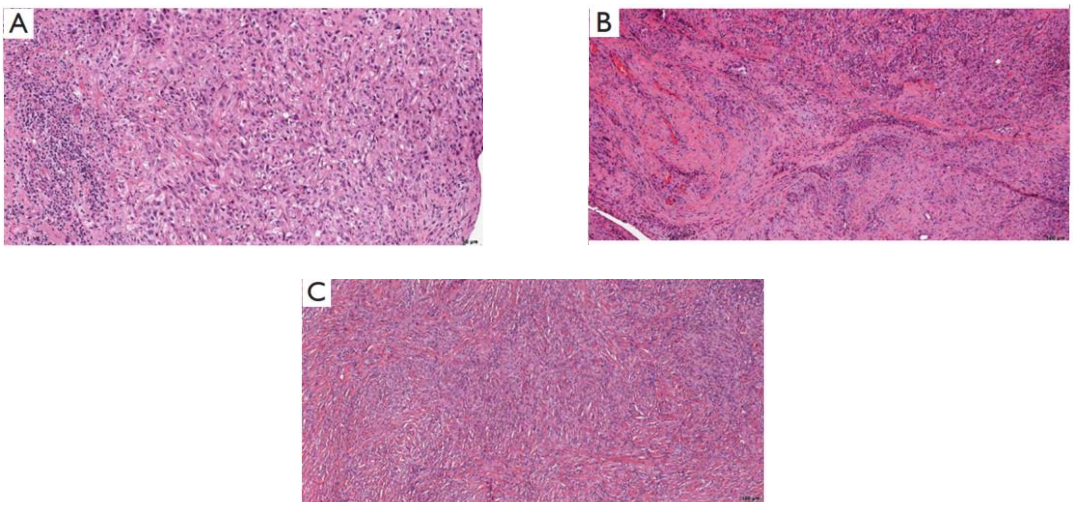


**Fig 1. Major histologic subtypes in MPM.** Representative histopathology images of the A) epithelioid, B) biphasic and C) sarcomatoïd histologic subtype of MPM. Histological classification remains a major criterion in outcomes and management of MPM patients. *Adapted from (17)*

*4.1.3 Current treatment strategies in MPM*

Until recently, a key element in the management of MPM was its resectability and histology. Patients with localized epithelioid or biphasic tumors were managed by multimodal approaches including surgery, radiotherapy and chemotherapy while patients with more extensive disease or sarcomatoid histology only receive systemic therapies with palliative radiation, (26).

Two surgical resection approaches were performed according to tumor burden: extra-pleural pneumonectomy (EPP) or extended pleural decortication (EPD). While both approaches aimed to macroscopically resect the tumor burden, EPP was associated to high morbidity and mortality which limited its clinical benefit for patients, (27). EPD had a far lesser morbidity and mortality burden with similar oncological outcomes (28-30). Additional local therapies were also tested before or after the surgery to improve patient outcome. Sugarbaker et al, perfused hyperthermic chemotherapy in the pleural cavity after MPM resection which was associated to better patient survival (31). De Perrot et al combined pre-operative hypofractionated radiation therapy with EPP. Results were encouraging regarding survival but limited by the toxicity of this approach (32). Friedberg

et al, combined radical pleurectomy with intrathoracic photodynamic therapy. Results showed patient median survivals of more than 30 months in this highly selected population (33).

In 2023, the MARS-2 trial was presented at the World Conference on Lung cancer (34). This randomized controlled trial compared, for patients with resectable MPM, chemotherapy only to chemotherapy + extended pleural decortication (EPD). The overall survival was comparable between groups and there were more adverse events and a lesser quality of life in the surgical group compared to chemotherapy only group. The role of surgery in MPM is therefore controversial. Until recently, the only non-surgical systemic therapy approach in MPM was cisplatin combined to pemetrexed (35, 36). This approach showed response in the majority of MPM with an improved survival of 10%. Immunotherapy was recently evaluated in MPM given its promising results in other chest malignancies. Immunotherapy consists in improving the efficacy of the host immune response directed against the cancer. Various approaches exist for this concept including adoptive T cell transfers, cancer vaccines and immune checkpoint inhibitors (ICIs), (37). The latter aims to block immune checkpoint molecules expressed by other cells that influence the activity of lymphocytes. As an example, cytotoxic T lymphocyte antigen-4 (CTLA-4) is an immune checkpoint molecule. It consists in a ligand on effector immune cells that interact with its receptor on antigen presenting cells. A second immune checkpoint molecule is programmed death-ligand 1 (PD-L1) and is expressed on tumor cells. It binds to the PD1 expressed at the immune cell surface, (38). Interactions of the immune checkpoint molecule with its ligand inhibit the function of immune cells. In T-cells, the inhibition could happen through the downregulation of the T cell receptors and MHC-1, a key molecule for cancer cells recognition. This leads to a decreased effectiveness of the immune cells. By competitively binding such immune checkpoints, ICI precludes the inhibition of the function of immune cells to happen. This results in an enhanced immune activity.

In MPM, a phase III trial comparing chemotherapy (standard of care) with dual ICI, an anti-CTLA-4 (ipililumab) and an anti-PD1 (nivolumab), in second line exhibited an improved survival in the immunotherapy group compared to chemotherapy of 4 months. This has made ICI therapy a pillar in the management of MPM (39). However, these results still require improvement. Given the critical role of the immune system in the response to

immune checkpoint inhibition therapy, the investigation of the tumor microenvironment and its influence on the immune system composition have gained more interest.

## 4.2 The tumor microenvironment

### *4.2.1 Overview of tumor microenvironment*

The establishment and progression of a tumor is complex and involves multiple factors. In addition to genetic alterations that drive tumor growth and dissemination the surrounding host cells were shown to play a semantic role in supporting these mechanisms. The tumor microenvironment refers to the diversity of elements surrounding the tumor niche (40) The TME can be separated in cellular and non-cellular elements. Cellular elements include immune cells and cells acting on the extracellular matrix (ECM) such as fibroblasts or endothelial cells. Non-cellular elements are components embedded close to the tumor and in the ECM such as cytokines, chemokines, or ECM fibers, (41). The interpretation of the interactions occurring in the TME is complex since each element can contribute to tumor progression or actively impair tumor spread according to the circumstances (40). With the recent rise in importance of immunotherapy, research on the TME immune microenvironment has gained significant interest. The ultimate aim is to decipher how the tumor and TME can affect the immune response against tumors alone or in combination with immunotherapies.

### *4.2.2 Immune microenvironment in malignant pleural mesothelioma*

MPM is known to harbor an altered immune microenvironment. The term “cold TME” is often used to refer to an immune desert inside a tumor, as opposed to “hot TME” harboring strong immune infiltration, (42, 43, Figure 2). MPM has a high intertumoral heterogeneity regarding the composition of its TME, mainly influenced by the histological subtype of the tumor. Epithelioid and biphasic tumors are more prone to display a poorly infiltrated TME while sarcomatoïd tumors are characterized by an immune riche TME, (42, 44). A possible explanation to this observation is the aggressive phenotype of sarcomatoïd tumors. Indeed, sarcomatoïd MPM have a higher mutational load which favor the generation of neoantigens and a better immune response generation. This

response is, however, inhibited by tumor related mechanism (45, 46). The main effector element in the immune response remains tumor infiltrating lymphocytes (TIL). In addition to the CD3+ markers used to discriminate TILs, additional membrane protein markers are used to define their function. For example, lymphocytes harboring CD8+ are categorized as effector cytotoxic T-cells which exert an activity against tumors. CD4+ T-cells enhanced through cytokines the function of CD8+ T cells and are referred to helper T-cells. In addition to their supportive functions, helper T cells also have an intrinsic cytotoxic activity, (47, 48).

In the past, TILs have been used as prognostic markers for MPM. It was demonstrated in samples from MPM patients that a higher count in CD8+ cells in the tumor was associated with better progression free survival (PFS), better OS and higher levels of necrotic cells. Moreover, lymph node invasion was negatively correlated to the presence of CD8+ cells. The trend is less clear for CD4+ T cells, that were associated with improved or a decreased OS, (49, 50). Importantly, the immune checkpoints harbored by TILs in MPM patients were highly predictive of survival. The expression of immune checkpoints in MPM is highly variable from one tumor to another and is closely related to histology. For example, PD-L1 is three times more frequently expressed in non-epithelioid MPM (30%) compared to epithelioid MPM (10%), (51). Because they inhibit the immune response, this observation explains why sarcomatoid tumors have worst survival than epithelioid ones. Additionally, even low levels of expression of PDL-1 by MPM tumor cells (<1%) show decreased survival compared to negative PDL-1 patients (52-54). Other immune checkpoints remain poorly investigated in MPM. For examples, CTLA-4 expression appeared highly variable across MPM patient samples, and a higher expression was observed in epithelioid compared to non-epithelioid tumors. A favorable prognostic effect on the survival was found for the expression of CTLA-4 in the tissue, (55). The role of immune checkpoints on patient survival remain inconsistent in the literature (56). Nevertheless, dual immune checkpoint inhibition therapy was significantly better in non-epithelioid histologies compared to others suggesting there may be an therapeutic opportunity in these patients including with upfront ICI therapy.

Furthermore, given their importance for tumor response, strategies to enhance the recruitment of TILS in the MPM TME have been suggested. Among them, modulation of

the vasculature and endothelial cell activation have been performed in my host lab and by others.

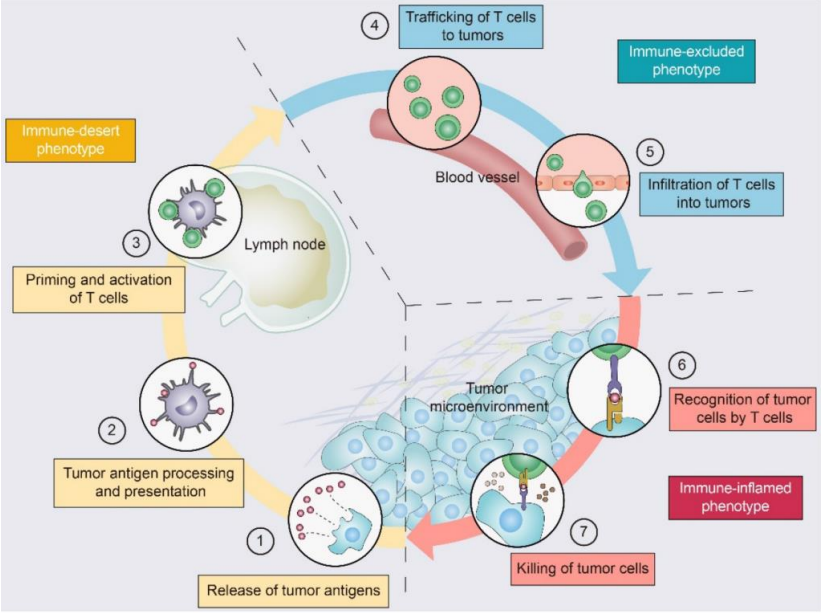


**Fig 2. Immune phenotype observed in tumors.** Several critical steps are needed to turn a cold TME into a richly infiltrated one. Absence of active immune cells against cancer cells consists in an immune-desert phenotype. Priming and activation of T cells by cancer-specific antigens are required to overcome this phenotype. Activation of T cells is not sufficient to ensure an effective immune response. Infiltration of the cytotoxic cells are keys to exert an effective tumor control. Lack of T cells infiltration results in an immune-excluded phenotype. *Adapted from (43)*

### *4.2.3 Vasculature in cancer*

The vasculature of cancer is characterized by an abnormal architecture and function. This aberrant morphological and functional vascularization is due to the unregulated secretion of growth factors such as the vascular endothelial growth factor A (VEGF-A) related to the need of energy of developing tumors. The abnormal function and increased permeability of vessels impacts on the TME composition by limiting immune cell recruitment or drug distribution, (57, 58). Because of the barriers anarchic vasculature represents to effectively treat the cancer, therapies have been developed to normalize these vessels.
Anti-angiogenic therapies were developed to target angiogenic factors. The first approach has been to inhibit the interaction between VEGF-A and its receptor. Bevacizumab, an antibody directed against VEGF-A is the first and most known anti-angiogenic therapy. Bevacizumab exhibited promising results in improving patient survival and is now part

of the standard of care for many cancers such as colorectal or breast cancers, (59-60). A second approach was to target the TME and its elements directly responsible for vessel growth. Macrophages are innate immune cells able of phagocytosis. Macrophages can either be recruited from the systemic circulation as monocyte derived cells, myeloid derived suppressive cells (MDSC) or be present in the tissue as tissue-resident macrophages, (61). Tumor associated macrophages (TAM) are macrophages found in the TME of the cancer and thought to support its growth. While there is no current consensus on their precise origin, a polarization of the macrophages, from a pro-inflammatory subtype (M1 macrophages) to a pro-tumoral subtype (M2 macrophages) seems to be initiated by the tumor and its TME and to partially explain the presence of TAMs, (62). M2 macrophages appeared to support abnormal angiogenesis. Therefore, targeting those cells with, for example, anti-CSF1-R, has shown promising effects with vascular normalization, (63).

High MPM vascular density was associated to a lower patient survival, (64). This suggests a favorable impact of anti-angiogenic drugs the normalize the tumor vasculature. Therefore, Bevacizumab, in combination with Cisplatin and Pemetrexed, is now used as second line therapy for epithelioid MPMs, (65, 66).

In addition to the abnormal vascular structure, the function of angiogenic vessels is impaired. Methods to improve this function have also been developed and tested.

### *4.2.4 Endothelial anergy and adhesion molecules in cancer*

Vessels are covered on their inner side by a monolayer of endothelial cells which constitute the endothelium of the vascular intima. Endothelial cells are polarized with a luminal membrane in contact with components circulating in the vascular lumen and basolateral membrane anchored it to the surrounding tissues, (67). ECs are the main effectors responsible for vessel function (barrier, hemostasis, vascular tone, and immune response regulation, (68)). ECs contribute to the immune response mainly by recruiting and allowing the immune cells from the circulation to enter the target site. This process first implies the activation of ECs. This activation takes place through two distinct pathways. The first pathway is mediated through GTP coupled receptors and lasts 10 to 20 minutes to ensure a controlled activation of the inflammatory phenotype. In case of sustained inflammation, pro-inflammatory cytokines such as IL-1 and TNF-α will trigger

their receptor at the surface of ECs, leading to the second pathway of EC activation. The latter is dependent on gene transcription and protein translation. This pathway is slower but lasts for longer periods (hours to days) . The recruitment function of ECs can then begin through the secretion of attractive cytokines and chemokines such as IL-8 or CCL-2, (69-71). Once leucocytes are attracted close to ECs, the presence of adhesion molecules and their ligands at the surface of leucocytes allows their firm arrest. This interaction happens in three phases: Tethering, rolling and firm arrest; with distinct adhesion molecules operating during each of these steps, (72). Once attached, the EC allows for leucocytes to cross the endothelium through a phenomenon call diapedesis. While it was admitted leucocytes transits between EC during diapedesis, more evidence suggests a cross cellular migration through EC cell, mainly during the phase I activation, (69), (Fig. 3).

The key players during this recruitment process are cellular adhesion molecules (CAM) presented by ECs. Among them, E-Selectin, ICAM-1 and VCAM-1 constitute the main CAM. E-Selectin is a type I transmembrane protein constituted by a N-terminal lectin-like domain, an epidermal growth factor (EGF) domain and a variable domain. It binds sialyl Lewis x (sLex) derived proteins expressed at the surface of immune cells, (70, 71). Mostly expressed by ECs, E-Selectin participates during the early phase to the recruitment of leucocytes by initiating the rolling of the latter (70). Intercellular adhesion molecules (ICAM) are a family of CAM with ICAM-1 being the most expressed protein of the family. ICAM-1 is a transmembrane protein with extracellular domain close to an immunoglobulin domain. It preferentially binds the β2-integrin called LFA-1. Its binding allows the firm arrest of the leucocyte at the endothelium, (72, 73). Vascular cell adhesion molecule 1 (VCAM-1) is a glycoprotein composed of a transmembrane domain, a cytoplasmic domain, and an extracellular domain with six or seven immunoglobulin-like domains binding preferentially, (74, 75). As ICAM-1, VCAM-1 promotes the full arrest of the leucocyte and facilitates the transmigration of immune cells into the inflammation site, (75). CAM participate actively to cancer immunity. Indeed the absence of CAM impaired the recruitment of a cancer immunity decreasing tumor control (76, 77). Despite their pro-inflammatory role, the impact of CAM on cancer control is still controversial: in addition to favoring leucocyte extravasation, recent evidence suggests CAM can also promote tumor progression and metastasis spread (78, 79). In addition, CAM also

stimulate interactions in the TME leading for example to the polarization of monocytes to M2 macrophages, (80) or to epithelial-to-mesenchymal transition in cancer cells, (81).
In cancer, ECs are characterized by a general loss of the previously mentioned functions. This state is designed as endothelial anergy. The resultant hypoxia and low pH within the TME are known to be immunosuppressive and preclude ECs from becoming responsive to inflammatory signals, (82, 83). In addition, the VEGF-A secretion appears to be responsible for the inhibition of the stimulatory signal given by IL-1 or TNF-α to EC, (84, 85). Because of the crucial role of ECs for the promotion of an immune response, therapies to relieve the vascular anergy in cancer have been proposed. In my thesis, I have used low-dose photodynamic therapy to relieve tumor vascular anergy and restore endothelial function and immune cell infiltration.

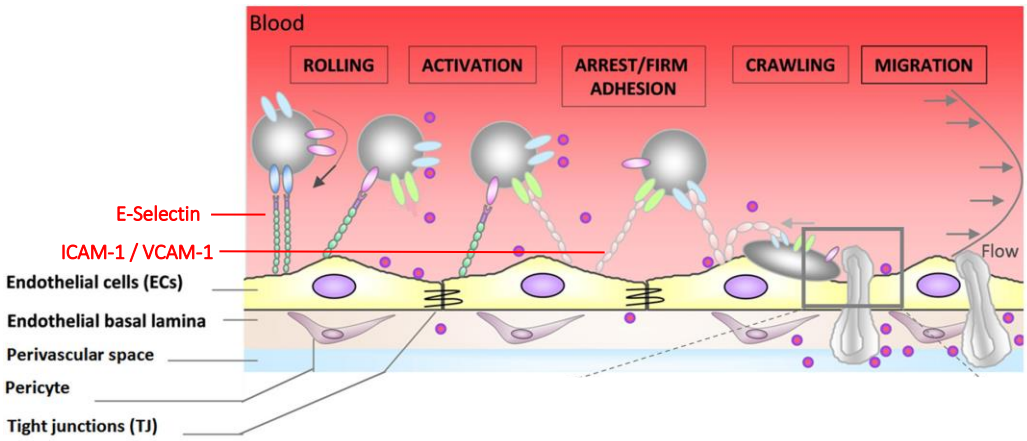


**Fig. 3 Cascade of interactions preceding diapedesis.** Circulating leucocytes closely interacts with endothelial cells during infiltration inside the tissues. E-Selectin typically plays its role during the initial interactions called rolling, while ICAM-1 and VCAM-1 interacts with leucocytes to provide the firm arrest of the circulating cells. *Adapted from (75)*

## 4.3 Photodynamic therapy

### *4.3.1 Origin and mechanism of action*

Photodynamic therapy (PDT) was developed in the early 20$^{th}$ century. Scientists observed that the exposure of certain molecules to light could mediate damage to cells. A german

scientist, Oscar Raab, observed in 1900 that the combination of specific wavelengths with a chemical component called acridine was lethal for *Paracemium* specie, (86). Few years later, scientists referred to the term photodynamic action by applying eosin followed by exposition to visible light to treat skin diseases, (87). Since, the described biological effect evolved from these initial experiences to the actual concept of PDT. This therapy consists in the activation of photosensitizer, an inert component reactive to light, with a specific light wavelength. The exposure of the photosensitizer to light will excite the molecule and deliver the energy for an electron to move to a first excited state. This will lead to the creation of reactive molecular species including reactive oxygen species (ROS), (88). Through their highly reactive properties, ROS are able to interact with many components of the cells such as proteins, lipids or nucleic acids. Therefore, ROS can lead to numerous physiological and pathological processes, (89). Since its first application in clinic in 1976 for bladder cancer, PDT is now used in various cancers with interesting results, (90). Because of their easy illumination, skin cancers seem to be the most suitable opportunity for PDT treatment. Given its low side effect profile, PDT offers an alternative treatment in non-surgical skin cancers. PDT was shown to be effective for the management of non-melanoma skin cancer such as basal carcinoma. However, the treatment with PDT was associated with higher recurrence rates (91). Authors observed similar results in melanoma. While PDT was an interesting palliative option for the treatment of melanoma, studies suggested that the combination of PDT with immunotherapy could be helpful to overcome melanoma resistance and thus, recurrences, (92). PDT treatment also benefit to other cancer types such as colorectal, head and neck or breast cancer. As for skin cancers, the adjunction of immunotherapy to PDT treatment seems promising, (93-95) The rational of combining PDT to immunotherapy is to benefit from the local tumor killing and immune stimulation effect of PDT and enhance host immunity against metastasis and recurrence: an abscopal effect. The abscopal effect designs the ability of a therapy to control tumors distant from the tumor site through the stimulation of the immune system. Studies have demonstrated the ability of PDT to mount an immune response that will attack tumors distant from the treatment site (96-98). Moreover, PDT seems to have an impact on the memory compartment of the immune system. Memory CD8+ T-cells are a long-term, heterogenous population of immune cells responsible for a rapid and effective immune reaction in case of a rechallenge by a previously encountered antigen, (99). In the context of cancer, memory immune cells are of great interest through their

effectiveness to prevent relapses. Tissue-resident CD8+ T-cells contribute to immune surveillance of tissue and preclude the initiation of a recurrent tumor, (100). The ability of PDT to stimulate memory immune cells have been observed in preclinical cancer models through an improved survival and tumor control after the rechallenge of the animals by the initial tumor cells, (101, 102). Altogether, these data support the combination of PDT with ICIs. Several studies demonstrated the efficacy of these two treatments in colon cancer and breast cancers (103-106). Interestingly, the timing between PDT and ICI therapies appears to be crucial to maximize their synergistic effects. Indeed, due to the interval between PDT treatment and CD8+ infiltration, an early administration of ICI before the infiltration of the tumor by the CD8+ would preclude to see any effect of the combination, (107).

A plethora of effects were attributed to PDT. It can induce cell damages and also modulate the immune and vascular compartments (Fig 4). Cell killing mediated by PDT is mainly related to the ROS generated which will react with cellular components such as the plasma membrane or organelles thus causing the disruption of the cell. In addition, cell damages followings PDT appear to be mediated through the apoptotic pathways. Both the intrinsic (mitochondria mediated) and extrinsic (Fas death receptor activation) pathways seem involved. In both pathways, the exposition to PDT leads to the activation of caspase 3/7 by caspase 8 (extrinsic) or caspase 9 (intrinsic) ultimately triggering apoptosis, (108). PDT treatment also affects the immune response. By creating a local inflammation, PDT enhances the production of cytokines at the site of the disease. Studies report an increased secretion of pro-inflammatory cytokines such as IL-1, IL-6 or IL-10 after treatment, (109-111). Those cytokines are responsible for an improved recruitment of immune cells at the site of illumination. In addition to cytokines, adhesion molecules induced by PDT appear to play a role in the recruitment of immune cells. Indeed, while PDT significantly increased leukocyte-endothelial cell interaction in tumors, PDT-induced leukocyte recruitment was significantly decreased in presence of anti-pan-selectin antibodies, (112). While various cell types are involved in the response, including NK cells or neutrophils, it appears that CD8+ T-cells are the main effectors of the immune response provided by PDT, (111-114). In the context of cancer, the depletion of CD8+ after PDT treatment abrogated the long-term control provided by PDT suggesting their substantial contribution to tumor control (113, 115). As targeting the vasculature of the cancer became an interesting approach to tackle tumor growth, the impact of PDT on the tumor vasculature has been studied. The

main action of PDT on the vasculature consists in direct damages to tumor vessels. Decreasing the vessels density inside the tumor results in a decrease in oxygen concentration ultimately favoring the shrinking of the tumor, (116-118). In addition, authors also reported the ability of PDT to generate thrombosis inside tumor vessels after treatment, (118, 119). PDT also interact with a main inflammation pathway: NF-κB. While the implications of NF-κB on tumors are various, it appears that PDT is able to enhance immune activity and reduce the ability of tumor cells to survive to oxygen stress through this pathway, (120). Given the importance of remodeling the TME, either acting on the immune environment or the vasculature, innovative approaches using PDT have been tried to specifically influence those compartments. In my thesis, we focus on low-dose photodynamic therapy targeting the endothelium.

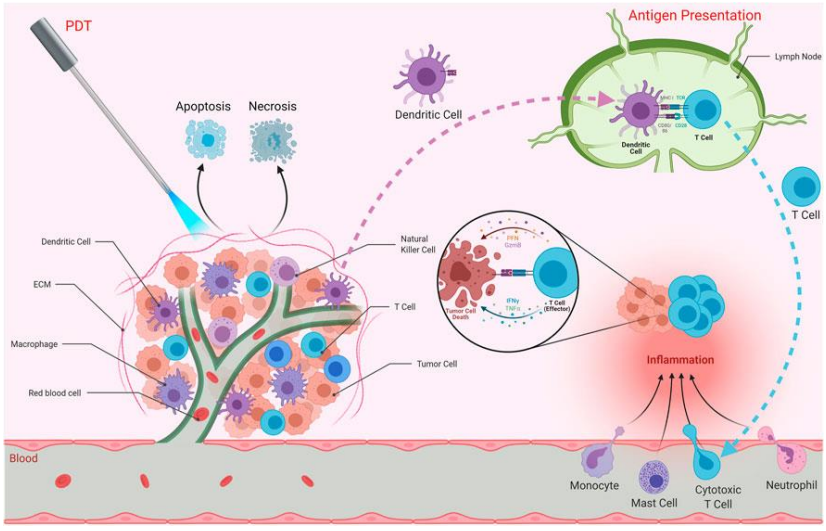


**Figure 4. Potentiation of immune system by PDT treatment.** Treatment of cancer cells by PDT induce apoptosis and necrosis. Those two phenomena in turns release antigens in the ECM that will be uptaken and presented to cytotoxic cells in lymph nodes by antigen presenting cells. Ultimately, this cascade of events contributes to the mounting of a specific immune response against the tumor. *Adapted from (88)*

*4.3.2 Vascular targeted low-dose photodynamic therapy*

PDT depends on multiple parameters such as the fluence, fluence rates and the timing between the photosensitizer injection and illumination. The fluence rate is the number of photons on a unit area per unit of time. The variation in the fluence rate heavily impacts

the tumor response to PDT, (121). Indeed, while high fluence rates were historically used in PDT treatment, it appeared they were associated to higher oxygen consumption by PDT which decreased its effect (121). Therefore, authors supported the use of lower fluence rate, e.g. from 112 to 14 mW/cm2, in order to preserve oxygen at the site of action and maximize the PDT effect. PDT used with lower fluence rate is called low-dose photodynamic therapy, (L-PDT). L-PDT was shown to increase tumor apoptosis compared to PDT with higher fluence rates. Moreover, L-PDT was able to enhance immune stimulation, with higher cytokine secretion and neutrophil recruitment compared to PDT at high fluence rates, (122). Additional research supported the increased effect of L-PDT on tumor control compared to conventional PDT. However, little is known regarding the contribution of the immune system to this improved phenotype, (123-125). Our group previously investigated the effect of L-PDT on the immune infiltration in a heterotopic murine model of MPM. In addition to an improved survival in presence of L-PDT treatment, an increased infiltration of CD8+ lymphocytes and a better activity of antigen presenting cells were observed early after treatment. Moreover, an up-regulation of E-Selectin was also correlated to the improved immune infiltration, (126). Modulating the timing between photosensitizer injection and illumination allowed to target the endothelium more specifically with our L-PDT treatment. Indeed, localization of the photosensitizer, mainly intra- and perivascular at the time of treatment can affect the endothelial cells more specifically, (Fig. 5). Targeting the vessels with L-PDT resulted in a remodeling of the tumor vasculature. By allowing a better coverage of the vessels by the pericytes, L-PDT decreases the leak from the blood vessels and the associated interstitial fluid pressure (IFP). A reduced IFP facilitates a better drug distribution through convection. This improved drug distribution has been shown to be selective for the tumoral tissue and led to a better uptake of macromolecules such as chemotherapy, (127, 128). The promising effects of PDT on the TME have led to the translation of this therapy to cancer patients.

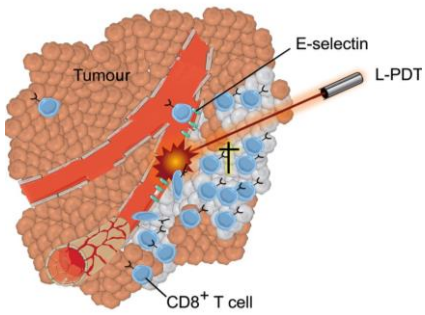

**Fig. 5 Vascular targeted low dose photodynamic therapy.** Vascular targeted L-PDT results in the release of ROS inside the vessels. Activation of endothelial cells by this process results in a relief of vascular anergy through the expression of E-Selectin. In addition, L-PDT favors the recruitment of CD8+ T cells at the tumor site. *Adapted from (126)*

Altogether, it seems that a better comprehension of the immune impact of PDT and its combination with immunotherapy is mandatory to exploit these approaches in cancers such as MPM.

## 4.4 HYPOTHESIS and Aims of the study

Because L-PDT has shown interesting immune modulating potential of the TME and that treatments to control MPM are urgently needed, we hypothesized that:

**Low dose photodynamic therapy modulates the expression of adhesion molecules on the tumor endothelium which favors immune infiltration and improved immune mediated MPM control.**

AIMS

AIM 1: Understand the impact of L-PDT on the tumor microenvironment (vascular and immune compartments) of MPM.

AIM 2: Assess how the immune remodeling and which immune components of the tumor microenvironment affects tumor control.

AIM3: Validate the clinical prognosis of E-Selectin and CD8+ T-cells in patients bearing MPM.

# 5. Summary of results and contributions

In the following chapters 7.1, 7.2 and 7.3, I present the findings of my thesis.

In the first chapter entitled "Low dose photodynamic therapy remodels the tumor microenvironment of malignant pleural mesothelioma" I first developed two orthotopic syngeneic models of MPM in mice that could be treated by L-PDT. Then, I investigated how L-PDT influences the vascular and immune compartments of the tumor microenvironment of MPM. Prior experiments published by my host laboratory had shown that L-PDT could induce E-Selectin expression in endothelial cells and improve the immune recruitment of antigen presenting cells and cytotoxic lymphocytes in the tumor bulk. However, the mechanism for these correlations was never clearly established. With Dre Sabrina Cavin and Dr. Yameng Hao, we first developed a mouse model for MPM where the cell line was injected orthotopically and the L-PDT could be delivered through the chest wall. In addition, we developed a second model of chronic thoracic window in order to perform intravital imaging (IVM) on the tumor. Next, with Dre Sabrina Cavin and Dr Christophe Gattlen, we determined the importance of the NF-κB pathway for E-Selectin expression as well as the E-Selectin expression importance for lymphocyte infiltration. Finally, with Dre Sabrina Cavin, we observed the immune recruitment induced by L-PDT was dependent on the E-Selectin expression and on the NF-κB signaling.

In the second chapter entitled "Induction of vascular E-Selectin and CD8+ T-cells infiltration are mandatory for MPM control provided by L-PDT", we validated the key role played by E-Selectin and CD8+ T-cells induced by L-PDT in the MPM tumor control. To do so, I performed a survival experiment where L-PDT treated mice were continuously depleted in E-Selectin. I observed a significant decrease in survival in mice where E-Selectin was abrogated compared to control, suggesting the crucial contribution of E-Selectin in improving the survival in MPM bearing mice. In a second survival experiment, mice were depleted in CD8+ T cells. Control provided by L-PDT on the tumor was lost in depleted animals suggesting the dramatic contribution of T-cells in the L-PDT mediated tumor control.

In the third project entitled "Clinical prognosis of endothelial E-Selectin expression and impact on CD8+ T-cell infiltration in MPM patient samples", I validated the outcomes provided by E-Selectin and CD8+ T cells in human MPM tissues through immunofluorescence staining. I found a basal higher expression of E-Selectin and an

increased expression after treatment were associated with an improved survival in MPM patients. Additionally, CD8+ T cells infiltration was positively correlated with survival in our cohort. Also, in tumors with a CD8+ T cells infiltration above the median, E-Selectin was positively correlated to CD8+ T-cells infiltration. The results of these three projects are constituting an article which is currently sent to journals for peer-review.

All along the project, Dr. Jean Yannis Perentes, Pr. Johanna Joyce and Dre. Sabrina Cavin provided their input and helped in the design of the experiments, article writing, congresses presentation preparation, and contributed substantially to the editing and writing of this thesis.

# 6. Material and Methods

*Cell lines*

Mouse malignant mesothelioma cells AB12 (Reference: RRID:CVCL_4405 ) derived from BALB/c mice exposed to crocidolite asbestos were kindly provided by Pr. Marc de Perrot, University Health Network, Toronto, Canada. AB12 luciferase-expressing cells were generated by transduction with a lentiviral vector containing a luciferase transgene and puromycin resistance gene (pLenti PGK V5-LUC Puro w543-1, Addgene). Once inoculated in mice, AB12 cells form biphasic MPM characterized by the presence of epithelioid and sarcomatoid cytomorphology cells. Cells were grown in culture in RPMI 1640 medium supplemented with 10% fetal bovine serum. 5 µg/ml of Puromycin (Puromycin ant-pr-1, Invivogen) was added for selection of luciferase expressing cells.
Immortalized human vascular endothelial cells EC-RF24 (ScienCell, RRID:CVCL_AX74) were seeded on poly-L-Lysine coated plates and maintained in endothelial basal medium-2 (EBM-2™ basal medium, CC-3156, Lonza) supplemented with appropriate growth factors (EGM-2™ SingleQuots™ Supplements, CC-4176, Lonza) and passaged at 80% confluence.

*Mouse and tumor models*

Animal experiments were conducted on 10- to 20-week-old BALB/c mice imported from Charles River Laboratories. The animals were acclimated for at least 1 week prior to the beginning of experiments and all animal experiments were conducted in accordance with the Animal Welfare Act and the National Institutes of Health 'Guidelines for the Care and Use of Laboratory Animals' and approved by the Committee for Animal Experiment for the Canton Vaud, Switzerland (authorization VD3574).
250'000 AB12 luciferase expressing cells were injected in 50uL of media directly inside the chest cavity under general anesthesia with ketamine/xylazine (65/4 mg/kg).
Evaluation of tumor size was performed every 2-3 days using the whole body intravital imaging system (IVIS) (IVIS spectrum, Perkin Elmer) 10 minutes after injection of 100 µl of D-Luciferin (Promega, P1041) at a concentration of 15mg/ml I.P. Animals were treated when the bioluminescence signal in tumors reached a value between $8.0 \times 10^6$ to $2.0 \times 10^7$

p/sec/cm2/sr. The animals were assigned to different treatment groups to obtain homogenous bioluminescence values between groups and a male to female ratio of 1:1. Animals with extra-thoracic tumors or undetectable tumor growth were excluded from the study.
At the end of all experiments, animals were sacrificed by IP injection of 0.1mg/kg Pentobarbital and perfused intracardially with saline solution.

*Photodynamic Therapy*

L-PDT was performed using the liposomal form of benzoporphyrin derivative monoacid ring A Visudyne® (Novartis Pharma AG, Basel, Switzerland), as a photosensitizer.

- In vivo L-PDT administration

Animals were anesthetized with a mixture of ketamine / xylazine (100/10 mg/kg) administered IP. Visudyne was resuspended in 0.9% NaCl at a concentration of 0.1 mg/ml benzoporphyrin derivative monoacid ring A and injected intravenously at a dose of 400 µg/kg body weight. After 10 min, a laser light of 568 nm was applied through the chest wall to the tumor and surrounding normal tissue by using a frontal light diffuser containing a lens (Medlight, Ecublens, Switzerland). The height between the light diffuser and chest wall was defined by measuring in real-time the fluence rate and the fluence in 11 mice using a previously described light dosimetry system (129-131) and set at 4.35 cm to treat the tumor with an irradiance of 50 mW/cm2. The treatment spot had a diameter of 25 mm, and the treatment time was of 198 s to reach a total light dose of 10J/cm2.
The drug-light conditions were chosen to modulate and favor stabilization of the tumor vasculature based on previously published studies (132).

- In vitro L-PDT treatment

EC-RF24 cells were serum-starved 6 hours before treatment and incubated with 50 ng/ml Visudyne for 15 min. The photosensitizer was removed with the media prior to light

exposition. Cells were then exposed to an irradiance of 5 mW/cm2 and a light dose of 0.15 J/cm2 (for L-PDT) as described previously, (132).

*Inhibition of canonical NF-κB pathway:*

- In vitro NF-κB pathway blockade in endothelial cells

Two different siRNA constructs targeting IKKγ (NEMO) were used to block the NF-κB pathway in endothelial cells, named, respectively siRNA1 (s16186, Ambion) and siRNA2 (s16187, Ambion). Negative control siRNA (Silencer™ Select Negative Control No. 1 siRNA, 4390843, Thermofisher) was used as control. Sequences of siRNAs are provided in Table 1.
Briefly, cells seeded in 60 mm dishes were transfected with 120 pmol of each siRNA (40 pmol/µL) using the Viafect transfection reagent (E4981, Promega) in a 4:1 ratio. Medium was changed 6h to 8h after transfection.

- In vivo NF-κB pathway blockade

A NEMO (IKKγ) binding domain (NBD) peptide containing the IKKα and IKKβ consensus binding sequence was used to inhibit NF-κB activity in vivo (Sigma Aldrich 480025). A mutated non-binding peptide (Sigma Aldrich 480030) was used as control. Inhibitory and control peptides were dissolved in a sterile solution of 10% DMSO in PBS to a final concentration of 1mg/ml according to a previously published protocol (133). 100 µl of the suspension were injected IP 15 minutes before PDT treatment.

*Table 1: Sequences of siRNA*

| | *Sense* | *Antisense* |
|---|---|---|
| *siRNA 1* | AAACAGGAGGUGAUCGAUAtt | UAUCGAUCACCUCCUGUUUgg |
| *siRNA 2* | GGAUCGAGGACAUGAGGAAtt | UUCCUCAUGUCCUCGAUCCtg |

*E-Selectin inhibition in vivo*

50 µL of anti-E-Selectin antibodies at a concentration of 0.6 µg/µl (BioXcell BE0294) were injected IV 30 minutes before treatment, according to a previously published protocol (134). After PDT treatment, antibodies were injected every 2 days until sacrifice to

maintain E-Selectin blockade along the course of the experiment. Controls were performed using appropriate IgG isotype control (BioXcell BP0090) at the same concentration.

*CD8 T-cell depletion*

3 days prior L-PDT treatment mice were injected IP with 0.2 mg of anti-CD8 antibody (BioXcell BP0061) once a day. After L-PDT, antibodies were injected every 2 days until sacrifice to maintain CD8 depletion during the course of the experiment, following a previously established protocol (135). Controls were performed using appropriate isotype control IgG (BioXcell BP0090) at the same concentration.

*Flow cytometry*

7 days after L-PDT treatment, tumors were collected and dissociated using tumor dissociation kit (Miltenyi). The dissociated tissue was filtered through a 40 μm mesh filter in HBSS and red blood cell were removed using 1mL of red blood cell lysis buffer (Biolegend) for 10 minutes. The single cell suspension was stained with the Zombie-near-infrared fixable viability kit (Biolegend) for 20 minutes at room temperature (RT) following standard protocol, washed with FACS buffer (2 mM EDTA and 0.5% BSA in PBS) and then FC-blocked (BD Biosciences) for 30 minutes on ice. After washing with FACS buffer, cells were incubated with directly conjugated antibodies (see Table 2). Stained samples were washed 3 times with FACS buffer. Sample acquisition was performed on a BD Symphony at the Flow Cytometry Core Facility of University of Lausanne. FlowJo v10.7.1 (BD) was used for analysis.

*Table 2: Antibodies used in flow cytometry*

| Primary antibody | Reactivity to | Concentration used | Reference | Manufacturer |
|---|---|---|---|---|
| FVD UV440 | Mouse | 1/700 | 423105 | Biolegend |
| CD16/32 | Mouse | 1/100 | 553141 | BD Bioscience |
| CD45 BUV805 | Mouse | 1/500 | 748370 | BD Bioscience |
| CD4 BUV615 | Mouse | 1/500 | 613006 | BD Bioscience |
| CD3 BUV395 | Mouse | 1/25 | 563565 | BD Bioscience |
| CD11b BV750 | Mouse | 1/750 | 101267 | Biolegend |

| | | | | |
|---|---|---|---|---|
| PD1 BV711 | Mouse | 1/100 | 135321 | Biolegend |
| LAG-3 BV421 | Mouse | 1/200 | 125221 | Biolegend |
| CTLA-4 PE | Mouse | 1/50 | 106305 | Biolegend |
| CD8 PE-Cy5.5 | Mouse | 1/200 | 35-0081-82 | Thermofisher |
| TCRβ Alexa 488 | Mouse | 1/250 | 109216 | Biolegend |
| TIGIT PE-Cy7 | Mouse | 1/50 | 142107 | Biolegend |

*Immunostaining*

Paraffin-embedded fixed samples or OCT embedded samples were cut in 8 µm thick sections and used for immunofluorescence staining of adhesion molecules and lymphocytes in mouse tumor tissues. Paraffin-embedded fixed samples were stained for adhesion molecules: Tissue section of whole slides and tissue microarray (TMA) slides were deparaffinized and rehydrated by heating slides at 60°C for 10 minutes on a heated plate followed by successive immersion in xylene (3 times 5 minutes), EtOH 100% (3 times 3 minutes), EtOH 90% (3 minutes), EtOH 70% (3 minutes) and water (2 times 3 minutes). Slides were then immersed in antibody retrieval pH 6 solution, heated in microwave at 800 Watts for 5 minutes and left 30 minutes at room temperature for cool down.

After 3 successive wash of 10 minutes with PBS, sections were mounted on a Shandon coverplate system (Epredia™ 72110017), blocked one hour with blocking solution composed of 5% normal donkey serum (NDS, Bio Rad, C06SB), 0.1% bovine serum albumin (BSA, Panreac Applichem, ref A1391,0100) in PBS and incubated overnight with primary antibodies in blocking buffer at 4°C. The day after, samples were washed with PBS and incubated with secondary antibody and DAPI (ThermoFisher Scientific Cat# D3571, RRID:AB_2307445) in blocking buffer for 1h at RT. Antibodies and concentrations used are provided in Table 3. At the end of the staining procedure, slides were mounted using Fluoromount-G mounting medium (Southern Biotech, ref: 0100-01).

The slides were scanned with Zeiss Axioscan Z.1 at x20 magnification, and the images were analyzed with Image J (FIJI). Thresholds between 80 and 120 were applied to separate noise from the signal. Thresholds values were then exported in the RG2B colocalization plug-in to measure colocalization displayed as pixel count.

Samples embedded in OCT were used for immunofluorescence of immune cells in mice tissue. OCT blocs were cut in 8 µm thick sections. Slides were fixed in methanol at -20°C for 10 min. After 3 times 10 minutes PBS wash, procedure was performed as for paraffin section. Antibodies used are presented in Table 3.

*Table 3 : Antibodies used in immunofluorescence*

| **Primary antibody** | **Organism** | **Reactivity to** | **Concentration used** | **Reference** | **Manufacturer** |
|---|---|---|---|---|---|
| E-Selectin | Rabbit | Mouse, Human | 1/25 | NBP1-45545SS | Novus Biological |
| ICAM-1 | Mouse | Mouse | 1/100 | NBP2-22541 | Novus Biological |
| VCAM-1 | Rabbit | Mouse | 1/100 | NBP2-67292 | Novus Biological |
| VE-Cadherin | Goat | Mouse | 1/200 | AF1002 | R&D System |
| CD3 | Rabbit | Mouse, Human | 1/100 | GTX16669 | Gene Tex |
| CD4 | Rat | Mouse, Human | 1/50 | 550280 | BD Pharmingen |
| CD8a | Rat | Mouse, Human | 1/50 | 550281 | BD Pharmingen |
| VE-Cadherin | Goat | Human | 1/100 | AF938 | R&D System |

| **Secondary antibody** | **Organism** | **Reactivity to** | **Concentration used** | **Reference** | **Manufacturer** |
|---|---|---|---|---|---|
| Alexa Fluor 488 | Donkey | Goat | 1/300 | A-11055 | Invitrogen |
| Alexa Fluor 568 | Goat | Mouse | 1/300 | A11031 | Invitrogen |

| | | | | | |
|---|---|---|---|---|---|
| Alexa Fluor 568 | Donkey | Rabbit | 1/300 | A-10042 | Thermo Fisher |
| Alexa Fluor 488 | Donkey | Rabbit | 1/300 | A-21206 | Thermo Fisher |
| Alexa Fluor 488 | Donkey | Rat | 1/300 | A-21208 | Thermo Fisher |
| Alexa Fluor 568 | Donkey | Rabbit | 1/300 | A-10042 | Thermo Fisher |
| Alexa Fluor 647 | Goat | Rat | 1/300 | A-21247 | Thermo Fisher |
| Alexa Fluor 647 | Donkey | Goat | 1/300 | A-31573 | Invitrogen |

*Immunofluorescent staining of EC-RF24 cells*

6 hours after PDT treatment, EC-RF 24 cells were fixed with 4% PFA. Blocking and staining were performed as described for tumor staining. Antibodies used are described in Table 3. Acquisition of 3 fields per well was performed using an Olympus Fluoview 3000 confocal microscope with a plan Apochromat 20×/0.75 WD 0.6mm DIC dry objective. To isolate the signal from adhesion molecules expressed at the membrane, nucleus was removed using mask from DAPI staining and thresholds of between 500 and 900 were applied to remove background noise.

*MPM tumor microarray*

77 MPM patient samples collected during initial biopsy and/or from surgical resection specimen (either extrapleural pneumectomy or pleural decortication) at the University Hospital of Bern, Switzerland, were included in a tumor microarray (TMA) in triplicate core under the ethical approval KEK-BE: 2016-01497. Analysis was performed on formalin fixed paraffin-embedded sections. In addition to the TMA, 5 formalin fixed paraffin-embedded patients samples collected at initial biopsy from the Lausanne University Hospital were added to the analysis. Tumor samples were deparaffinized by heating on 60°C plate for 10 minutes followed by successive immersion in xylene (3 times 5 minutes), EtOH 100% (3 times 3 minutes), EtOH 90% (3 minutes), EtOH 70% (3 minutes) and water (2 times 3 minutes). Serial antibody retrieval solution immersions were performed. Tumor samples were immersed in a pH6 antibody retrieval solution and heated in microwave at 800 Watts for 5 minutes followed by a 30-minute cooldown. Solution was discarded and slides were then immerged in another pH9 antibody retrieval

solution. Slides were heated in microwave at 800 Watts for 5 minutes and put to cool down in the solution for 30 minutes. Following steps of the procedure were performed as described in the immunostaining section.

*MPM tissue microarray – Analysis*

Individual tumors in the TMA were isolated with QuPath and exported to FIJI for analysis. Patient samples were available in triplicates before and/or after treatment. Samples before treatment were collected during diagnostic biopsy while post-treatment samples originated from the surgical resection. Only cores derived from the tumor center were used in the analysis. Thresholds between 70 and 120 were applied to separate noise from the signal. Thresholds values were then exported in the RG2B colocalization plug-in to measure colocalization signal displayed as pixel count. Non-vascular E-Selectin were obtained by subtracting colocalization area between VE-Cadherin and E-Selectin to the total E-Selectin area.

*Western Blot*

Cells were lysed in RIPA buffer after L-PDT treatment and samples in SDS-PAGE sample buffer were separated on 10% acrylamide gels and electroblotted onto nitrocellulose membranes. Membranes were blocked in PBS-Tween with 5% milk and incubated with polyclonal anti-E-selectin/CD62E antibody (NBP1-45545, Novus Biologicals, 1:1000), anti-phospho-IκBα (2859S, Cell Signaling Technology, 1:1000), anti-total-IκBα (9242S, Cell Signaling Technology), anti-IKKγ (sc-166398, Santa Cruse, 1:1000) or anti-GAPDH antibody (G9545, SIGMA, 1:5000). Appropriate HRP secondary antibodies were used for detection (Jackson Immunoresearch Laboratories, 1:5000). Antibodies were diluted into PBS-Tween 0.1%. Between each step, 3 wash with PBS-Tween 0.1% was performed. Acquisition was realized on Vilber, Fusion Fx. Densitometric quantifications of specific bands were performed using the ImageJ/Fiji software.

*Statistical analysis*

Statistical analyses were performed using GraphPad Prism version 8.0.1 for Windows (GraphPad Software, Inc., San Diego, CA, USA). The significance between means of more

than 2 experimental groups was assessed by using one-way analysis of variance followed by Tukey's multiple comparisons post hoc test when the F value was significant. When 2 sets of data were compared, a two-tailed Student's t-test was applied. Test for normal distribution (Shapiro-Wilk test), outliers identifiers tests, equality of variance test were applied consistently. If data were not normally distributed, Kruskal-Wallis test was applied. All data are expressed as mean ± standard deviation. Survival analyses were performed using Kaplan-Meier analysis with log-rank (Mantel-Cox) test applied. Hazard Ratio were calculated using Mantel-Haenszel method. $P < 0.05$ was considered significant.

# 7. Results

## 7.1 Low dose photodynamic therapy remodels the tumor microenvironment of malignant pleural mesothelioma

### Development of two orthotopic MPM immunocompetent mouse models PDT application

Studying the TME *in vivo* requires replicating the tumor development as closely as possible to the human setting. This implies an orthotopic growth and treatment of the tumor. Thus, I first developed an orthotopic model of MPM that could be treated by L-PDT. Growing MPM tumors in the pleura is well established, (136). However, assessing tumor growth was the first challenge. I used AB12 cells which are syngeneic BALB/c MPM cells developed from exposure of mice to crocidolite asbestos (136). To follow tumor within the chest cavity, I transduced tumor cells with luciferase. In the presence of luciferin, transfected cells produce photons that can be imaged by an in vivo imaging system (IVIS). I then confirmed the signal measured corresponded to the tumor bulk in the chest cavity. Preliminary cohorts of mice were first used to establish the growth of AB12 cells implanted in BALB/c mice. I observed that a photon count of $1x10^7$ p/sec/cm2/sr was the minimum to ensure robust and reproducible tumor growth (Fig. 6.1). Thus, I set this point as the established tumor cutoff to decide when L-PDT treatment could be performed. This allowed high reproducible cohorts of animals along the experiments.

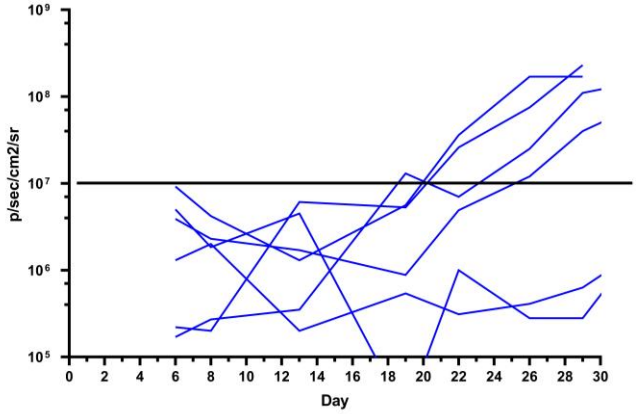


**Fig. 6.1: Development of an orthotopic MPM model for transthoracic L-PDT** Representative growth curves of a preliminary cohort of mice to investigate the dynamic of orthotopic AB12 growth. Each line represents a mice. Results are obtained from IVIS.

Delivering the suited dose of L-PDT directly in the chest of the mice was the second challenge for the establishment of the model. Chest wall thickness is a factor to account for when exposing the chest to the laser. Moreover, mice present a unique thoracic cavity (only one pleural space) which implies to intubate the mice for any incision in the chest to avoid a bilateral pneumothorax and death by asphyxia. To avoid having to intubate and open the chest of animals for therapy, given the chest cavity of mice is thin and similar, I developed a model in which light could be delivered directly through the chest wall (Fig. 6.2A). Using an investigational cohort of 11 wild type animals in which we placed 2 light sensors within the chest cavity (at different depths), I determined the laser characteristics for reproducible light delivery in the chest . We ensured of the homogeneous distribution of the laser inside the cavity. In addition, a third probe was placed at the surface of the chest to evaluate the loss of light due to the thoracic wall, (Fig. 6.2B). For each animal, the height of the laser required to reach the targeted dose inside the chest was recorded. After 11 animals, the graph showed in Fig. 6.2C was drawn and we conclude that a height of 4.35 cm was satisfying our conditions (irradiance of 50 mW/cm2, total light dose of 10J/cm2) with a low variability between animals. Each animal was terminally anesthetized at the end of the experiment.

A

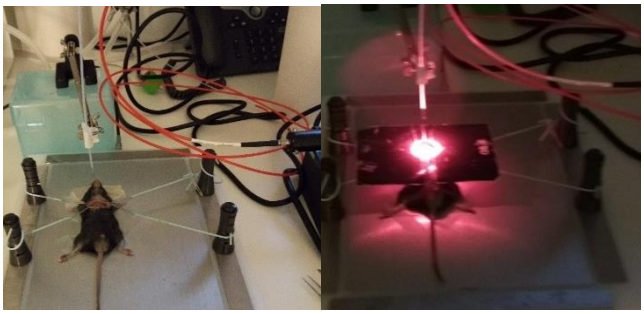

B

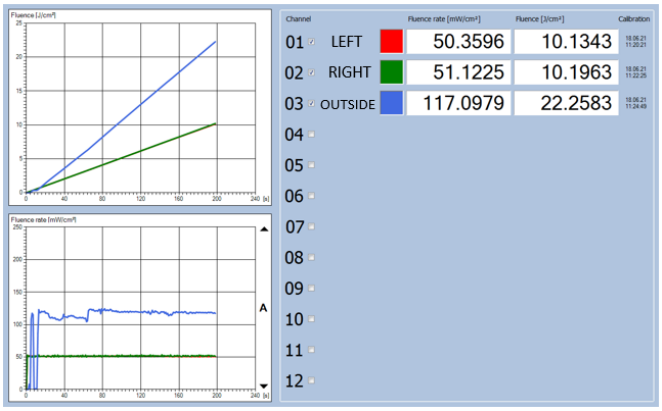


Over the chest Inside the chest - Left Inside the chest - Right

C

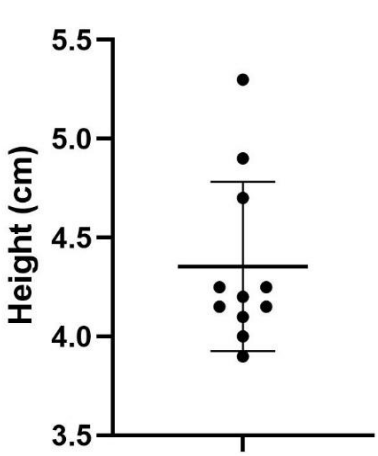

**Fig. 6.2: Development of an orthotopic MPM model for transthoracic L-PDT** : A) Illustrative image of orthotopically delivered L-PDT in thoracic cavity. Chest cavity remained close during the procedure. B) Representative quantification of the fluence (top curves) and fluence rates (bottom curves) measured to establish the conditions for the L-PDT in vivo model. 2 probes were placed into the animal (right and left chest) and 1 at the top of the rib cage. C) Quantification of the laser height required to deliver 50 mW/cm$^2$ through the chest, n=11 animals.

In parallel, we also developed a mouse thoracic window model to be able to treat with L-PDT and also image using two photon laser scanning imaging methods.

Intravital imaging (IVM) allow the live observation of biological events in living tissue. In the context of tumors, IVM can track the events regulating the progression of cancer from local establishment to metastasis dissemination. With the growing interest of investigating the TME, IVM plays a role in interrogating the immune regulation taking place in the microenvironment of the tumors, (136, 137). Different models of window have been described to image various organs and their disease in mice such as brain or skin, (139, 140). Recently, Condeelis group described a surgical protocol to implant a thoracic window, (141). The group used this model to investigate breast metastasis development in the lung.

The window I helped to develop consists in a titanium frame implanted in the rib cage of the animal that allows, through a coverslip, the intravital imaging of the underlying tissue/tumor. Sabrina Cavin and I adapted the protocol from the previous study from Condeelis group (141) and established a new window model (more stable and more practical under the microscope). We brought modifications to the original window frame in order to fit the two-photons available in the facility. We also engineered a solution to reduce the breathing artefact of the animal during the imaging. All these modifications required to establish a new surgical protocol. This was done successfully with the ability to keep mice alive for more than 6 weeks and image the lung under the window during this period. This model is now being used in the project of Damien Marie who investigate the TME of lung cancer with it. Results of his study are planned to be part of a peer-reviewed article and will include our thoracic window model.

*Surgical protocol for the implantation of a chronic thoracic window*

The main challenge for the surgery was to perform an air sealed implantation of the window in the chest cage of the animal through a limited invasive approach to allow a good recovery and a long imaging time period. C57BL/6 mice were anesthetized using a mix of Ketamine-Xylazine at a dose of 100 mg/kg. Due to the unique thoracic cavity in mice, the animals were intubated using a BD Venflon catheter after exposure of the trachea. The mice is then placed on the left lateral side. An incision is performed 1cm above costal edge and 1cm away from the median line of the sternum. After dissection of the fat and the muscular plane, chest wall is exposed and ribs 2 to 6 are resected in a circular way. A purse string suture was performed surrounding the chest opening. The frame was inserted, and lungs recruited before closing the pleural cavity by placing the glass coverslip. A second purse string suture was performed to adapt the skin inside the groove of the titanium frame. Animals were then extubated and monitored until the animal had fully recovered. Oral antibiotics (10mL of Bactrim 200/40mg in 250mL of water) was administered until the end of the experiment. The analgesia was insured by subcutaneous (0.1mg/kg) Temgesic injections twice a day for 3 days and oral Temgesic (0.3mg/mL) and Dafalgan (1mg/mL) for 7 days.

*Intravital imaging and correction of the breathing artefact*

Animals generally fully recover from their surgery after a couple of hours but their mobility and feeding are completely normal by the 4$^{th}$ postoperative day. (Fig 7A). IVM was performed using a two-photon microscope. To avoid breathing artefacts, we developed two solutions: first, we used a stabilizing plate fitting the window groove (Fig. 7B). The chest was slightly elevated with this maneuver and made the window more independent of the rib cage movement

Second, we set an electronic pad under the animal that gated the laser scanner imaging at fixed timepoints of the respiratory cycle thus improving significantly the imaging quality. To investigate the MPM microenvironment in real time, we used Rhodamine 6-G (R6G) and Pacific blue dextran to label the circulating leucocytes (in red) and the vessels (in blue) respectively. We manage to clearly observe vessels and circulating leucocytes inside the healthy lung tissue, (Fig. 7C). The next step was to develop a tumor model expressing a green fluorescent protein (GFP) to image in real time the tumor with its vessels and its immune infiltration. However, we were never able to have a reproducible MPM mouse model with or without GFP expression within the timeframe of our thoracic window. We did, however, manage to obtain a reproducible lung cancer model in the thoracic window model. Therefore, in a second project led by my colleague Damien Marie, we are now investigating the TME of lung cancer using this intravital imaging model.

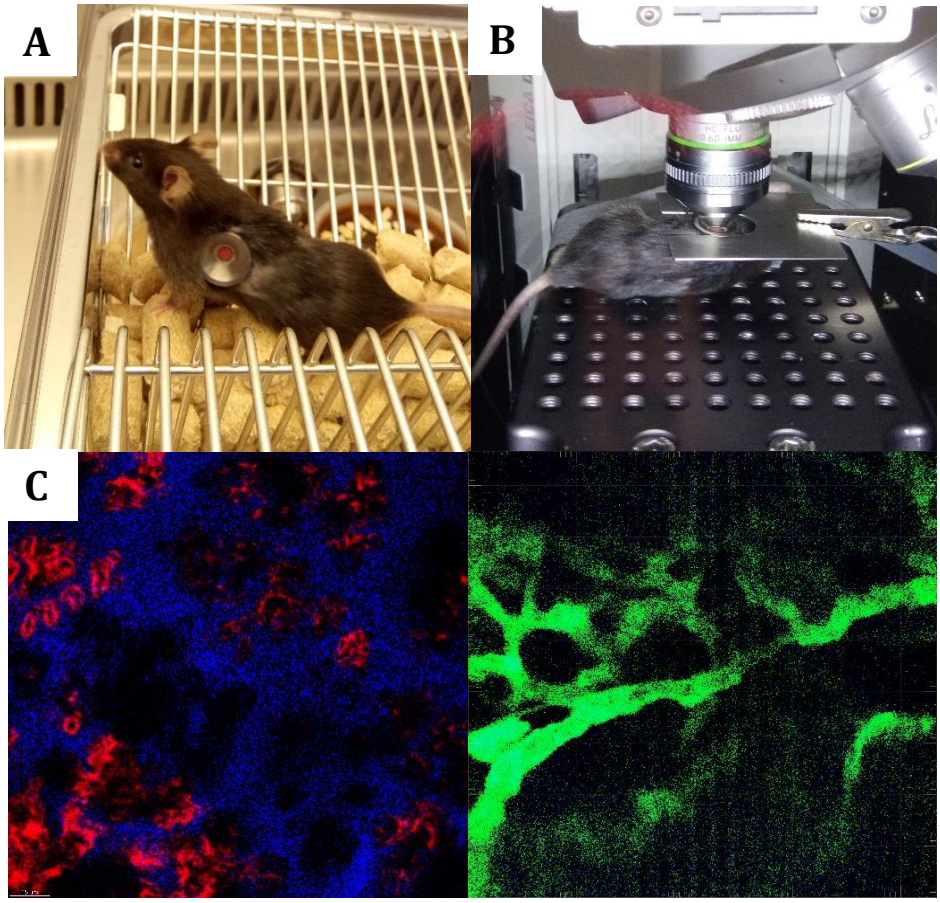


**Fig. 7: Model of intravital imaging through a thoracic window:** a) C57BL/6 mice implanted with the chronic thoracic window. Surgery protocol is well established and provides a survival rate of more than 80%. Mice can be kept alive with a functional window up to 6 weeks. B) Set-up under 2-photons microscope with the x16 immersion lens. A stabilizing plate is used to compensate for breathing movement shifts. C) *Left:* Live image at x16 magnification of healthy lung using the window. Circulating leucocytes are marked in red with Rhodamine 6G and vessels in blue with Pacific-Blue Dextran. *Right:* Vessels of healthy lung stained with FITC-Dextran.

**Low dose photodynamic therapy promotes vascular endothelial E-Selectin via NF-κB**

To understand the TME remodeling provided by L-PDT, we sought to understand how L-PDT could induce E-Selectin as observed in our previous publication. We first used an in vitro model in which EC-RF24 endothelial cells are cultured and can be treated by L-PDT. We first determined the kinetics of E-Selectin expression in EC-RF24 (Fig. 8.1 A). We found that L-PDT caused a peak of E-Selectin expression at 9 hours which remained elevated up to 24 hours following therapy (Fig. 8.1 B-D). Because the NF-κB transcription factor was shown to be involved in the regulation of E-Selectin (142), we monitored IκBα phosphorylation, a key mediator in the NF-κB canonical pathway activation. IκBα phosphorylation occurred between three- and twenty-four-hours following L-PDT in vitro, as determined by western blot analysis (Fig. 8.1 B-C).

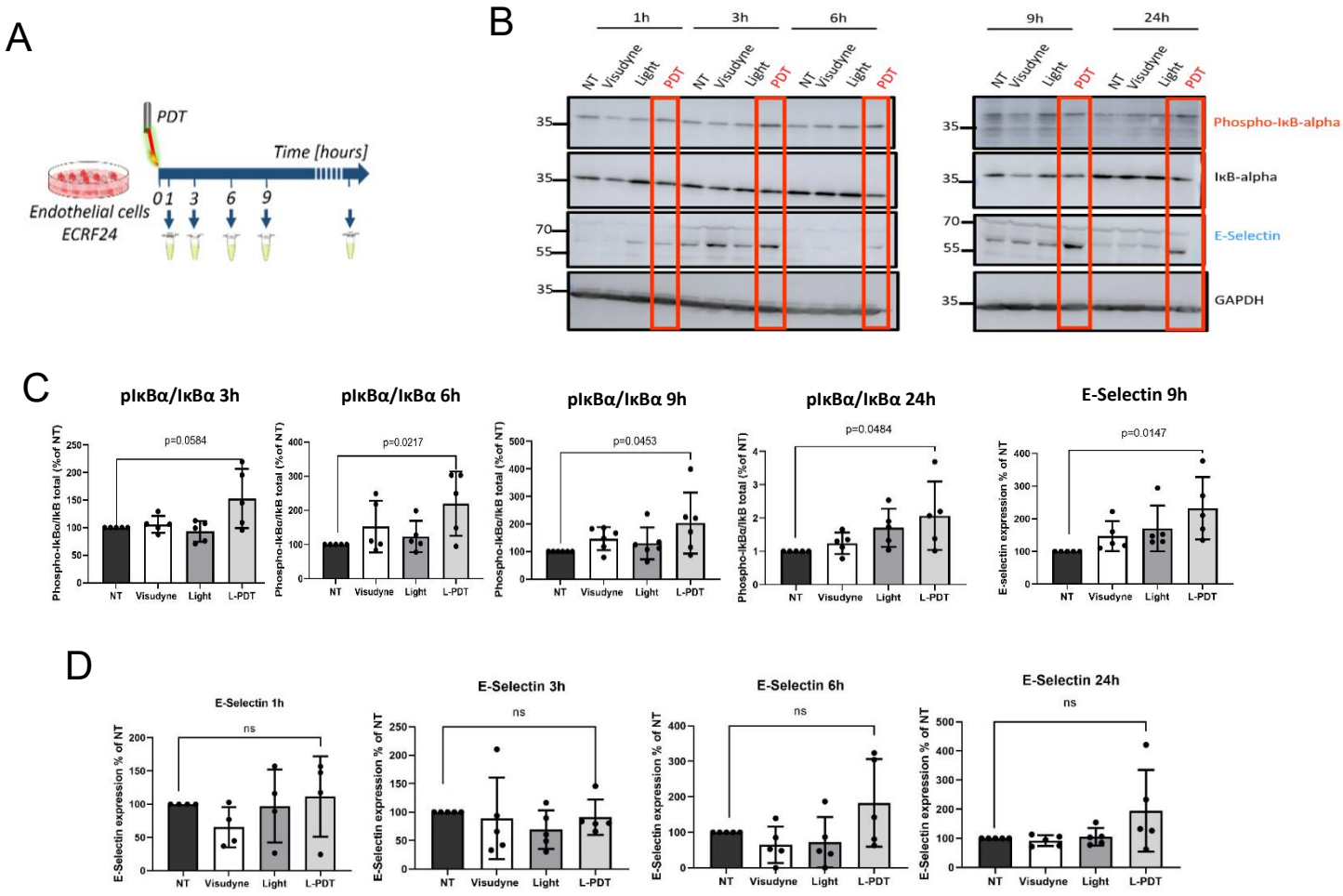

**Fig. 8.1: E-Selectin expression following L-PDT is mediated by the NF-κB pathway** A) Schematic representation of in vitro experiments: ECRF-24 cells were treated by L-PDT and protein lysate was collected at 1h, 3h, 6h, 9h and 24h after treatment. B) Western blot analysis of lysates from not treated (NT) ECRF-24 cells or treated with Visudyne (50ng/mL), Light (0.15 J/cm$^2$) or L-PDT for the indicated time using anti-phospho-Iκα, anti-total IκBα, anti-E-selectin and anti-GAPDH antibodies with densitometric quantification of 5 experiments (C). All values were normalized to the amount of GAPDH. D) Additional timepoints of E-Selectin expression after treatment in EC-RF24 endothelial cells. Timepoints were replicated between n=4 to n=6.. * : p< 0.05, ** : p<0.01, ***: p<0.001, ****: p< 0.0001. One-Way ANOVA tests were used. p-value under 0.05 are considered as significant.

To confirm a role for canonical NF-κB pathway in E-Selectin induction following L-PDT, we used two different siRNAs to silence NEMO (IKKγ). We observed a silencing of 48% for siRNA 1, 65% for siRNA 2 and 2% for control siRNA (Fig. 8.2 A). Using EC-RF24 cells transfected with each NEMO siRNA construct, we found that E-selectin upregulation following L-PDT was abrogated (mean expression of 0.98 for L-PDT with control siRNA vs 0.37 (p=0.0079) and 0.41 (p=0.0076) for L-PDT with siRNA 1 or 2 respectively, Fig. 8.2 B-C).

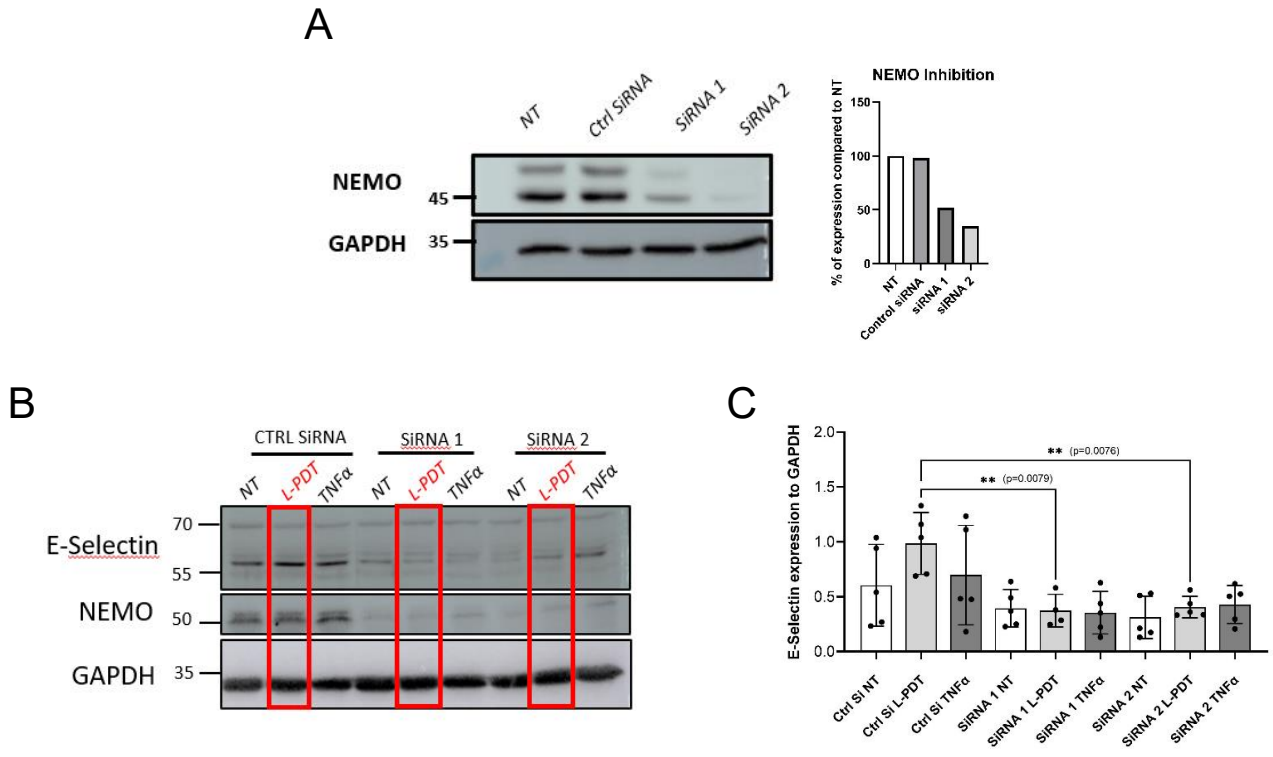


**Fig. 8.2: E-Selectin expression following L-PDT is mediated by the NF-κB pathway** A) Representative western blot of NEMO inhibition in presence of Si RNA in EC-RF24 cells. Percentage of silencing were obtained comparing intensity of NT signal with intensity from other siRNA signals. Quantification on the right. B) Western blot analysis of lysates from not treated (NT) ECRF-24 cells or treated with Visudyne (50ng/mL), Light (0.15 J/cm$^2$), L-PDT or TNFα 20ng/ml for 6h for the indicated time using anti-NEMO, anti-E-selectin and anti-GAPDH antibodies with densitometric quantification of 5 experiments (C). * : p< 0.05, ** : p<0.01, ***: p<0.001, ****: p< 0.0001. One-Way ANOVA tests were used. p-value under 0.05 are considered as significant.

We validated these findings by the monitoring of E-Selectin expression with immunofluorescence staining on wild EC-RF24 compared to EC-RF24 cells transfected with NEMO siRNAs, (Fig. 8.3 A-F). Thus E-Selectin induced L-PDT relies on canonical NF-κB signaling. We next aimed to extend these findings in vivo.

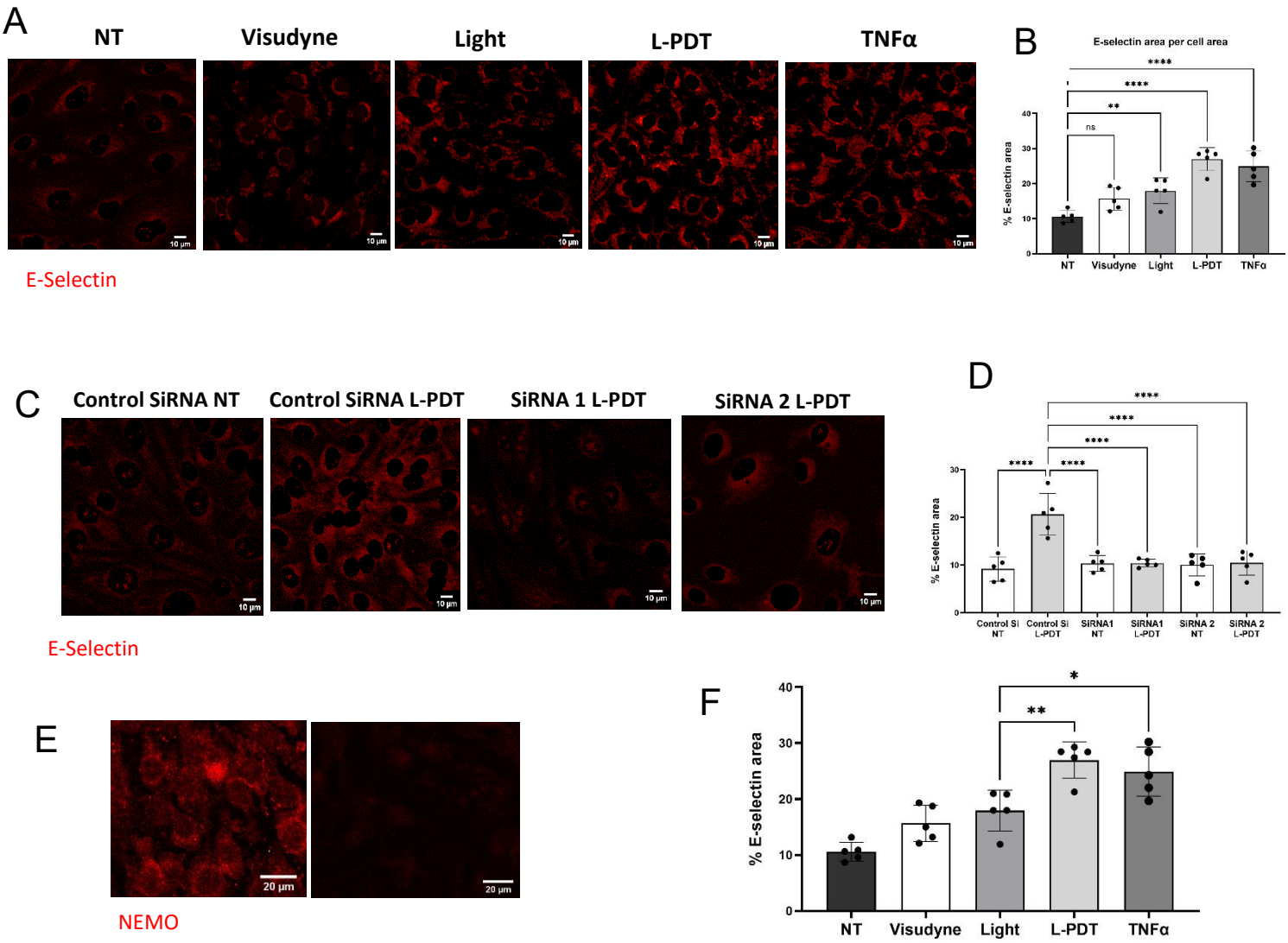


**Fig. 8.3: E-Selectin expression following L-PDT is mediated by the NF-κB pathway** A) Representative images of immunofluorescence staining of ECRF-24 cells treated with Visudyne (50ng/mL), Light (0.15 J/cm$^2$), L-PDT or TNFα 20ng/ml for 6h with quantification of 5 experiments (B); E-selectin appears in red. C) Representative images of immunofluorescence staining of ECRF-24 cells treated or not with L-PDT in presence of NEMO siRNA with quantification of 5 experiments (D). E) Representative image of NEMO inhibition between untreated and siRNA 2 cells. F) Quantification of expression of E-selectin in ECRF-24 cells treated by light, L-PDT or TNFα investigated by immunofluorescence. * : p< 0.05, ** : p<0.01, ***: p<0.001, ****: p< 0.0001. One-Way ANOVA tests were used. p-value under 0.05 are considered as significant.

We then used our orthotopic MPM model to validate our in vitro findings. We assessed the role of the NF-κB pathway in the upregulation of endothelial E-Selectin following L-PDT in vivo. For this, we disrupted the formation of the IKK complex using a NEMO binding domain (NBD) peptide that prevents the formation of the IKK complex and inhibits canonical NF-κB activation (Fig. 9A); as control a non-binding peptide was used (133). We found that while L-PDT caused a significant increase in endothelial E-Selectin compared to untreated control (NT), the presence of the NBD totally prevented this, ($p<0.05$ compared to L-PDT group, Fig. 9 C-D). Interestingly, this phenotype was also observed for other trans-endothelial adhesion molecules such as ICAM-1 and VCAM-1, which were upregulated with L-PDT but remained similar to NT in the presence of NBD (Fig. 9 C-D). In contrast, the non-binding peptide did not impact L-PDT-mediated adhesion molecule induction. There was no difference in MPM vessel density in the presence or absence of the NBD peptide assessed by the VE-Cadherin expression levels (Fig. 9B).

Given the essential role of adhesion molecules for the recruitment of immune cells, we next investigated how NBD affected the tumor immune microenvironment. We found that the infiltration of CD8+ T cells following L-PDT in MPM was impaired in response to the NBD but not to the control peptide ($p<0.001$ compared to L-PDT group and $p<0.0001$ compared to L-PDT + Control peptide group, Fig. 9 E-F). Finally, granzyme B expression by intra-tumoral CD8 T cells was induced in response to L-PDT and prevented upon NBD peptide co-administration (Fig. 9 E-F). This suggests a critical role for NF-κB mediated E-Selectin induction following L-PDT to mount CD8+ T cell response.


A
NBD L-PDT
D0 D1
MPM cell implantation
immuno-fluorescence
B
VE-Cadherin Area
% of Tumor Area
ns
NT (n=6)
L-PDT (n=6)
L-PDT +NBD (n=7)
L-PDT + Control (n=4)

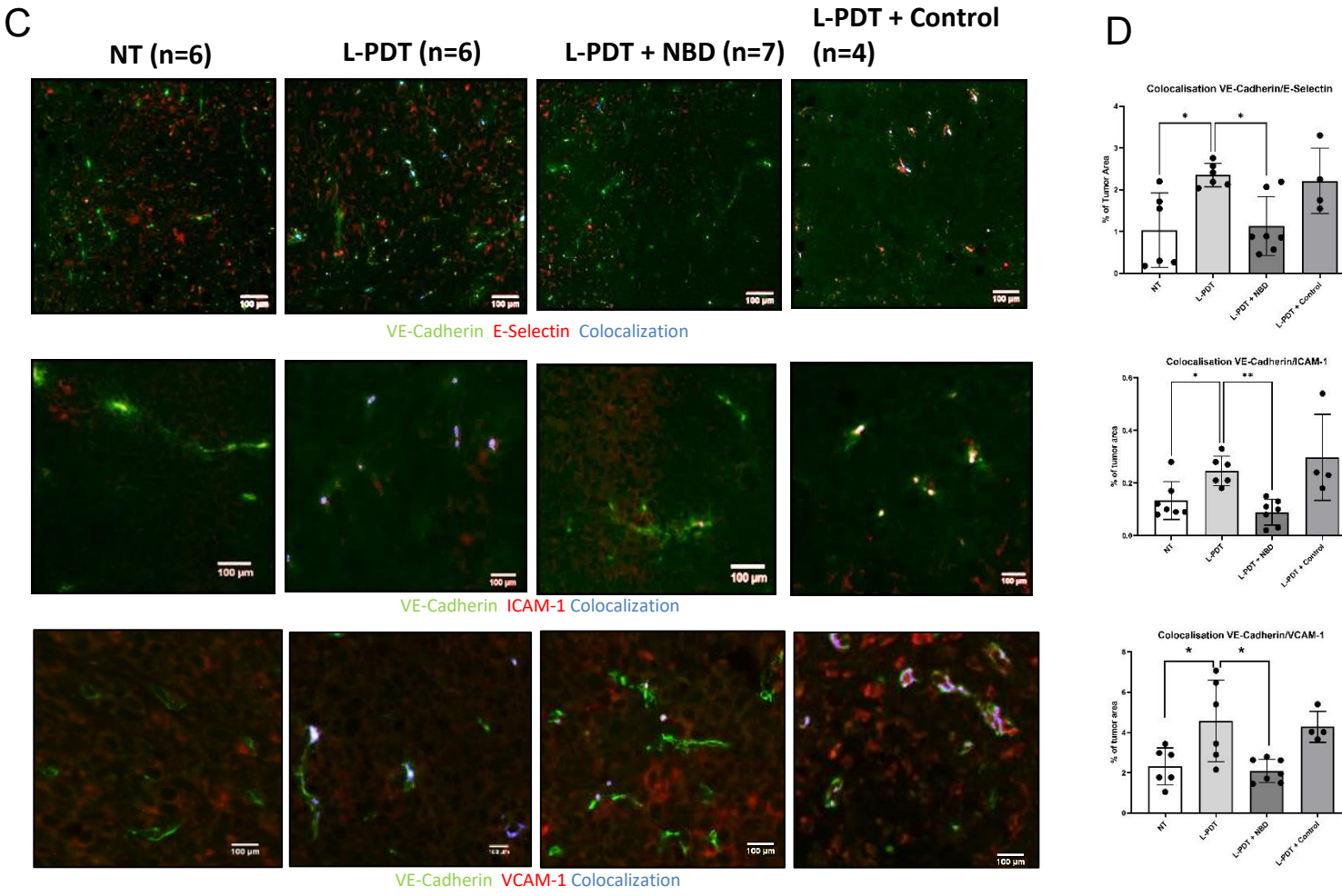
C
NT (n=6)
L-PDT (n=6)
L-PDT + NBD (n=7)
L-PDT + Control (n=4)
VE-Cadherin E-Selectin Colocalization
VE-Cadherin ICAM-1 Colocalization
VE-Cadherin VCAM-1 Colocalization
100 µm
D
Colocalisation VE-Cadherin/E-Selectin
Colocalisation VE-Cadherin/ICAM-1
Colocalisation VE-Cadherin/VCAM-1
% of Tumor Area
% of tumor area
NT
L-PDT
L-PDT + NBD
L-PDT + Control

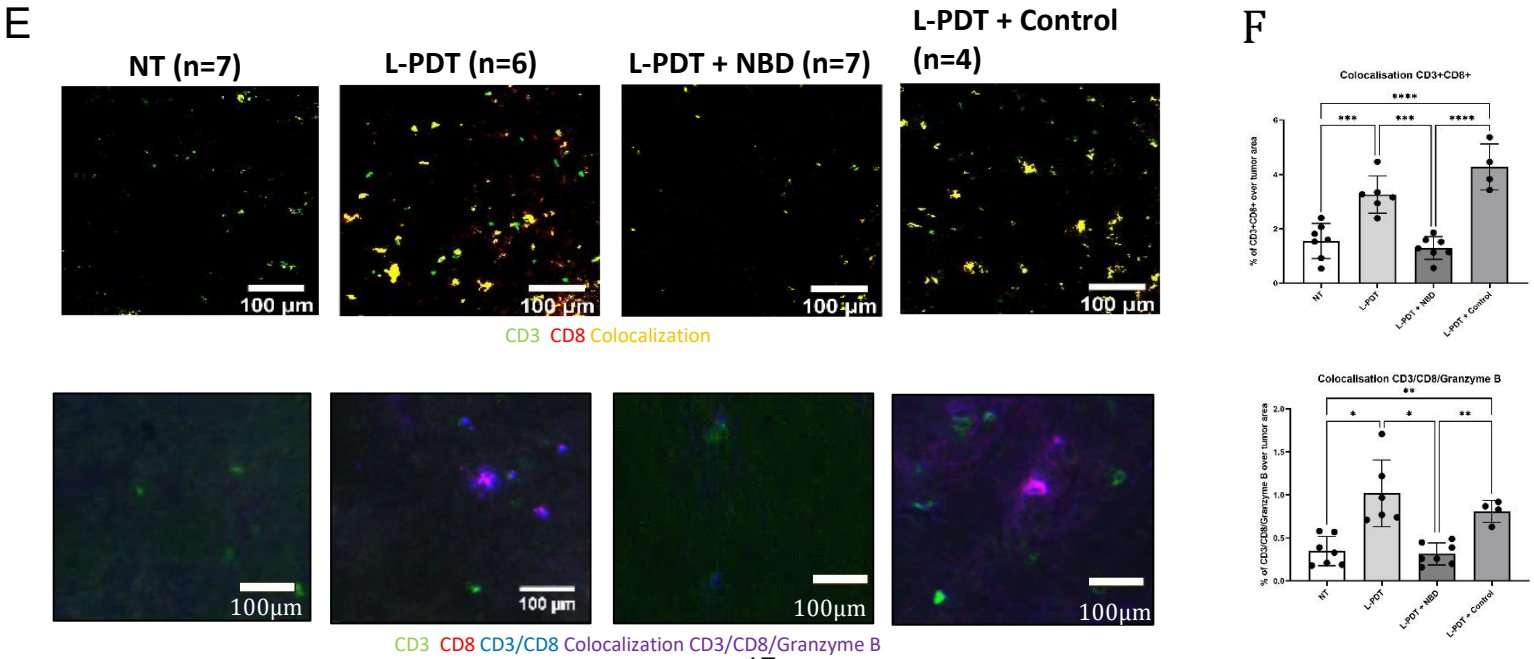
E
NT (n=7)
L-PDT (n=6)
L-PDT + NBD (n=7)
L-PDT + Control (n=4)
CD3 CD8 Colocalization
CD3 CD8 CD3/CD8 Colocalization CD3/CD8/Granzyme B
100 µm
100µm
F
Colocalisation CD3+CD8+
% of CD3+CD8+ over tumor area
Colocalisation CD3/CD8/Granzyme B
% of CD3/CD8/Granzyme B over tumor area
NT
L-PDT
L-PDT + NBD
L-PDT + Control

**Fig. 9: Peptide-based inhibition of IκB kinase (IKK) complex formation in vivo abrogates the expression of tumor endothelial E-Selectin following L-PDT in MPM**. A) Schematic representation of NF-kB pathway blockade experiment in MPM tumor bearing mice treated with L-PDT. B) Quantification of expression of VE-Cadherin in orthotopic MPM tumor. C) Illustrative images of E-Selectin, ICAM-1, VCAM-1 (in red), VE-Cadherin (in green) expression in MPM tumors. Colocalization appears in blue. D) Quantification of colocalization area of VE-Cadherin and E-Selectin E-Selectin, ICAM-1 or VCAM-1 over tumor area in immunofluorescence staining of MPM tumors, n=26. E) Illustrative images of CD3+ (in green) and CD8+ cells (in red) (top) and CD3+ CD8+ Granzyme B (in purple, bottom) in MPM tumor by immunofluorescence staining. Colocalization between CD3+ and CD8+ appears in blue. F) Quantification of CD3+ CD8+ T cells (top) and CD3+ CD8+ Granzyme B+ cells (bottom) over tumor area by immunofluorescence, n=24. NBD: NEMO Binding domain peptide. * : p< 0.05, ** : p<0.01, ***: p<0.001, ****: p< 0.0001, One-Way ANOVA tests were used. p-value under 0.05 are considered as significant. D: Day

## E-Selectin is essential for immune infiltration of L-PDT treated MPM

Finally, we validated the contribution of E-Selectin to the immune recruitment induced by L-PDT. We applied L-PDT in the orthotopic MPM syngeneic mouse model and assessed the impact of E-Selectin inhibition with an antibody, injected 30 minutes before L-PDT, on immune cell recruitment (Fig. 10A). At 24 hours, the abundance of tumor infiltrating T-cells was assessed by immunofluorescence (Fig 10B). We observed a significant recruitment of CD3+/CD8+ and of CD3+/CD4+ T cells in the tumor bed following L-PDT, which returned to control levels upon E-Selectin inhibition (Fig 10B-E). Interestingly, L-PDT with or without E-Selectin blockade did not affect overall tumor vessel density assessed by the quantification of VE-Cadherin (Fig. 10 F). To further investigate the remodeling provided by L-PDT, we looked at longer timepoints after treatment: At 7 days, the recruitment of CD3+ and CD3+/CD8+ cells was significantly enhanced in L-PDT treated tumors compared to control tumors as determined by flow cytometry, while overall CD45+ content was comparable between groups (Fig. 10G-J).

A

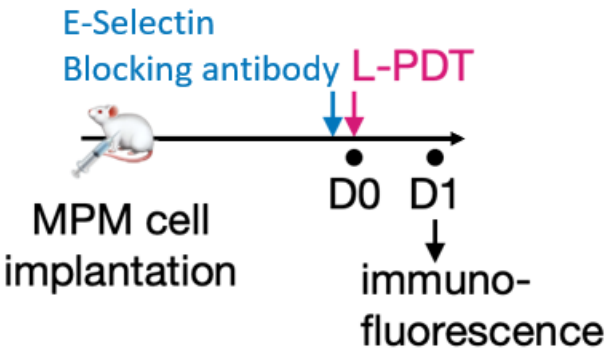
E-Selectin
Blocking antibody
L-PDT
D0
D1
MPM cell implantation
immuno-fluorescence

B

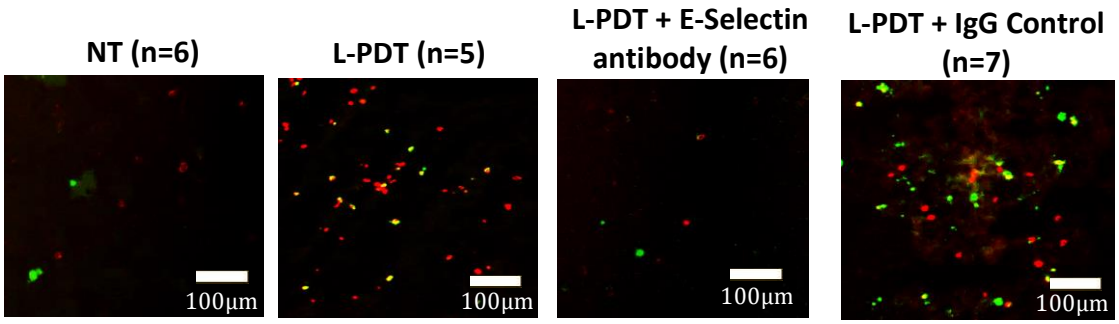
NT (n=6)
L-PDT (n=5)
L-PDT + E-Selectin antibody (n=6)
L-PDT + IgG Control (n=7)
100µm
CD3 CD8 Colocalization

C

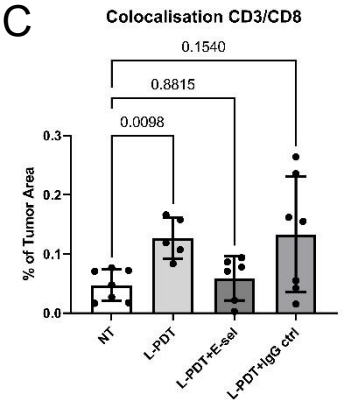
Colocalisation CD3/CD8
0.1540
0.8815
0.0098
% of Tumor Area
NT
L-PDT
L-PDT+E-sel
L-PDT+IgG ctrl

D

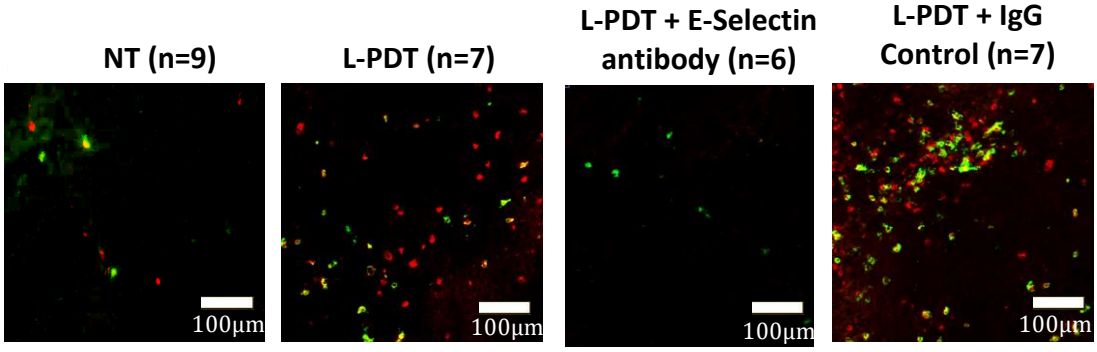
NT (n=9)
L-PDT (n=7)
L-PDT + E-Selectin antibody (n=6)
L-PDT + IgG Control (n=7)
100µm
CD3 CD4 Colocalization

E

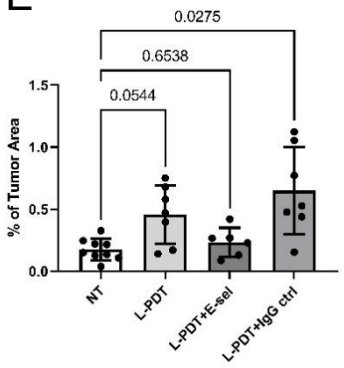
0.0275
0.6538
0.0544
% of Tumor Area
NT
L-PDT
L-PDT+E-sel
L-PDT+IgG ctrl

F

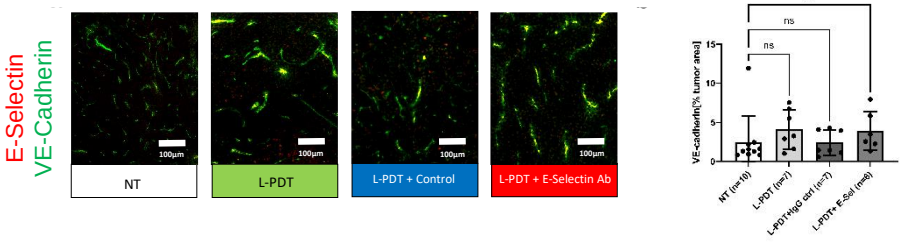
E-Selectin
VE-Cadherin
NT
L-PDT
L-PDT + Control
L-PDT + E-Selectin Ab
ns

G

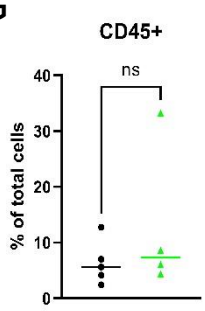
CD45+
ns
% of total cells

H

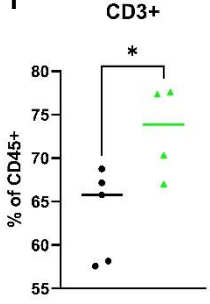
CD3+
*
% of CD45+

I

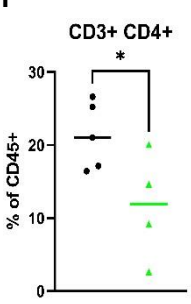
CD3+ CD4+
*
% of CD45+

J

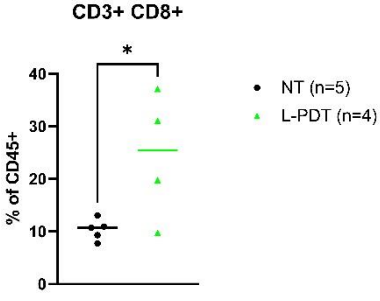
CD3+ CD8+
*
% of CD45+
NT (n=5)
L-PDT (n=4)

**Fig. 10: Low dose photodynamic therapy promotes T lymphocyte infiltration through vascular endothelial E-Selectin.** A) Schematic representation of the experiment inhibiting E-Selectin in MPM tumor bearing mice treated with L-PDT. B) Illustrative image of CD3+ CD8+ cells infiltrating MPM. CD3, CD8 and their colocalization appear respectively in green, red and yellow. C) Quantification of area of CD3+ CD8+ colocalization over tumor area, n=24. D) Illustrative image of CD3+ CD4+ cells infiltrating MPM. CD3, CD4 and their colocalization appearing respectively in green, red and yellow. E) Quantification of area of CD3+ CD4+ colocalization over tumor area, n=29. F) Representative images of E-selectin and VE-Cadherin inside MPM tumors and quantification. Flow cytometry (n=9) of G) CD45+ cells among total cells, H) CD3+ cells among CD45+ cells, I) CD3+ CD4+ cells among CD45+ cells and J) CD3+ CD8+ cells among CD45+ cells from MPM bearing mice treated or not with L-PDT. * : $p< 0.05$. One-Way ANOVA tests or two-tailed unpaired t-tests were used accordingly. p-value under 0.05 are considered as significant. D: Day

## 7.2 Induction of vascular E-Selectin and CD8+ T-cells infiltration are mandatory for the MPM control provided by L-PDT

### E-Selectin and CD8+ T-Cells are essential for tumor control following low-dose photodynamic therapy

Given the importance of CD8+ T-cells in controlling tumor development, we next investigated the impact of E-Selectin inhibition following L-PDT on MPM control. For this purpose, we monitored the tumor response to L-PDT with or without long-term E-selectin inhibition (Fig. 11.1 A). Tumor growth was significantly decreased with L-PDT + IgG compared to untreated conditions (mean reduction in tumor size by 89.8%+/-35.3, p=0.0249, Fig. 11.1 B-C,) and translated into a survival advantage (mean survival of 8 days in L-PDT compared to 6.5 days in controls, p=0.0195, Hazard Ratio 0.08, 95% Confidence Interval (CI) 0.009752 - 0.6708, Fig. 11.1 D). Interestingly, in the presence of an E-Selectin blocking antibody, tumor growth was comparable to control and the survival advantage of L-PDT was lost (Fig. 11.1 D).

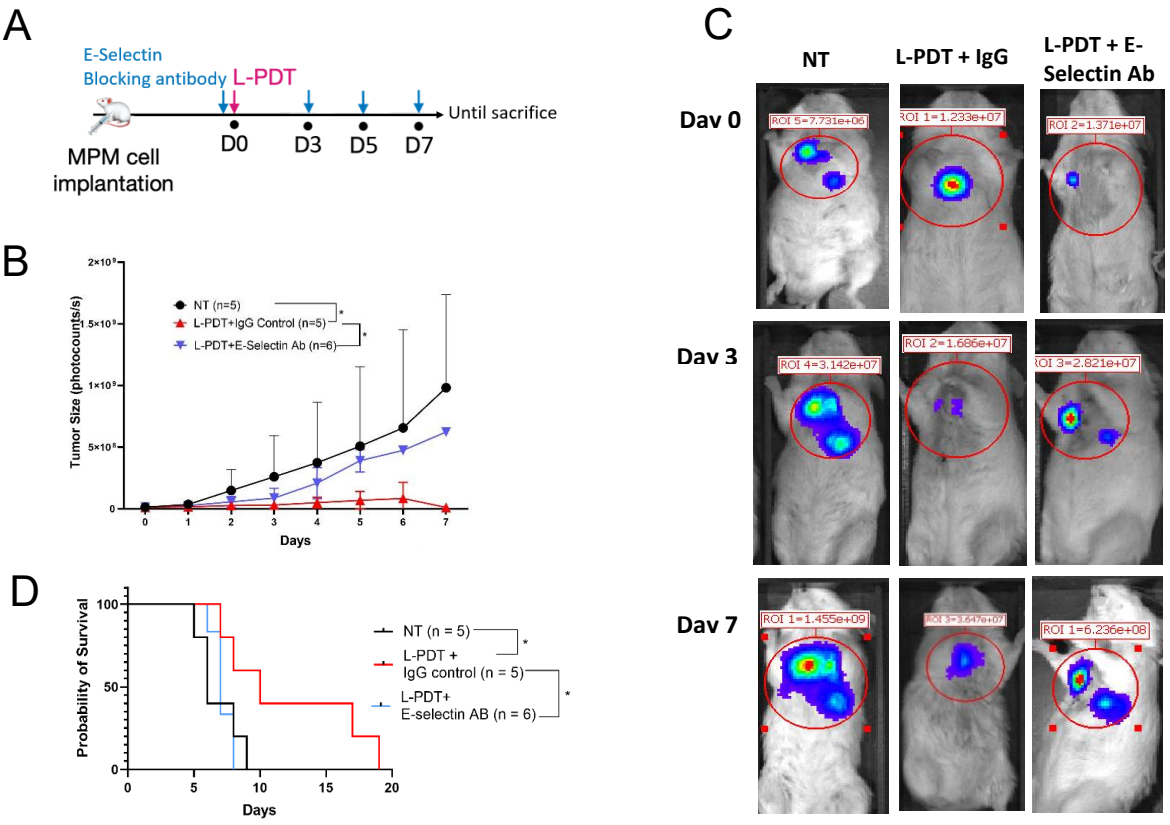

**Fig. 11.1: E-Selectin is essential for tumor control following low-dose photodynamic therapy.** A) Schematic representation of the experiment inhibiting E-Selectin in MPM tumor bearing mice treated with L-PDT. B) Tumor growth curve observed by IVIS in photocount per second of untreated animals (n=5) or treated with L-PDT with IgG control (n=5) or L-PDT with E-Selectin inhibition (n=6). Two-tailed unpaired t-test was used as statistical test. C) Representative images of tumor growth followed by bioluminescence among treatment groups at day 0, day 3 and day 7 after treatment. D) Kaplan-Meier analysis of the survival between animals included in the tumor growth assessment. * : p< 0.05, ** : p<0.01. p-value under 0.05 are considered as significant. D: Day

Given the L-PDT correlated with enhanced CD8+ T lymphocyte infiltration, we next determined the contribution of these immune in the observed phenotype. We depleted CD8+ T-cells in mice using an anti-CD8 antibody injection. Tumor bearing mice were then treated with L-PDT. Tumor control following L-PDT was abrogated in the presence of the anti-CD8 antibody, with tumor volumes and animal survivals comparable to the untreated group (6.4 x107 p/sec/cm2/sr in L-PDT with IgG Control vs 3.4x108 p/sec/cm2/sr in L-PDT with anti-CD8, p=0.0149 and median survival of 8 days in L-PDT with IgG Control vs 7 days in L-PDT with anti-CD8, Hazard Ratio: 0.09, 95% CI 0.01370 - 0.5411, p= 0.083) (Fig. 11.2 A-B). CD8+ T cell depletion did not affect the overall amount of VE-Cadherin, (Fig. 11.2 C) suggesting a stable vascular density in the MPM tumors. Together, these results indicate a central role for E-selectin and CD8+ T-cells in mediating the L-PDT efficacy.

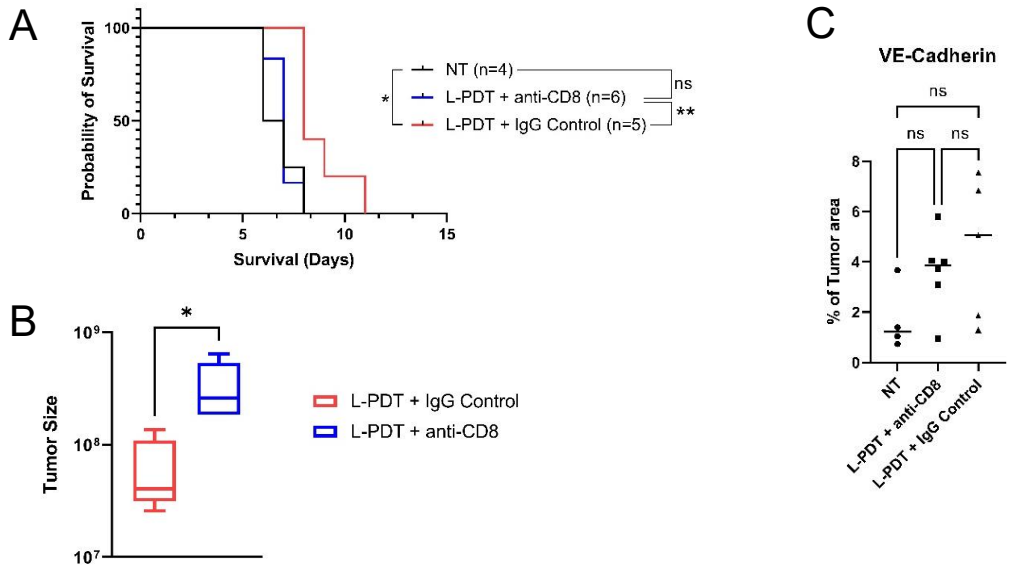


**Fig. 11.2: E-Selectin is essential for tumor control following low-dose photodynamic therapy.** A) Kaplan-Meier analysis of the survival between animals depleted or not in CD8+ population and treated with L-PDT or untreated, (n=15). B) Tumor size comparison at median survival between CD8+ depleted and non-depleted animals using two-tailed unpaired t-test, (n=11). C) Quantification of immunofluorescence investigating the expression of VE-Cadherin (on the left) and vascular E-Selectin (on the right) in untreated mice (NT) or mice treated with L-PDT following or not CD8+ depletion. * : p< 0.05, ** : p<0.01. p-value under 0.05 are considered as significant. D: Day

## 7.3 Clinical prognosis of endothelial E-Selectin expression and impact on CD8+ T-cell infiltration in MPM patient samples

### Vascular E-Selectin expression is associated with better survival in malignant pleural mesothelioma patients

In order to investigate the impact of vascular E-Selectin on the survival of MPM patients, we analyzed a large number of tumor tissues from 82 patients with a total of 105 samples when including pre- and post-treatment samples. The majority of these patients had received chemotherapy exclusively or in combination with surgery and/or radiation therapy. Among these patients, 54 tumors presented an epithelioid histology, 21 a biphasic and 7 were sarcomatoid. In this cohort, 21 patients underwent surgical resection and similar chemotherapy regimens with matched pre- (initial biopsy) and post-treatment (surgical specimen) samples. We first compared tumors with an increased in E-Selectin post treatment (n=13) compared to sample with decreased or stable E-Selectin expression (n=8) (Fig. 12.1 A). Patients with higher tumor associated vascular E-Selectin presented a better survival compared to patients with lower levels, (median survival: 24 months versus 8 months, p=0.0027, Fig. 12.1 B). This change was significant in patients with epithelioid tumors (median survival: 24 months versus 9 months, p=0.0007, Fig. 12.1 C). In the biphasic and sarcomatoid subgroups, no survival analysis could be obtained because of sample underrepresentation in this surgical cohort. The median expression of vascular E-Selectin across all subtypes was 2.18%. Patients with an E-Selectin expression higher than the median had significant better survival compared to patients with lower than median expression. This observation was found when pooling all histologies and when considering epithelioid tumors, (Fig. 12.1 D-E). However, no difference was found in biphasic or sarcomatoid tumor group, (Fig. 12.1 F). Finally, VE-Cadherin and non-vascular E-selectin expression had no impact on survival across different histologies (Fig. 12.1 G-H).

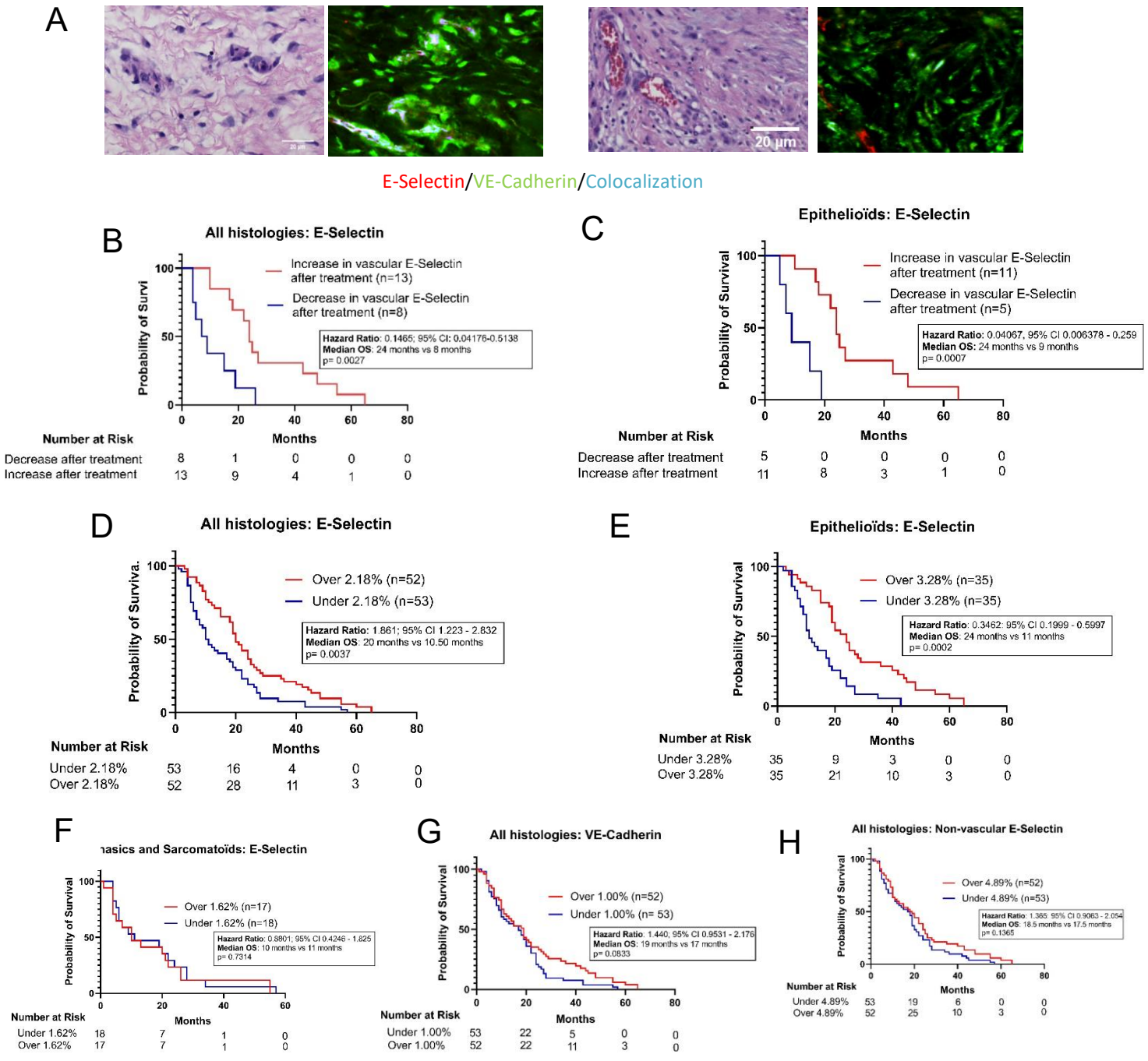


**Fig. 12.1: Vascular E-Selectin expression is associated with better survival in malignant pleural mesothelioma patients** A) Representative images of vascular E-Selectin and VE-cadherin expression with colocalization signal in blue and respective Hematoxylin/Eosin coloration. Image on the left shows a tumor with high vascular E-Selectin expression while image on the right correspond to a tumor with low expression. Kaplan Meier analysis between patients presenting an increase (red) or a decrease (blue) in vascular E-Selectin expression after treatment including B) all histologies, C) only including epithelioïd tumors. Kaplan Meier analysis associating vascular E-Selectin to survival in months in: D) MPM patients of the cohort independently of histology subtype; E) only epithelioïdes patient. Survival curves associating survival with respectively F) E-Selectin in biphasic and sarcomatoïd patients, G) VE-Cadherin across all histologies, H) non-vascular E-Selectin in all histologies. Cut-off was determined as the median of the value of interest. p-value under 0.05 are considered as significant.

We next investigated lymphocyte infiltration in these samples (Fig. 12.2 A). Neoadjuvant treatment increased infiltration in CD8+ T cells in 10 patients and remained the same or decreased in 9 patients. Patients with a CD8+ T-cell infiltration higher than the median exhibited a better survival compared to patients with lower values (median survival of 19.5 months versus 11 months, p=0.0056), (Fig. 12.2 B). This was also observed when separating epithelioid from biphasic and sarcomatoid tumors, (Fig 12.2 C-D). We did not find a survival difference between patients with higher or lower CD8+ infiltration after treatment, (12.2 E). Additionally, in the patients with CD3/CD8+ lymphocyte infiltration above the median, we found a positive correlation between recruited CD3/CD8 lymphocytes and vascular E-Selectin expression (Fig. 12.2 F). Altogether, our findings show a correlation between vascular E-Selectin expression and CD3/CD8+ lymphocyte recruitment and patient outcome.

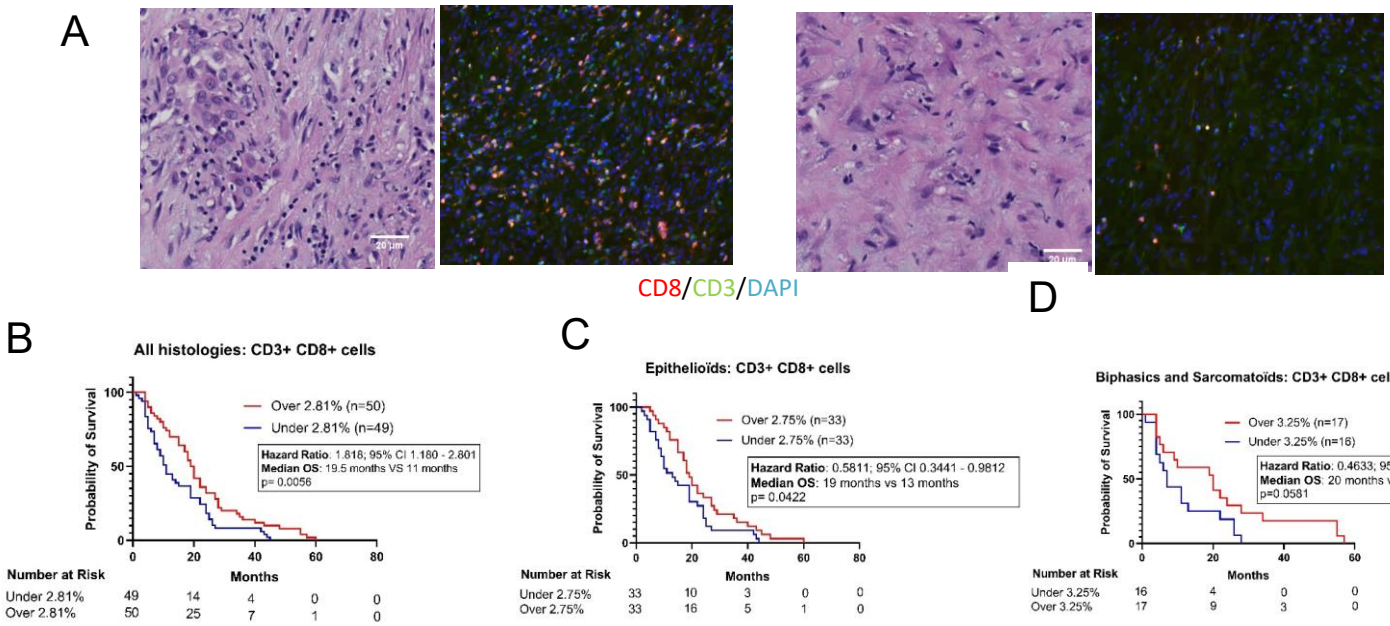

**Fig. 12.2: Vascular E-Selectin expression is associated with better survival in malignant pleural mesothelioma patients** . A) Representative images of CD3+ CD8+ expression with respective Hematoxylin/Eosin coloration. Image on the left shows a tumor with high CD8 infiltration while image on the right correspond to a tumor with low infiltration. Kaplan Meier analysis between patients with high and low infiltration of CD3/CD8 cells across B) all histologies or C) among epithelioid tumors only or D) biphasic and sarcomatoïd tumors only. Cut-off was determined as the median of the value of interest. E) Survival curves between patients presenting post-treatment higher or lower values of CD3+/CD8+ cells. F) Pearson correlation between vascular E-Selectin and CD3/CD8 cells in patient with above the median CD3+ CD8+ cells infiltration. p-value under 0.05 are considered as significant.

# 8. Discussion

During my MD-PhD thesis, I investigated how L-PDT could remodel the TME and the immune infiltration of a MPM murine model. More specifically, I investigated how L-PDT affected the tumor vasculature and adhesion molecule expression within MPM and how this affected the immune infiltration and tumor control. I established a mechanism involving NF-κB induced E-selectin expression favoring CD8+ T cell infiltration leading to immune mediated tumor control. Each element was necessary and sufficient to induce L-PDT dependent tumor control.

I first found that L-PDT induced endothelial E-Selectin expression through the activation of the NF-κB pathway in vitro and in vivo. This increased E-Selectin expression was associated to higher MPM infiltration by active CD8+ and CD4+ lymphocytes. This recruitment was mandatory for the L-PDT induced tumor control. The inhibition of E-Selectin or CD8+ lymphocytes by antibodies abrogated the impact of L-PDT on MPM regression. An axis involving NF-κB and E-Selectin was therefore uncovered for the effective recruitment of lymphocytes following L-PDT. These preclinical results were validated in MPM patient samples where E-Selectin and CD8+ T-cells were positively correlated to each other and to patient survival. Altogether, this suggests that L-PDT could be an interesting treatment for MPM alone or in combination with immunotherapies.

## 8.1 Modulation of the MPM tumor immune microenvironment following L-PDT

In the era of immunotherapy, numerous approaches have been described to reprogram TME of poorly infiltrated tumors or switch immunosuppressive environments into pro-inflammatory ones. (143, 144), Hanahan et al described the hallmarks of cancer which represent the angular stone to understand and establish treatment targets to overcome cancer barriers.

A first hallmark is tumor inflammation. In order to grow, cancer must avoid the host immunity to react against it (145, 146). In a previous study from our group, (126), we observed L-PDT improved the ratio of CD8+ over CD4+ CD103+, a Treg subtype in mice. Thus, L-PDT seems to favor an adaptive immune response through a favorable CD8+ over CD4 ratio supporting an immune mediated response. T regulators (Treg) are CD4+ T-cells expressing the transcription factor FOXP3. Tregs appear to be an essential TME immunosuppressive player that favor the development of cancer, (147). This is further supported by the poor prognosis associated with high infiltration of Treg in various cancers, (147-149). Tregs exert their function through numerous mechanisms. As their effector counterpart CD8+ T cells, Tregs are able to use perforin and granzyme to kill effector cells of the anti-tumor immunity, (150). In addition, Tregs are known to secrete anti-inflammatory cytokines such as IL-10 or TGF-β and to compete with other T-cells for pro-inflammatory cytokine stimulation such as IL-2, (151-152). Altogether, Tregs participate to shift the immune environment to a pro-tumoral phenotype by precluding the action of cytotoxic T-cells.

Here, we observed a concurrent upregulation of CD3+CD4+ and CD3+CD8+ T cells 24h after L-PDT followed by a drop in CD3+CD4+ cells 7 days after treatment. We were not able to distinguish the proportion of Tregs within the total CD3+CD4+ T cell population. However, given L-PDT provided a significant survival advantage, this suggests a dominant CD8+ response over Tregs. Furthermore, the specific CD8+ inhibition abrogated the survival advantage provided by L-PDT.

We found that L-PDT could activate the NF-κB pathway. This pathway is important to create an inflammatory environment through the secretion of inflammatory cytokines

such as IL-1, (153). In addition, a role for adhesion molecule expression at the surface of the endothelium to promote immune cell recruitment was also demonstrated. Here, we found a positive impact of NF-κB on the expression of adhesion molecules E-Selectin, ICAM1 and VCAM1. The impact of NF-κB on tumor progression however remains a matter of debate. On the one hand, the pro-tumoral role of NF-κB was first deciphered through the study of mutational signatures in tumors: several tumors such as breast harbor gene mutations of the NF-κB subunits or IκB proteins (154). The IKKα mutation led to the renewal of breast tumor progenitors and was associated with bad outcome (155). Other pro-tumor implications of NF-κB include cell adhesion protein promotion which facilitate the development of metastasis (156), mesenchymal-epithelial differentiation and radioresistance, (157). On another hand, NF-κB also carries an anti-tumoral role through its maintenance in effector T-cell homeostasis and survival (158). In MPM patients, the contribution of NF-κB has been evaluated for the tumor response to ICIs. In patients treated with anti-CTLA-4 and/or anti-PD1, an upregulation of NF-κB in the immune or tumor cells correlated with tumor response (159, 136). Here, we found a positive contribution of NF-κB in MPM following L-PDT through the expression of adhesion molecules that favored immune infiltration. The inhibition of the pathway led to a reduction in E-Selectin expression and CD8+ T cell recruitment in MPM tumors. Thus, the contribution of L-PDT to the inflammatory landscape could also participate to shift from an immunosuppressive TME to an anti-tumor microenvironment. We found that the recruitment of those immune cells was promoted following the expression of adhesion molecules, notably E-Selectin at the surface of the vessels through NF-κB. While NF-κB is a rapidly induced inflammation pathway, here we observed a late activation of the signaling following L-PDT. This is in line with literature as reported by Volanti et al who observed induction of NF-κB by PDT happening few hours after treatment (160). Authors state this late activation could be due to an alternative phosphorylation of IκBα happening in endothelial cells exposed to PDT. In addition, IL-6 appears to play a critical role in the vascular inflammation mediated by NF-κB, (161). It has been reported activation of NF-kB by IL-6 could be slow, suggesting its contribution to L-PDT induced activation, (162). Altogether, this reinforces the impact of L-PDT on the tumor vasculature which also represents an important hallmark of cancer: angiogenesis.

Tumor vasculature is a major component of the TME and affect both response to treatment and the immune polarization of the TME. It is well established that the

architecture of the vasculature is aberrant in tumors (163, 164). Vascular normalization remains an effective way to tackle cancer growth, (165). This can be performed by inhibiting VEGF signaling, the major growth factor responsible for angiogenesis (166-168). Vasculature normalization remains a contested approach since the improvement of the vascular architecture could also favor tumor growth and dissemination through better oxygen and nutrient distribution. However, Hamzah et al showed that vascular normalization improved tumor immune infiltration which largely overcame the better nutrient distribution. (169). This suggests the dramatic impact of the immune system on controlling tumor growth and spread. In addition to inhibiting angiogenesis, it is possible to remodel the vasculature via endothelial and pericyte modulation (170, 171). L-PDT was previously shown to improve the vascular transport by enhancing the pericyte-endothelial association. This vascular stabilization following L-PDT caused a decrease in intrinsic vascular permeability and a drop in interstitial fluid pressure. This ultimately translated into a better drug distribution inside tumors, (127, 128). In my thesis, I highlighted a second new vascular modulation provided by L-PDT. Following exposition to the treatment, endothelial cells are able to recover from the vascular anergy through the NF-κB pathway. This occurred through the activation of the canonical NF-κB signaling as NEMO blockade impaired the L-PDT effect. Interestingly, NF-κB activation by L-PDT occurred several hours after therapy suggesting a cascade effect between the creation of free oxygen radicals and ultimately NF-κB activation (172, 173). The activation of the endothelium allows the expression of adhesion molecules at the surface of the vessels such as E-Selectin, ICAM-1 and VCAM-1. In conclusion, I deciphered that L-PDT could relief the vascular anergy which translates into a better tumor infiltration and thus an improved tumor control. Those links were not clearly established in the context of L-PDT before. While the role of adhesion molecule in cancer remains unclear, their implication in the contribution of the immune system to fight tumor growth implies to review both their pro and anti-tumor role in cancer.

## 8.2 Contribution of adhesion molecules in cancer development and immunotherapy

Cellular adhesion molecules (CAM) are key elements for the diapedesis of circulating immune cells into the inflammation site, (174, 175). Through their immune promotion function, CAM are crucial to establish a directed immune response against the tumor. However, the expression of CAM is not restricted to immune and endothelial cells; indeed, cancer cells are capable to present and bind to CAM at the surface of host cells, (176, 177). By their adhesion function, CAM have the capacity to promote the invasion and circulation of tumor cells similarly to the recruitment of immune cells by the vasculature. This ambivalent contribution to cancer progression has been extensively studied and CAM remained a target for the inhibition of cancer spread for many years, (178-180). However, the wide acceptance of immunotherapy led to reconsider the therapeutic potential of enhancing CAM in order to favor an immune response in combination with immunotherapeutic approaches. There are three main CAM that were found to be upregulated by L-PDT in our project: ICAM-1, VCAM-1 and E-Selectin.

Here we found that vascular E-Selectin and not tumor E-Selectin were important for the L-PDT mediated tumor control and immune infiltration. Our findings are further backed by the patient samples. Tumor vs stromal expression of E-Selectin can have different effects on tumor progression. Tumor expression for example was shown to favor metastasis. In our TMA, E-selectin was not prognostic for patient outcome. Interestingly, vascular E-selectin did predict CD8 infiltration and tumor control. This was also the case in patient samples where vascular E-selectin correlated with CD8 infiltration and outcome.

ICAM-1 was shown to actively contribute to the diffusion of cancer cells to distant sites mainly when the protein is harbored by tumor cells. ICAM-1 is required in the various steps of the metastatic cascade. By triggering the TGF-β/SMAD signaling, ICAM-1 is able to favor the epithelial-to-mesenchymal transition of cancer cells, (181). Once in the circulation, ICAM-1 is implicated in the formation of clusters of circulating tumor cells, (182). Finally, ICAM-1 also contributes to the trans endothelial migration of tumor cells, (177). Conversely, studies trying to abrogate the expression of ICAM-1 observed a poorer tumor control when inhibited. Indeed, authors reported a depleted immune TME regarding numerous cells populations such as lymphocytes and neutrophils, (182-185). In our study, we observed a significant upregulation of ICAM-1 located at the surface of the endothelium. This upregulation could result from the vascular targeting profile of our

L-PDT conditions and may explain the enhanced immune infiltration leading to the positive outcome observed on animals treated by L-PDT.

The expression of VCAM-1 on cancer cells is also associated with an increase in cancer cells metastasis, (186, 187). Conversely, the anti-tumor potential of VCAM-1 when expressed at the surface of endothelial cells, is supported by the literature. Nakajima et al, (188), observed upregulation of VCAM-1 and E-Selectin at the surface of endothelial cells was ultimately associated with an improved infiltration of immune cells resulting in better tumor control. Regarding the potential combination with immunotherapy, VCAM-1 appears to enhance effects of pulsed dendritic vaccination and antigen-specific vaccination, (189, 190).

Finally, E-Selectin is implicated in the metastasis process. Cancer cells could express either E-Selectin or selectin ligands at their surface to promote migration away from the primary site, (164). Therefore, research investigated the blocking of E-Selectin in cancer. Approaches to deplete E-Selectin varied from inhibitors to genetic mouse model. Results reported a decrease in the development of metastasis but also a reduced pro-tumoral infiltration in Th2 macrophages, (191-193). However, a key principle to better understand the balanced impact of CAM on cancer progression is the site of expression. As detailed by Sackstein et al, (194) the expression of CAM at the tumor site was crucial for the homing of effector immune cells while other research has supported a contribution of CAM on the metastatic process of tumors (176, 191). In addition, E-Selectin expression was shown to improve the outcome of immunotherapy. The expression of E-Selectin by CAR-T cells appears to be essential for the CAR-T to reach the tumor site, (195). In a similar fashion, E-Selectin seems critical for the homing of lymphocytes, thus improving the mounting of a specific anti-tumor response, (196).

In my thesis, we deciphered L-PDT was able to induce CAM at the surface of endothelial cells through the NF-κB pathway. This upregulation appears crucial to the TME remodeling provided by L-PDT by allowing the recruitment of active immune cells inside the tumor. Conversely, upon E-Selectin depletion, we find a decreased infiltration in immune cells after L-PDT. To note, only vascular E-Selectin was upregulated following L-PDT. Moreover, E-Selectin induction appears required for the tumor growth control. Upon depletion of E-Selectin, mice loose the survival advantage given by L-PDT. With those findings, we highlighted the importance of the site of expression for E-Selectin. Indeed, we found vascular targeted L-PDT was able to induce vascular E-Selectin while sparing

adjacent tissues and cells. This selective upregulation led to an improvement in immune infiltration significantly contributing to the survival of MPM bearing mice. To confirm the positive role of E-Selectin when expressed at the surface of endothelial cells, we finally confirmed our findings in the clinical setting using MPM patient samples.

## 8.3 Clinical implication of immune infiltrate and adhesion molecules in MPM

In the context of MPM, the scarcity of studies on adhesion molecules in this cancer limits the inferences that could be drawn. Ruco et al, (197), investigated specifically the impact of ICAM-1 and VCAM-1 in cultured malignant mesothelioma cell lines and malignant mesothelioma patient biopsies. They observed an intense expression of both molecules in neoplastic cells in patient samples. In vitro, ICAM-1 was constitutively expressed in all mesothelioma cell lines while VCAM-1 was present in only one-half of these cells. The other half could have VCAM-1 induction following exposure to inflammatory cytokines such as TNF-α. At the gene expression levels, (198), others observed an overexpression of E-Selectin in all cell lines what was correlated with a worse prognosis. A limitation of those studies is they did not investigate CAM expression outside of cancer cells. Such investigations have been led by Tsagkouli et al, (199), by analyzing both serum and pleural level of CAM in MPM patients. They observed that while ICAM-1 and VCAM-1 did not correlate with clinical outcomes, both high pleural and serum E-Selectin levels appear to carry a better prognosis and a lower tumor grade, reinforcing the consideration that the location of CAM is crucial in tipping the balance of their contribution to tumor repression. Conversely, Dick et al found no correlation between survival and E-Selectin, ICAM-1 and VCAM-1 expression in pleural effusion of MPM patient. Those results underline additional investigations are required regarding the predictive value of adhesion molecules in MPM, (200).

Given the impact of the CAM location, we analyzed 82 MPM patient samples, looking for implication of E-Selectin, inside and outside of the vessels, in the survival prognosis. We found vascular E-Selectin expression was positively correlated to survival as the level of CD8+ cells infiltration in the tumor while E-Selectin outside the vessels did not correlate with clinical outcomes. Regarding the CD8+ infiltration, CD8+ cells have shown to carry a favorable prognosis in MPM. Indeed, a higher count in CD8+ cells in the tumor was

associated with better PFS, better OS and higher levels of necrotic cells. Moreover, presence of CD8+ cells was negatively correlated with lymph node invasion, (49, 50). In my thesis, CD8+ cells infiltration was found to be positively correlated with survival as well in MPM patients. This was true in both epithelioid and biphasic and sarcomatoid tumors. Finally, a correlation between E-Selectin expression and CD8+ lymphocytes infiltration was found in highly infiltrated tumors, suggesting the synergic contribution of vascular CAM and immune cells in improving the survival of MPM patients. Thus, patients derived results reinforce the clinical relevance of L-PDT for MPM patients through its ability to enhance vascular E-Selectin. In addition, L-PDT, by relieving cold TME and vascular anergy, could constitute an interesting adjunct of current immunotherapies in MPM.

## 8.4 Clinical translation of L-PDT in MPM

Our preclinical results support the translation of L-PDT as an adjunct of the current treatments for MPM. While promising, several points regarding this translation remain to be discussed.

Indeed, we first investigated the role of E-Selectin and CD8+ T-cells on the survival of MPM bearing mice following L-PDT. We observed that their selective inhibition led to a significant decrease in survival and tumor growth control, a link that was not known in the context of MPM. These preclinical results were further confirmed with the TMA study. We found that patients with increased level of E-Selectin survived longer compared to patients with low levels. The same conclusion was drawn regarding CD8+ T-cells expression with tumor presenting a higher infiltration was associated with a higher survival. Moreover, patients with CD8+ T-cells infiltration above the median presented a significant correlation between vascular E-Selectin expression and CD8+ cells infiltration. This supports the critical contribution of both E-Selectin and CD8+ T-cells in the clinical outcomes of MPM patients. Interestingly, patients with a higher E-Selectin expression after neoadjuvant treatment survived longer compared to patients with a decreased expression. Thus, L-PDT, through its potential in inducing endothelial E-Selectin and CD8+ infiltration could improve the survival in MPM patients.

Since the recent MARS-2 trial, (34), the role of surgery has recently been questioned. The latter randomized resectable MPM patients to chemotherapy alone versus chemotherapy plus surgery and showed no difference in OS or PFS with more adverse events in the surgery group. Caution is thus warranted with the use of surgery. In addition, intraoperative PDT of MPM triggers inflammation limiting anti-tumor immune responses (201). Therefore, my thesis suggests a supportive role for L-PDT in the management of MPM. Indeed, most patients clinically suffer from dyspnea because of the pleural effusion they develop. A standard approach consists in performing a thoracoscopy and talc pleurodesis to relief the symptoms. My study supports the addition of a L-PDT therapy in the context of MPM which could be used as a tumor immune priming approach to enhance the impact of subsequent immunotherapy during this operation. Major advantages of L-PDT include its very low toxicity, precise delivery at the site of interest and effectiveness. Moreover, L-PDT has been shown to effectively remodel the tumor vasculature in MPM, enhancing the distribution of macromolecules in the tumor while sparring adjacent healthy tissues (132). In addition, the stimulation of active immune cells following L-PDT indicates L-PDT could also synergize with ICI by improving their tumor targeting.

Of course, the potential of combining L-PDT with ICI remains to be investigated and goes beyond the scope of this thesis. To investigate the possible synergy between L-PDT and ICI, additional characterization of the TME is required, notably regarding the timing between ICI administration and L-PDT treatment. For this, the use of the thoracic window model that was developed for this thesis could be a valuable tool to better combine L-PDT with immunotherapies. This study is also beyond the scope of this thesis but the methods and the endpoints seem established.

## 9. Conclusion

MPM is a challenging disease characterized by vascular anergy and an altered immune TME. While immunotherapeutic approaches have presented encouraging results, overall survival increase remains modest suggesting room for improvement. L-PDT have previously shown to positively impact on MPM. In my thesis, I showed the positive outcomes provided by L-PDT are linked to a vascular and immune modulation of the MPM TME. Specifically, L-PDT enhances endothelial CAM expression through the NF-κB pathway. This in turn, support the infiltration of active CD8+ T cells that allows a better

tumor control. Finally, we highlighted the crucial impact of vascular E-Selectin in MPM patients on their survival prognosis. The reprogramming of the TME conferred by L-PDT remains to be investigated in combination with ICI. Altogether, this study suggests the potential translational impact of L-PDT for MPM patients.

# 10. References


1. Khan YS, Lynch DT. Histology, Lung. 2022 May 8. In: StatPearls [Internet]. Treasure Island (FL): StatPearls Publishing; 2022 Jan–. PMID: 30521210.
2. Chaudhry R, Bordoni B. Anatomy, Thorax, Lungs. 2022 Jul 25. In: StatPearls [Internet]. Treasure Island (FL): StatPearls Publishing; 2023 Jan–. PMID: 29262068.
3. Murray JF. The structure and function of the lung. Int J Tuberc Lung Dis. 2010 Apr;14(4):391-6. PMID: 20202294.
4. Guillot L, Nathan N, Tabary O, Thouvenin G, Le Rouzic P, Corvol H, Amselem S, Clement A. Alveolar epithelial cells: master regulators of lung homeostasis. Int J Biochem Cell Biol. 2013 Nov;45(11):2568-73. doi: 10.1016/j.biocel.2013.08.009. Epub 2013 Aug 27. PMID: 23988571.
5. Charalampidis C, Youroukou A, Lazaridis G, Baka S, Mpoukovinas I, Karavasilis V, Kioumis I, Pitsiou G, Papaiwannou A, Karavergou A, Tsakiridis K, Katsikogiannis N, Sarika E, Kapanidis K, Sakkas L, Korantzis I, Lampaki S, Zarogoulidis K, Zarogoulidis P. Pleura space anatomy. J Thorac Dis. 2015 Feb;7(Suppl 1):S27-32. doi: 10.3978/j.issn.2072-1439.2015.01.48. PMID: 25774304; PMCID: PMC4332049.
6. Zielinska-Krawczyk M, Krenke R, Grabczak EM, Light RW. Pleural manometry-historical background, rationale for use and methods of measurement. Respir Med. 2018 Mar;136:21-28. doi: 10.1016/j.rmed.2018.01.013. Epub 2018 Jan 31. PMID: 29501243.
7. Li J. Ultrastructural study on the pleural stomata in human. Funct Dev Morphol. 1993;3(4):277-80. PMID: 7949406.
8. Finley DJ, Rusch VW. Anatomy of the pleura. Thorac Surg Clin. 2011 May;21(2):157-63, vii. doi: 10.1016/j.thorsurg.2010.12.001. PMID: 21477764
9. Okiemy G, Foucault C, Avisse C, Hidden G, Riquet M. Lymphatic drainage of the diaphragmatic pleura to the peritracheobronchial lymph nodes. Surg Radiol Anat. 2003 Apr;25(1):32-5. doi: 10.1007/s00276-002-0081-y. Epub 2003 Apr 4. PMID: 12677463
10. Bénard A, Podolska MJ, Czubayko F, Kutschick I, Klösch B, Jacobsen A, Naschberger E, Brunner M, Krautz C, Trufa DI, Sirbu H, Lang R, Grützmann R, Weber GF. Pleural Resident Macrophages and Pleural IRA B Cells Promote Efficient Immunity Against Pneumonia by

Inducing Early Pleural Space Inflammation. Front Immunol. 2022 Apr 14;13:821480. doi: 10.3389/fimmu.2022.821480. PMID: 35493510; PMCID: PMC9047739.

11. Didier Jean, Marie-Claude Jaurand. Causes and pathophysiology of malignant pleural mesothelioma. Lung Cancer Management, 2015, 4 (5), pp.219-229. ff10.2217/lmt.15.21ff. ffinserm-02483449f
12. Chernova T and al, Long-Fiber Carbon Nanotubes Replicate Asbestos-Induced Mesothelioma with Disruption of the Tumor Suppressor Gene Cdkn2a (Ink4a/Arf). Curr Biol. 2017 Nov 6;27(21):3302-3314.e6.
13. BTS statement on malignant mesothelioma in the UK, 2007, Thorax 2007;62:ii1-ii19.
14. Betti M, Aspesi A, Sculco M, Matullo G, Magnani C, Dianzani I. Genetic predisposition for malignant mesothelioma: A concise review. Mutat Res Rev Mutat Res. 2019 Jul-Sep;781:1-10. doi: 10.1016/j.mrrev.2019.03.001. Epub 2019 Mar 6. PMID: 31416570.
15. Neumann V, Löseke S, Nowak D, Herth FJ, Tannapfel A. Malignant pleural mesothelioma: incidence, etiology, diagnosis, treatment, and occupational health. Dtsch Arztebl Int. 2013 May;110(18):319-26. doi: 10.3238/arztebl.2013.0319. Epub 2013 May 3. PMID: 23720698; PMCID: PMC3659962.
16. Alì G, Bruno R, Fontanini G. The pathological and molecular diagnosis of malignant pleural mesothelioma: a literature review. J Thorac Dis. 2018 Jan;10(Suppl 2):S276-S284. doi: 10.21037/jtd.2017.10.125. PMID: 29507796; PMCID: PMC5830567.
17. Brcic L, Kern I. Clinical significance of histologic subtyping of malignant pleural mesothelioma. Transl Lung Cancer Res. 2020 Jun;9(3):924-933. doi: 10.21037/tlcr.2020.03.38. PMID: 32676358; PMCID: PMC7354152.
18. Galateau Salle F, Le Stang N, Nicholson AG, Pissaloux D, Churg A, Klebe S, Roggli VL, Tazelaar HD, Vignaud JM, Attanoos R, Beasley MB, Begueret H, Capron F, Chirieac L, Copin MC, Dacic S, Danel C, Foulet-Roge A, Gibbs A, Giusiano-Courcambeck S, Hiroshima K, Hofman V, Husain AN, Kerr K, Marchevsky A, Nabeshima K, Picquenot JM, Rouquette I, Sagan C, Sauter JL, Thivolet F, Travis WD, Tsao MS, Weynand B, Damiola F, Scherpereel A, Pairon JC, Lantuejoul S, Rusch V, Girard N. New Insights on Diagnostic Reproducibility of Biphasic Mesotheliomas: A Multi-Institutional Evaluation by the International Mesothelioma Panel From the MESOPATH Reference Center. J Thorac Oncol. 2018 Aug;13(8):1189-1203. doi: 10.1016/j.jtho.2018.04.023. Epub 2018 Apr 30. PMID: 29723687; PMCID: PMC7558835.
19. Dudnik E, Bar J, Moore A, Gottfried T, Moskovitz M, Dudnik J, Shochat T, Allen AM, Zer A, Rotem O, Peled N, Urban D. BAP1-Altered Malignant Pleural Mesothelioma: Outcomes With Chemotherapy, Immune Check-Point Inhibitors and Poly(ADP-Ribose) Polymerase

Inhibitors. Front Oncol. 2021 Mar 10;11:603223. doi: 10.3389/fonc.2021.603223. PMID: 33777745; PMCID: PMC7987904.

20. De Rienzo A, Chirieac LR, Hung YP, Severson DT, Freyaldenhoven S, Gustafson CE, Dao NT, Meyerovitz CV, Oster ME, Jensen RV, Yeap BY, Bueno R, Richards WG. Large-scale analysis of BAP1 expression reveals novel associations with clinical and molecular features of malignant pleural mesothelioma. J Pathol. 2021 Jan;253(1):68-79. doi: 10.1002/path.5551. Epub 2020 Oct 15. PMID: 32944962; PMCID: PMC7756745.
21. Sato T, Sekido Y. NF2/Merlin Inactivation and Potential Therapeutic Targets in Mesothelioma. Int J Mol Sci. 2018 Mar 26;19(4):988. doi: 10.3390/ijms19040988. PMID: 29587439; PMCID: PMC5979333.
22. Fennell DA, Baas P, Taylor P, Nowak AK, Gilligan D, Nakano T, Pachter JA, Weaver DT, Scherpereel A, Pavlakis N, van Meerbeeck JP, Cedrés S, Nolan L, Kindler H, Aerts JGJV. Maintenance defactinib versus placebo after first-line chemotherapy in patients with merlin-stratified pleural mesothelioma: COMMAND-a double-blind, randomized, phase II study. J Clin Oncol. 2019;37(10):790–798. doi: 10.1200/JCO.2018.79.0543.
23. Alhejaily A, Day AG, Feilotter HE, Baetz T, Lebrun DP. Inactivation of the CDKN2A tumor-suppressor gene by deletion or methylation is common at diagnosis in follicular lymphoma and associated with poor clinical outcome. Clin Cancer Res. 2014 Mar 15;20(6):1676-86. doi: 10.1158/1078-0432.CCR-13-2175. Epub 2014 Jan 21. PMID: 24449825.
24. Jennings CJ, Murer B, O'Grady A, Hearn LM, Harvey BJ, Kay EW, Thomas W. Differential p16/INK4A cyclin-dependent kinase inhibitor expression correlates with chemotherapy efficacy in a cohort of 88 malignant pleural mesothelioma patients. Br J Cancer. 2015 Jun 30;113(1):69-75. doi: 10.1038/bjc.2015.187. Epub 2015 Jun 9. PMID: 26057448; PMCID: PMC4647524.
25. Dacic S, Kothmaier H, Land S, Shuai Y, Halbwedl I, Morbini P, Murer B, Comin C, Galateau-Salle F, Demirag F, Zeren H, Attanoos R, Gibbs A, Cagle P, Popper H. Prognostic significance of p16/cdkn2a loss in pleural malignant mesotheliomas. Virchows Arch. 2008 Dec;453(6):627-35. doi: 10.1007/s00428-008-0689-3. Epub 2008 Oct 29. PMID: 18958493.
26. Nicolini F, Bocchini M, Bronte G, Delmonte A, Guidoboni M, Crinò L, Mazza M. Malignant Pleural Mesothelioma: State-of-the-Art on Current Therapies and Promises for the Future. Front Oncol. 2020 Jan 24;9:1519. doi: 10.3389/fonc.2019.01519. PMID: 32039010; PMCID: PMC6992646.
27. Treasure T, Lang-Lazdunski L, Waller D, Bliss JM, Tan C, Entwisle J, Snee M, O'Brien M, Thomas G, Senan S, O'Byrne K, Kilburn LS, Spicer J, Landau D, Edwards J, Coombes G,

Darlison L, Peto J; MARS trialists. Extra-pleural pneumonectomy versus no extra-pleural pneumonectomy for patients with malignant pleural mesothelioma: clinical outcomes of the Mesothelioma and Radical Surgery (MARS) randomised feasibility study. Lancet Oncol. 2011 Aug;12(8):763-72. doi: 10.1016/S1470-2045(11)70149-8. Epub 2011 Jun 30. PMID: 21723781; PMCID: PMC3148430.

28. Zhou N, Rice DC, Tsao AS, Lee PP, Haymaker CL, Corsini EM, Antonoff MB, Hofstetter WL, Rajaram R, Roth JA, Swisher SG, Vaporciyan AA, Walsh GL, Mehran RJ, Sepesi B. Extrapleural Pneumonectomy Versus Pleurectomy/Decortication for Malignant Pleural Mesothelioma. Ann Thorac Surg. 2022 Jan;113(1):200-208. doi: 10.1016/j.athoracsur.2021.04.078. Epub 2021 May 8. PMID: 33971174.
29. Lang-Lazdunski L, Bille A, Lal R, Cane P, McLean E, Landau D, Steele J, Spicer J. Pleurectomy/decortication is superior to extrapleural pneumonectomy in the multimodality management of patients with malignant pleural mesothelioma. J Thorac Oncol. 2012 Apr;7(4):737-43. doi: 10.1097/JTO.0b013e31824ab6c5. PMID: 22425923.
30. Taioli E, Wolf AS, Flores RM. Meta-analysis of survival after pleurectomy decortication versus extrapleural pneumonectomy in mesothelioma. Ann Thorac Surg. 2015 Feb;99(2):472-80. doi: 10.1016/j.athoracsur.2014.09.056. Epub 2014 Dec 20. PMID: 25534527.
31. Sugarbaker DJ, Gill RR, Yeap BY, Wolf AS, DaSilva MC, Baldini EH, Bueno R, Richards WG. Hyperthermic intraoperative pleural cisplatin chemotherapy extends interval to recurrence and survival among low-risk patients with malignant pleural mesothelioma undergoing surgical macroscopic complete resection. J Thorac Cardiovasc Surg. 2013 Apr;145(4):955-963. doi: 10.1016/j.jtcvs.2012.12.037. Epub 2013 Feb 21. PMID: 23434448.
32. Cho BCJ, Donahoe L, Bradbury PA, Leighl N, Keshavjee S, Hope A, Pal P, Cabanero M, Czarnecka K, McRae K, Tsao MS, de Perrot M. Surgery for malignant pleural mesothelioma after radiotherapy (SMART): final results from a single-centre, phase 2 trial. Lancet Oncol. 2021 Feb;22(2):190-197. doi: 10.1016/S1470-2045(20)30606-9. Epub 2021 Jan 12. PMID: 33450184.
33. Friedberg JS, Culligan MJ, Mick R, Stevenson J, Hahn SM, Sterman D, Punekar S, Glatstein E, Cengel K. Radical pleurectomy and intraoperative photodynamic therapy for malignant pleural mesothelioma. Ann Thorac Surg. 2012 May;93(5):1658-65; discussion 1665-7. doi: 10.1016/j.athoracsur.2012.02.009. PMID: 22541196; PMCID: PMC4394024.
34. Lim E, Waller D, Lau K, et al. MARS 2: A multicentre randomised trial comparing (extended) pleurectomy decortication versus no radical surgery for mesothelioma. Presented at WCLC 2023. September 9-12, 2023. Abstract PL03.10.

35. Vogelzang NJ, Rusthoven JJ, Symanowski J, Denham C, Kaukel E, Ruffie P, Gatzemeier U, Boyer M, Emri S, Manegold C, Niyikiza C, Paoletti P. Phase III study of pemetrexed in combination with cisplatin versus cisplatin alone in patients with malignant pleural mesothelioma. J Clin Oncol. 2003 Jul 15;21(14):2636-44. doi: 10.1200/JCO.2003.11.136. PMID: 12860938.(34)
36. Baas P, Fennell D, Kerr KM, Van Schil PE, Haas RL, Peters S; ESMO Guidelines Committee. Malignant pleural mesothelioma: ESMO Clinical Practice Guidelines for diagnosis, treatment and follow-up. Ann Oncol. 2015 Sep;26 Suppl 5:v31-9. doi: 10.1093/annonc/mdv199. Epub 2015 Jul 28. PMID: 26223247.
37. Waldman AD, Fritz JM, Lenardo MJ. A guide to cancer immunotherapy: from T cell basic science to clinical practice. Nat Rev Immunol. 2020 Nov;20(11):651-668. doi: 10.1038/s41577-020-0306-5. Epub 2020 May 20. PMID: 32433532; PMCID: PMC7238960.
38. Iranzo P, Callejo A, Assaf JD, Molina G, Lopez DE, Garcia-Illescas D, Pardo N, Navarro A, Martinez-Marti A, Cedres S, Carbonell C, Frigola J, Amat R, Felip E. Overview of Checkpoint Inhibitors Mechanism of Action: Role of Immune-Related Adverse Events and Their Treatment on Progression of Underlying Cancer. Front Med (Lausanne). 2022 May 30;9:875974. doi: 10.3389/fmed.2022.875974. PMID: 35707528; PMCID: PMC9189307
39. Baas P, Scherpereel A, Nowak AK, Fujimoto N, Peters S, Tsao AS, Mansfield AS, Popat S, Jahan T, Antonia S, Oulkhouir Y, Bautista Y, Cornelissen R, Greillier L, Grossi F, Kowalski D, Rodríguez-Cid J, Aanur P, Oukessou A, Baudelet C, Zalcman G. First-line nivolumab plus ipilimumab in unresectable malignant pleural mesothelioma (CheckMate 743): a multicentre, randomised, open-label, phase 3 trial. Lancet. 2021 Jan 30;397(10272):375-386. doi: 10.1016/S0140-6736(20)32714-8. Epub 2021 Jan 21. Erratum in: Lancet. 2021 Feb 20;397(10275):670. PMID: 33485464.
40. Bożyk A, Wojas-Krawczyk K, Krawczyk P, Milanowski J. Tumor Microenvironment-A Short Review of Cellular and Interaction Diversity. Biology (Basel). 2022 Jun 18;11(6):929. doi: 10.3390/biology11060929. PMID: 35741450; PMCID: PMC9220289.
41. Farc O, Cristea V. An overview of the tumor microenvironment, from cells to complex networks (Review). Exp Ther Med. 2021 Jan;21(1):96. doi: 10.3892/etm.2020.9528. Epub 2020 Nov 26. PMID: 33363607; PMCID: PMC7725019.
42. Yang K, Yang T, Yang T, Yuan Y, Li F. Unraveling tumor microenvironment heterogeneity in malignant pleural mesothelioma identifies biologically distinct immune subtypes enabling prognosis determination. Front Oncol. 2022 Sep 27;12:995651. doi: 10.3389/fonc.2022.995651. PMID: 36237331; PMCID: PMC9552848.

43. Liu YT, Sun ZJ. Turning cold tumors into hot tumors by improving T-cell infiltration. Theranostics. 2021 Mar 11;11(11):5365-5386. doi: 10.7150/thno.58390. PMID: 33859752; PMCID: PMC8039952.
44. Blum Y, Meiller C, Quetel L, Elarouci N, Ayadi M, Tashtanbaeva D, Armenoult L, Montagne F, Tranchant R, Renier A, de Koning L, Copin MC, Hofman P, Hofman V, Porte H, Le Pimpec-Barthes F, Zucman-Rossi J, Jaurand MC, de Reyniès A, Jean D. Dissecting heterogeneity in malignant pleural mesothelioma through histo-molecular gradients for clinical applications. Nat Commun. 2019 Mar 22;10(1):1333. doi: 10.1038/s41467-019-09307-6. PMID: 30902996; PMCID: PMC6430832.
45. Pagano M, Ceresoli LG, Zucali PA, Pasello G, Garassino M, Grosso F, Tiseo M, Soto Parra H, Zanelli F, Cappuzzo F, Grossi F, De Marinis F, Pedrazzoli P, Gnoni R, Bonelli C, Torricelli F, Ciarrocchi A, Normanno N, Pinto C. Mutational Profile of Malignant Pleural Mesothelioma (MPM) in the Phase II RAMES Study. Cancers (Basel). 2020 Oct 13;12(10):2948. doi: 10.3390/cancers12102948. PMID: 33065998; PMCID: PMC7601196.
46. Jardim DL, Goodman A, de Melo Gagliato D, Kurzrock R. The Challenges of Tumor Mutational Burden as an Immunotherapy Biomarker. Cancer Cell. 2021 Feb 8;39(2):154-173. doi: 10.1016/j.ccell.2020.10.001. Epub 2020 Oct 29. PMID: 33125859; PMCID: PMC7878292.
47. Hendry S, Salgado R, Gevaert T, Russell PA, John T, Thapa B, Christie M, van de Vijver K, Estrada MV, Gonzalez-Ericsson PI, Sanders M, Solomon B, Solinas C, Van den Eynden GGGM, Allory Y, Preusser M, Hainfellner J, Pruneri G, Vingiani A, Demaria S, Symmans F, Nuciforo P, Comerma L, Thompson EA, Lakhani S, Kim SR, Schnitt S, Colpaert C, Sotiriou C, Scherer SJ, Ignatiadis M, Badve S, Pierce RH, Viale G, Sirtaine N, Penault-Llorca F, Sugie T, Fineberg S, Paik S, Srinivasan A, Richardson A, Wang Y, Chmielik E, Brock J, Johnson DB, Balko J, Wienert S, Bossuyt V, Michiels S, Ternes N, Burchardi N, Luen SJ, Savas P, Klauschen F, Watson PH, Nelson BH, Criscitiello C, O'Toole S, Larsimont D, de Wind R, Curigliano G, André F, Lacroix-Triki M, van de Vijver M, Rojo F, Floris G, Bedri S, Sparano J, Rimm D, Nielsen T, Kos Z, Hewitt S, Singh B, Farshid G, Loibl S, Allison KH, Tung N, Adams S, Willard-Gallo K, Horlings HM, Gandhi L, Moreira A, Hirsch F, Dieci MV, Urbanowicz M, Brcic I, Korski K, Gaire F, Koeppen H, Lo A, Giltnane J, Rebelatto MC, Steele KE, Zha J, Emancipator K, Juco JW, Denkert C, Reis-Filho J, Loi S, Fox SB. Assessing Tumor-Infiltrating Lymphocytes in Solid Tumors: A Practical Review for Pathologists and Proposal for a Standardized Method from the International Immuno-Oncology Biomarkers Working Group: Part 2: TILs in Melanoma, Gastrointestinal Tract Carcinomas, Non-Small Cell Lung Carcinoma and Mesothelioma, Endometrial and Ovarian Carcinomas, Squamous Cell Carcinoma of the Head and Neck, Genitourinary

Carcinomas, and Primary Brain Tumors. Adv Anat Pathol. 2017 Nov;24(6):311-335. doi: 10.1097/PAP.0000000000000161. PMID: 28777143; PMCID: PMC5638696.

48. Zitvogel L, Tesniere A, Kroemer G. Cancer despite immunosurveillance: immunoselection and immunosubversion. Nat Rev Immunol. 2006 Oct;6(10):715-27. doi: 10.1038/nri1936. Epub 2006 Sep 15. PMID: 16977338.
49. Yamada N, Oizumi S, Kikuchi E, Shinagawa N, Konishi-Sakakibara J, Ishimine A, Aoe K, Gemba K, Kishimoto T, Torigoe T, Nishimura M. CD8+ tumor-infiltrating lymphocytes predict favorable prognosis in malignant pleural mesothelioma after resection. Cancer Immunol Immunother. 2010 Oct;59(10):1543-9. doi: 10.1007/s00262-010-0881-6. Epub 2010 Jun 22. PMID: 20567822.
50. Anraku M, Cunningham KS, Yun Z, Tsao MS, Zhang L, Keshavjee S, Johnston MR, de Perrot M. Impact of tumor-infiltrating T cells on survival in patients with malignant pleural mesothelioma. J Thorac Cardiovasc Surg. 2008 Apr;135(4):823-9. doi: 10.1016/j.jtcvs.2007.10.026. PMID: 18374762.
51. Borgeaud M, Kim F, Friedlaender A, Lococo F, Addeo A, Minervini F. The Evolving Role of Immune-Checkpoint Inhibitors in Malignant Pleural Mesothelioma. J Clin Med. 2023 Feb 22;12(5):1757.
52. Mansfield AS, Roden AC, Peikert T, Sheinin YM, Harrington SM, Krco CJ, Dong H, Kwon ED. B7-H1 expression in malignant pleural mesothelioma is associated with sarcomatoid histology and poor prognosis. J Thorac Oncol. 2014 Jul;9(7):1036-1040. doi: 10.1097/JTO.0000000000000177. PMID: 24926549; PMCID: PMC4058651.
53. Cedrés S, Ponce-Aix S, Zugazagoitia J, Sansano I, Enguita A, Navarro-Mendivil A, Martinez-Marti A, Martinez P, Felip E. Analysis of expression of programmed cell death 1 ligand 1 (PD-L1) in malignant pleural mesothelioma (MPM). PLoS One. 2015 Mar 16;10(3):e0121071. doi: 10.1371/journal.pone.0121071. PMID: 25774992; PMCID: PMC4361537.
54. Rrapaj E, Giacometti L, Spina P, Salvo M, Baselli GA, Veggiani C, Rena O, Trisolini E, Boldorini RL. Programmed cell death 1 ligand 1 (PD-L1) expression is associated with poor prognosis of malignant pleural mesothelioma patients with good performance status. Pathology. 2021 Jun;53(4):462-469. doi: 10.1016/j.pathol.2020.09.018. Epub 2020 Dec 4. PMID: 33272690.
55. Roncella S, Laurent S, Fontana V, Ferro P, Franceschini MC, Salvi S, Varesano S, Boccardo S, Vigani A, Morabito A, Canessa PA, Giannoni U, Rosenberg I, Valentino A, Fedeli F, Merlo DF, Ceppi M, Riggio S, Romani M, Saverino D, Poggi A, Pistillo MP. CTLA-4 in mesothelioma patients: tissue expression, body fluid levels and possible relevance as a

prognostic factor. Cancer Immunol Immunother. 2016 Aug;65(8):909-17. doi: 10.1007/s00262-016-1844-3. Epub 2016 May 20. PMID: 27207606.

56. Sule Kutlar Dursun F, Alabalik U. Investigation of pd-l1 (cd274), pd-l2 (pdcd1lg2), and ctla-4 expressions in malignant pleural mesothelioma by immunohistochemistry and real-time polymerase chain reaction methods. Pol J Pathol. 2022;73(2):111-119. doi: 10.5114/pjp.2022.119752. PMID: 36172747.
57. Carmeliet P, Jain RK. Principles and mechanisms of vessel normalization for cancer and other angiogenic diseases. Nat Rev Drug Discov. 2011 Jun;10(6):417-27. doi: 10.1038/nrd3455. PMID: 21629292.
58. Viallard C, Larrivée B. Tumor angiogenesis and vascular normalization: alternative therapeutic targets. Angiogenesis. 2017 Nov;20(4):409-426. doi: 10.1007/s10456-017-9562-9. Epub 2017 Jun 28. PMID: 28660302.
59. Ferrara N, Hillan KJ, Novotny W. Bevacizumab (Avastin), a humanized anti-VEGF monoclonal antibody for cancer therapy. Biochem Biophys Res Commun. 2005 Jul 29;333(2):328-35. doi: 10.1016/j.bbrc.2005.05.132. PMID: 15961063.
60. Garcia J, Hurwitz HI, Sandler AB, Miles D, Coleman RL, Deurloo R, Chinot OL. Bevacizumab (Avastin®) in cancer treatment: A review of 15 years of clinical experience and future outlook. Cancer Treat Rev. 2020 Jun;86:102017. doi: 10.1016/j.ctrv.2020.102017. Epub 2020 Mar 26. PMID: 32335505.
61. Pan Y, Yu Y, Wang X, Zhang T. Tumor-Associated Macrophages in Tumor Immunity. Front Immunol. 2020 Dec 3;11:583084. doi: 10.3389/fimmu.2020.583084. Erratum in: Front Immunol. 2021 Dec 10;12:775758. PMID: 33365025; PMCID: PMC7751482.
62. Zou Z, Lin H, Li M, Lin B. Tumor-associated macrophage polarization in the inflammatory tumor microenvironment. Front Oncol. 2023 Feb 2;13:1103149. doi: 10.3389/fonc.2023.1103149. PMID: 36816959; PMCID: PMC9934926.
63. Priceman SJ, Sung JL, Shaposhnik Z, Burton JB, Torres-Collado AX, Moughon DL, Johnson M, Lusis AJ, Cohen DA, Iruela-Arispe ML, Wu L. Targeting distinct tumor-infiltrating myeloid cells by inhibiting CSF-1 receptor: combating tumor evasion of antiangiogenic therapy. Blood. 2010 Feb 18;115(7):1461-71. doi: 10.1182/blood-2009-08-237412. Epub 2009 Dec 11. PMID: 20008303; PMCID: PMC2826767.
64. Edwards JG, Cox G, Andi A, Jones JL, Walker RA, Waller DA, O'Byrne KJ. Angiogenesis is an independent prognostic factor in malignant mesothelioma. Br J Cancer. 2001 Sep 14;85(6):863-8. doi: 10.1054/bjoc.2001.1997. PMID: 11556838; PMCID: PMC2375086
65. Zalcman G, Mazieres J, Margery J, Greillier L, Audigier-Valette C, Moro-Sibilot D, Molinier O, Corre R, Monnet I, Gounant V, Rivière F, Janicot H, Gervais R, Locher C, Milleron B, Tran Q, Lebitasy MP, Morin F, Creveuil C, Parienti JJ, Scherpereel A; French Cooperative

Thoracic Intergroup (IFCT). Bevacizumab for newly diagnosed pleural mesothelioma in the Mesothelioma Avastin Cisplatin Pemetrexed Study (MAPS): a randomised, controlled, open-label, phase 3 trial. Lancet. 2016 Apr 2;387(10026):1405-1414. doi: 10.1016/S0140-6736(15)01238-6. Epub 2015 Dec 21. Erratum in: Lancet. 2016 Apr 2;387(10026):e24. PMID: 26719230.

66. Popat S, Baas P, Faivre-Finn C, Girard N, Nicholson AG, Nowak AK, Opitz I, Scherpereel A, Reck M; ESMO Guidelines Committee. Electronic address: clinicalguidelines@esmo.org. Malignant pleural mesothelioma: ESMO Clinical Practice Guidelines for diagnosis, treatment and follow-up☆. Ann Oncol. 2022 Feb;33(2):129-142. doi: 10.1016/j.annonc.2021.11.005. Epub 2021 Nov 30. PMID: 34861373.
67. Krüger-Genge A, Blocki A, Franke RP, Jung F. Vascular Endothelial Cell Biology: An Update. Int J Mol Sci. 2019 Sep 7;20(18):4411. doi: 10.3390/ijms20184411. PMID: 31500313; PMCID: PMC6769656.
68. Sturtzel C. Endothelial Cells. Adv Exp Med Biol. 2017;1003:71-91. doi: 10.1007/978-3-319-57613-8_4. PMID: 28667554.
69. Pober JS, Sessa WC. Evolving functions of endothelial cells in inflammation. Nat Rev Immunol. 2007 Oct;7(10):803-15. doi: 10.1038/nri2171. PMID: 17893694.
70. Øynebråten I, Bakke O, Brandtzaeg P, Johansen FE, Haraldsen G. Rapid chemokine secretion from endothelial cells originates from 2 distinct compartments. Blood. 2004 Jul 15;104(2):314-20. doi: 10.1182/blood-2003-08-2891. Epub 2004 Mar 25. PMID: 15044249.
71. Ridiandries A, Tan JT, Bursill CA. The Role of CC-Chemokines in the Regulation of Angiogenesis. Int J Mol Sci. 2016 Nov 8;17(11):1856. doi: 10.3390/ijms17111856. PMID: 27834814; PMCID: PMC5133856.
72. Alon R, Feigelson S. From rolling to arrest on blood vessels: leukocyte tap dancing on endothelial integrin ligands and chemokines at sub-second contacts. Semin Immunol. 2002 Apr;14(2):93-104. doi: 10.1006/smim.2001.0346. PMID: 11978081.
73. Bevilacqua MP. Endothelial-leukocyte adhesion molecules. Annu Rev Immunol. 1993;11:767-804. doi: 10.1146/annurev.iy.11.040193.004003. PMID: 8476577.
74. Bui TM, Wiesolek HL, Sumagin R. ICAM-1: A master regulator of cellular responses in inflammation, injury resolution, and tumorigenesis. J Leukoc Biol. 2020 Sep;108(3):787-799. doi: 10.1002/JLB.2MR0220-549R. Epub 2020 Mar 17. PMID: 32182390; PMCID: PMC7977775.
75. Hubbard AK, Rothlein R. Intercellular adhesion molecule-1 (ICAM-1) expression and cell signaling cascades. Free Radic Biol Med. 2000 May 1;28(9):1379-86.

76. Cook-Mills JM, Marchese ME, Abdala-Valencia H. Vascular cell adhesion molecule-1 expression and signaling during disease: regulation by reactive oxygen species and antioxidants. Antioxid Redox Signal. 2011 Sep 15;15(6):1607-38. doi: 10.1089/ars.2010.3522. Epub 2011 May 11. PMID: 21050132; PMCID: PMC3151426.
77. Cerutti C, Ridley AJ. Endothelial cell-cell adhesion and signaling. Exp Cell Res. 2017 Sep 1;358(1):31-38. doi: 10.1016/j.yexcr.2017.06.003. Epub 2017 Jun 8. PMID: 28602626; PMCID: PMC5700119.
78. Weishaupt C, Steinert M, Brunner G, Schulze HJ, Fuhlbrigge RC, Goerge T, Loser K. Activation of human vascular endothelium in melanoma metastases induces ICAM-1 and E-selectin expression and results in increased infiltration with effector lymphocytes. Exp Dermatol. 2019 Nov;28(11):1258-1269. doi: 10.1111/exd.14023. Epub 2019 Sep 9. PMID: 31444891.
79. Fisher DT, Chen Q, Skitzki JJ, Muhitch JB, Zhou L, Appenheimer MM, Vardam TD, Weis EL, Passanese J, Wang WC, Gollnick SO, Dewhirst MW, Rose-John S, Repasky EA, Baumann H, Evans SS. IL-6 trans-signaling licenses mouse and human tumor microvascular gateways for trafficking of cytotoxic T cells. J Clin Invest. 2011 Oct;121(10):3846-59. doi: 10.1172/JCI44952. Epub 2011 Sep 19. PMID: 21926464; PMCID: PMC3195455.
80. Burdick MM, Henson KA, Delgadillo LF, Choi YE, Goetz DJ, Tees DF, Benencia F. Expression of E-selectin ligands on circulating tumor cells: cross-regulation with cancer stem cell regulatory pathways? Front Oncol. 2012 Aug 20;2:103. doi: 10.3389/fonc.2012.00103. PMID: 22934288; PMCID: PMC3422812
81. Di D, Chen L, Wang L, Sun P, Liu Y, Xu Z, Ju J. Downregulation of human intercellular adhesion molecule-1 attenuates the metastatic ability in human breast cancer cell lines. Oncol Rep. 2016 Mar;35(3):1541-8. doi: 10.3892/or.2016.4543. Epub 2016 Jan 5. PMID: 26751847.
82. Shen CK, Huang BR, Yeh WL, Chen CW, Liu YS, Lai SW, Tseng WP, Lu DY, Tsai CF. Regulatory effects of IL-1β in the interaction of GBM and tumor-associated monocyte through VCAM-1 and ICAM-1. Eur J Pharmacol. 2021 Aug 15;905:174216. doi: 10.1016/j.ejphar.2021.174216. Epub 2021 May 28. PMID: 34058204.
83. Chen M, Wu C, Fu Z, Liu S. ICAM1 promotes bone metastasis via integrin-mediated TGF-β/EMT signaling in triple-negative breast cancer. Cancer Sci. 2022 Nov;113(11):3751-3765. doi: 10.1111/cas.15532. Epub 2022 Aug 26. PMID: 35969372; PMCID: PMC9633300.
84. Huinen ZR, Huijbers EJM, van Beijnum JR, Nowak-Sliwinska P, Griffioen AW. Anti-angiogenic agents - overcoming tumour endothelial cell anergy and improving

immunotherapy outcomes. Nat Rev Clin Oncol. 2021 Aug;18(8):527-540. doi: 10.1038/s41571-021-00496-y. Epub 2021 Apr 8. PMID: 33833434.

85. Chouaib S, Noman MZ, Kosmatopoulos K, Curran MA. Hypoxic stress: obstacles and opportunities for innovative immunotherapy of cancer. Oncogene. 2017 Jan 26;36(4):439-445. doi: 10.1038/onc.2016.225. Epub 2016 Jun 27. PMID: 27345407; PMCID: PMC5937267
86. Raab, O. Uber die Wirkung fluoreszierender Stoffe auf Infusorien. Zeitung Biol. 39, 524–526 (1900).
87. von Tappeiner, H. & Jodlbauer, A. Die sensiblilisierende Wirkung fluoreszierender Substanzer Gesammte Untersuchungen uber die photodynamische Erscheinerung (Voger, F. C., Leipzig, 1907).
88. Gunaydin G, Gedik ME, Ayan S. Photodynamic Therapy-Current Limitations and Novel Approaches. Front Chem. 2021 Jun 10;9:691697. doi: 10.3389/fchem.2021.691697. PMID: 34178948; PMCID: PMC8223074.
89. Brieger K, Schiavone S, Miller FJ Jr, Krause KH. Reactive oxygen species: from health to disease. Swiss Med Wkly. 2012 Aug 17;142:w13659. doi: 10.4414/smw.2012.13659. PMID: 22903797.
90. Kelly JF, Snell ME. Hematoporphyrin derivative: a possible aid in the diagnosis and therapy of carcinoma of the bladder. J Urol. 1976 Feb;115(2):150-1. doi: 10.1016/s0022-5347(17)59108-9. PMID: 1249866.
91. Cohen DK, Lee PK. Photodynamic Therapy for Non-Melanoma Skin Cancers. Cancers (Basel). 2016 Oct 4;8(10):90. doi: 10.3390/cancers8100090. PMID: 27782043; PMCID: PMC5082380.
92. Baldea I, Giurgiu L, Teacoe ID, Olteanu DE, Olteanu FC, Clichici S, Filip GA. Photodynamic Therapy in Melanoma - Where do we Stand? Curr Med Chem. 2018;25(40):5540-5563. doi: 10.2174/0929867325666171226115626. PMID: 29278205.
93. Kaleta-Richter M, Kawczyk-Krupka A, Aebisher D, Bartusik-Aebisher D, Czuba Z, Cieślar G. The capability and potential of new forms of personalized colon cancer treatment: Immunotherapy and Photodynamic Therapy. Photodiagnosis Photodyn Ther. 2019 Mar;25:253-258. doi: 10.1016/j.pdpdt.2019.01.004. Epub 2019 Jan 3. PMID: 30611864.
94. Meulemans J, Delaere P, Vander Poorten V. Photodynamic therapy in head and neck cancer: indications, outcomes, and future prospects. Curr Opin Otolaryngol Head Neck Surg. 2019 Apr;27(2):136-141. doi: 10.1097/MOO.0000000000000521. PMID: 30724766.
95. Ostańska E, Aebisher D, Bartusik-Aebisher D. The potential of photodynamic therapy in current breast cancer treatment methodologies. Biomed Pharmacother. 2021

May;137:111302. doi: 10.1016/j.biopha.2021.111302. Epub 2021 Jan 28. PMID: 33517188.

96. Lou J, Aragaki M, Bernards N, Chee T, Gregor A, Hiraishi Y, Ishiwata T, Leung C, Ding L, Kitazawa S, Koga T, Sata Y, Ogawa H, Chen J, Kato T, Yasufuku K, Zheng G. Repeated photodynamic therapy mediates the abscopal effect through multiple innate and adaptive immune responses with and without immune checkpoint therapy. Biomaterials. 2023 Jan;292:121918. doi: 10.1016/j.biomaterials.2022.121918. Epub 2022 Nov 17. PMID: 36442438.
97. Lou J, Aragaki M, Bernards N, Kinoshita T, Mo J, Motooka Y, Ishiwata T, Gregor A, Chee T, Chen Z, Chen J, Kaga K, Wakasa S, Zheng G, Yasufuku K. Repeated porphyrin lipoprotein-based photodynamic therapy controls distant disease in mouse mesothelioma via the abscopal effect. Nanophotonics. 2021 Aug 3;10(12):3279-3294. doi: 10.1515/nanoph-2021-0241. PMID: 36405502; PMCID: PMC9646247
98. Xie Q, Li Z, Liu Y, Zhang D, Su M, Niitsu H, Lu Y, Coffey RJ, Bai M. Translocator protein-targeted photodynamic therapy for direct and abscopal immunogenic cell death in colorectal cancer. Acta Biomater. 2021 Oct 15;134:716-729. doi: 10.1016/j.actbio.2021.07.052. Epub 2021 Jul 27. PMID: 34329783; PMCID: PMC8802307.
99. Netea MG, Domínguez-Andrés J, Barreiro LB, Chavakis T, Divangahi M, Fuchs E, Joosten LAB, van der Meer JWM, Mhlanga MM, Mulder WJM, Riksen NP, Schlitzer A, Schultze JL, Stabell Benn C, Sun JC, Xavier RJ, Latz E. Defining trained immunity and its role in health and disease. Nat Rev Immunol. 2020 Jun;20(6):375-388. doi: 10.1038/s41577-020-0285-6. Epub 2020 Mar 4. PMID: 32132681; PMCID: PMC7186935.
100. Byrne A, Savas P, Sant S, Li R, Virassamy B, Luen SJ, Beavis PA, Mackay LK, Neeson PJ, Loi S. Tissue-resident memory T cells in breast cancer control and immunotherapy responses. Nat Rev Clin Oncol. 2020 Jun;17(6):341-348. doi: 10.1038/s41571-020-0333-y. Epub 2020 Feb 28. PMID: 32112054.
101. Huis In 't Veld RV, Lara P, Jager MJ, Koning RI, Ossendorp F, Cruz LJ. M1-derived extracellular vesicles enhance photodynamic therapy and promote immunological memory in preclinical models of colon cancer. J Nanobiotechnology. 2022 Jun 3;20(1):252. doi: 10.1186/s12951-022-01448-z. PMID: 35658868; PMCID: PMC9164362.
102. Yu X, Gao D, Gao L, Lai J, Zhang C, Zhao Y, Zhong L, Jia B, Wang F, Chen X, Liu Z. Inhibiting Metastasis and Preventing Tumor Relapse by Triggering Host Immunity with Tumor-Targeted Photodynamic Therapy Using Photosensitizer-Loaded Functional

Nanographenes. ACS Nano. 2017 Oct 24;11(10):10147-10158. doi: 10.1021/acsnano.7b04736. Epub 2017 Sep 18. PMID: 28901740.

103. Yuan Z, Fan G, Wu H, Liu C, Zhan Y, Qiu Y, Shou C, Gao F, Zhang J, Yin P, Xu K. Photodynamic therapy synergizes with PD-L1 checkpoint blockade for immunotherapy of CRC by multifunctional nanoparticles. Mol Ther. 2021 Oct 6;29(10):2931-2948. doi: 10.1016/j.ymthe.2021.05.017. Epub 2021 May 21. PMID: 34023507; PMCID: PMC8530932.
104. Hao Y, Chung CK, Gu Z, Schomann T, Dong X, Veld RVHI', Camps MGM, Ten Dijke P, Ossendorp FA, Cruz LJ. Combinatorial therapeutic approaches of photodynamic therapy and immune checkpoint blockade for colon cancer treatment. Mol Biomed. 2022 Aug 17;3(1):26. doi: 10.1186/s43556-022-00086-z. PMID: 35974207; PMCID: PMC9381671.
105. Kleinovink JW, Fransen MF, Löwik CW, Ossendorp F. Photodynamic-Immune Checkpoint Therapy Eradicates Local and Distant Tumors by CD8+ T Cells. Cancer Immunol Res. 2017 Oct;5(10):832-838. doi: 10.1158/2326-6066.CIR-17-0055. Epub 2017 Aug 29. PMID: 28851692.
106. Huang Z, Wei G, Zeng Z, Huang Y, Huang L, Shen Y, Sun X, Xu C, Zhao C. Enhanced cancer therapy through synergetic photodynamic/immune checkpoint blockade mediated by a liposomal conjugate comprised of porphyrin and IDO inhibitor. Theranostics. 2019 Jul 29;9(19):5542-5557. doi: 10.7150/thno.35343. PMID: 31534502; PMCID: PMC6735384.
107. Wu Q, Chen Y, Li Q, Chen J, Mo J, Jin M, Yang Q, Rizzello L, Tian X, Luo L. Time Rules the Efficacy of Immune Checkpoint Inhibitors in Photodynamic Therapy. Adv Sci (Weinh). 2022 Jul;9(21):e2200999. doi: 10.1002/advs.202200999. Epub 2022 Apr 25. PMID: 35470595; PMCID: PMC9313507.
108. Buytaert E, Dewaele M, Agostinis P. Molecular effectors of multiple cell death pathways initiated by photodynamic therapy. Biochim Biophys Acta. 2007 Sep;1776(1):86-107. doi: 10.1016/j.bbcan.2007.07.001. Epub 2007 Jul 6. PMID: 17693025.
109. Gollnick SO, Liu X, Owczarczak B, Musser DA, Henderson BW. Altered expression of interleukin 6 and interleukin 10 as a result of photodynamic therapy in vivo. Cancer Res. 1997 Sep 15;57(18):3904-9. PMID: 9307269.
110. Yom SS, Busch TM, Friedberg JS, Wileyto EP, Smith D, Glatstein E, Hahn SM. Elevated serum cytokine levels in mesothelioma patients who have undergone pleurectomy or extrapleural pneumonectomy and adjuvant intraoperative photodynamic therapy. Photochem Photobiol. 2003 Jul;78(1):75-81. doi: 10.1562/0031-8655(2003)078<0075:esclim>2.0.co;2. PMID: 12929752.
111. Gollnick SO, Evans SS, Baumann H, Owczarczak B, Maier P, Vaughan L, Wang WC, Unger E, Henderson BW. Role of cytokines in photodynamic therapy-induced local and systemic

inflammation. Br J Cancer. 2003 Jun 2;88(11):1772-9. doi: 10.1038/sj.bjc.6600864. PMID: 12771994; PMCID: PMC2377133.

112. Wang Y, Perentes JY, Schäfer SC, Gonzalez M, Debefve E, Lehr HA, van den Bergh H, Krueger T. Photodynamic drug delivery enhancement in tumours does not depend on leukocyte-endothelial interaction in a human mesothelioma xenograft model. Eur J Cardiothorac Surg. 2012 Aug;42(2):348-54.
113. Hendrzak-Henion JA, Knisely TL, Cincotta L, Cincotta E, Cincotta AH. Role of the immune system in mediating the antitumor effect of benzophenothiazine photodynamic therapy. Photochem Photobiol. 1999 May;69(5):575-81. PMID: 10333764.
114. Castano AP, Mroz P, Hamblin MR. Photodynamic therapy and anti-tumour immunity. Nat Rev Cancer. 2006 Jul;6(7):535-45. doi: 10.1038/nrc1894. PMID: 16794636; PMCID: PMC2933780.
115. Korbelik M, Krosl G, Krosl J, Dougherty GJ. The role of host lymphoid populations in the response of mouse EMT6 tumor to photodynamic therapy. Cancer Res. 1996 Dec 15;56(24):5647-52. PMID: 8971170.
116. Henderson BW, Waldow SM, Mang TS, Potter WR, Malone PB, Dougherty TJ. Tumor destruction and kinetics of tumor cell death in two experimental mouse tumors following photodynamic therapy. Cancer Res. 1985 Feb;45(2):572-6. PMID: 3967232.
117. Busch TM, Wileyto EP, Emanuele MJ, Del Piero F, Marconato L, Glatstein E, Koch CJ. Photodynamic therapy creates fluence rate-dependent gradients in the intratumoral spatial distribution of oxygen. Cancer Res. 2002 Dec 15;62(24):7273-9. PMID: 12499269.
118. Fingar VH, Kik PK, Haydon PS, Cerrito PB, Tseng M, Abang E, Wieman TJ. Analysis of acute vascular damage after photodynamic therapy using benzoporphyrin derivative (BPD). Br J Cancer. 1999 Apr;79(11-12):1702-8. doi: 10.1038/sj.bjc.6690271. PMID: 10206280; PMCID: PMC2362794.
119. Star WM, Marijnissen HP, van den Berg-Blok AE, Versteeg JA, Franken KA, Reinhold HS. Destruction of rat mammary tumor and normal tissue microcirculation by hematoporphyrin derivative photoradiation observed in vivo in sandwich observation chambers. Cancer Res. 1986 May;46(5):2532-40. PMID: 3697992.
120. Piette J. Signalling pathway activation by photodynamic therapy: NF-κB at the crossroad between oncology and immunology. Photochem Photobiol Sci. 2015 Aug;14(8):1510-7.
121. Sitnik TM, Hampton JA, Henderson BW. Reduction of tumour oxygenation during and after photodynamic therapy in vivo: effects of fluence rate. Br J Cancer. 1998 May;77(9):1386-94. doi: 10.1038/bjc.1998.231. PMID: 9652753; PMCID: PMC2150183
122. Henderson BW, Gollnick SO, Snyder JW, Busch TM, Kousis PC, Cheney RT, Morgan J. Choice of oxygen-conserving treatment regimen determines the inflammatory response

and outcome of photodynamic therapy of tumors. Cancer Res. 2004 Mar 15;64(6):2120-6. doi: 10.1158/0008-5472.can-03-3513. PMID: 15026352.

123. van den Boogert J, van Staveren HJ, de Bruin RW, Eikelaar JH, Siersema PD, van Hillegersberg R. Photodynamic therapy for esophageal lesions: selectivity depends on wavelength, power, and light dose. Ann Thorac Surg. 1999 Nov;68(5):1763-9. doi: 10.1016/s0003-4975(99)01003-6. PMID: 10585056.
124. Efendiev KT, Alekseeva PM, Shiryaev AA, Skobeltsin AS, Solonina IL, Fatyanova AS, Reshetov IV, Loschenov VB. Preliminary low-dose photodynamic exposure to skin cancer with chlorin e6 photosensitizer. Photodiagnosis Photodyn Ther. 2022 Jun;38:102894. doi: 10.1016/j.pdpdt.2022.102894. Epub 2022 Apr 28. PMID: 35490962.
125. Liu AH, Sun X, Wei XQ, Zhang YZ. Efficacy of multiple low-dose photodynamic TMPYP4 therapy on cervical cancer tumour growth in nude mice. Asian Pac J Cancer Prev. 2013;14(9):5371-4. doi: 10.7314/apjcp.2013.14.9.5371. PMID: 24175828.
126. Cavin S, Gkasti A, Faget J, Hao Y, Letovanec I, Reichenbach M, Gonzalez M, Krueger T, Dyson PJ, Meylan E, Perentes JY. Low-dose photodynamic therapy promotes a cytotoxic immunological response in a murine model of pleural mesothelioma. Eur J Cardiothorac Surg. 2020 Oct 1;58(4):783-791. doi: 10.1093/ejcts/ezaa145. PMID: 32372095.
127. Perentes JY, Wang Y, Wang X, Abdelnour E, Gonzalez M, Decosterd L, Wagnieres G, van den Bergh H, Peters S, Ris HB, Krueger T. Low-Dose Vascular Photodynamic Therapy Decreases Tumor Interstitial Fluid Pressure, which Promotes Liposomal Doxorubicin Distribution in a Murine Sarcoma Metastasis Model. Transl Oncol. 2014 May 13;7(3):393–9. doi: 10.1016/j.tranon.2014.04.010. Epub ahead of print. PMID: 24836648; PMCID: PMC4145392.
128. Cavin S, Riedel T, Rosskopfova P, Gonzalez M, Baldini G, Zellweger M, Wagnières G, Dyson PJ, Ris HB, Krueger T, Perentes JY. Vascular-targeted low dose photodynamic therapy stabilizes tumor vessels by modulating pericyte contractility. Lasers Surg Med. 2019 Aug;51(6):550-561. doi: 10.1002/lsm.23069. Epub 2019 Feb 19. PMID: 30779366.
129. Krueger T, Altermatt HJ, Mettler D, Scholl B, Magnusson L, Ris HB. Experimental photodynamic therapy for malignant pleural mesothelioma with pegylated mTHPC. Lasers Surg Med. 2003;32(1):61-8. doi: 10.1002/lsm.10113. PMID: 12516073.
130. Wang X, Gronchi F, Bensimon M, Mercier T, Decosterd LA, Wagnières G, Debefve E, Ris HB, Letovanec I, Peters S, Perentes JY. Treatment of pleural malignancies by photo-induction combined to systemic chemotherapy: Proof of concept on rodent lung tumors and feasibility study on porcine chest cavities. Lasers Surg Med. 2015 Dec;47(10):807-16.

131. Krueger T, Pan Y, Tran N, Altermatt HJ, Opitz I, Ris HB. Intraoperative photodynamic therapy of the chest cavity in malignant pleural mesothelioma bearing rats. Lasers Surg Med. 2005 Oct;37(4):271-7
132. Cavin S, Riedel T, Rosskopfova P, Gonzalez M, Baldini G, Zellweger M et al. Vascular-targeted low dose photodynamic therapy stabilizes tumor vessels by modulating pericyte contractility. Lasers Surg Med 2019;51:550–61.
133. McCorkell KA, May MJ. NEMO-binding domain peptide inhibition of inflammatory signal-induced NF-κB activation in vivo. Methods Mol Biol. 2015;1280:505-25.
134. Casanova-Acebes M, Nicolás-Ávila JA, Li JL, García-Silva S, Balachander A, Rubio-Ponce A, Weiss LA, Adrover JM, Burrows K, A-González N, Ballesteros I, Devi S, Quintana JA, Crainiciuc G, Leiva M, Gunzer M, Weber C, Nagasawa T, Soehnlein O, Merad M, Mortha A, Ng LG, Peinado H, Hidalgo A. Neutrophils instruct homeostatic and pathological states in naive tissues. J Exp Med. 2018 Nov 5;215(11):2778-2795
135. De La Maza L, Wu M, Wu L, Yun H, Zhao Y, Cattral M et al. In situ vaccination after accelerated hypofractionated radiation and surgery in a mesothelioma mouse model. Clin Cancer Res 2017;23:5502–13.
136. Grasso CS, Tsoi J, Onyshchenko M, Abril-Rodriguez G, Ross-Macdonald P, Wind-Rotolo M, Champhekar A, Medina E, Torrejon DY, Shin DS, Tran P, Kim YJ, Puig-Saus C, Campbell K, Vega-Crespo A, Quist M, Martignier C, Luke JJ, Wolchok JD, Johnson DB, Chmielowski B, Hodi FS, Bhatia S, Sharfman W, Urba WJ, Slingluff CL Jr, Diab A, Haanen JBAG, Algarra SM, Pardoll DM, Anagnostou V, Topalian SL, Velculescu VE, Speiser DE, Kalbasi A, Ribas A. Conserved Interferon-γ Signaling Drives Clinical Response to Immune Checkpoint Blockade Therapy in Melanoma. Cancer Cell. 2020 Oct 12;38(4):500-515.e3.
137. Entenberg D, Oktay MH, Condeelis JS. Intravital imaging to study cancer progression and metastasis. Nat Rev Cancer. 2023 Jan;23(1):25-42. doi: 10.1038/s41568-022-00527-5. Epub 2022 Nov 16. PMID: 36385560; PMCID: PMC9912378.
138. Boulch M, Grandjean CL, Cazaux M, Bousso P. Tumor Immunosurveillance and Immunotherapies: A Fresh Look from Intravital Imaging. Trends Immunol. 2019 Nov;40(11):1022-1034. doi: 10.1016/j.it.2019.09.002. Epub 2019 Oct 23. PMID: 31668676.
139. Croci D, Zomer A, Kowal J, Joyce JA. Cranial imaging window implantation technique for longitudinal multimodal imaging of the brain environment in live mice. STAR Protoc. 2023 Mar 24;4(2):102197. doi: 10.1016/j.xpro.2023.102197. Epub ahead of print. PMID: 36964905; PMCID: PMC10050773.
140. Seynhaeve ALB, Ten Hagen TLM. Intravital Microscopy of Tumor-associated Vasculature Using Advanced Dorsal Skinfold Window Chambers on Transgenic Fluorescent Mice. J

Vis Exp. 2018 Jan 19;(131):55115. doi: 10.3791/55115. PMID: 29443052; PMCID: PMC5908657.

141. Entenberg D, Voiculescu S, Guo P, Borriello L, Wang Y, Karagiannis GS, Jones J, Baccay F, Oktay M, Condeelis J. A permanent window for the murine lung enables high-resolution imaging of cancer metastasis. Nat Methods. 2018 Jan;15(1):73-80. doi: 10.1038/nmeth.4511. Epub 2017 Nov 27. PMID: 29176592; PMCID: PMC5755704.
142. Schindler U, Baichwal VR. Three NF-kappa B binding sites in the human E-selectin gene required for maximal tumor necrosis factor alpha-induced expression. Mol Cell Biol. 1994 Sep;14(9):5820-31.
143. Hanahan D. Hallmarks of Cancer: New Dimensions. Cancer Discov. 2022 Jan;12(1):31-46. doi: 10.1158/2159-8290.CD-21-1059. PMID: 35022204.
144. Hanahan D, Weinberg RA. Hallmarks of cancer: the next generation. Cell. 2011 Mar 4;144(5):646-74. doi: 10.1016/j.cell.2011.02.013. PMID: 21376230.
145. Willimsky G, Blankenstein T. Sporadic immunogenic tumours avoid destruction by inducing T-cell tolerance. Nature. 2005 Sep 1;437(7055):141-6. doi: 10.1038/nature03954. PMID: 16136144.
146. Zitvogel L, Tesniere A, Kroemer G. Cancer despite immunosurveillance: immunoselection and immunosubversion. Nat Rev Immunol. 2006 Oct;6(10):715-27. doi: 10.1038/nri1936. Epub 2006 Sep 15. PMID: 16977338.
147. Togashi Y, Shitara K, Nishikawa H. Regulatory T cells in cancer immunosuppression - implications for anticancer therapy. Nat Rev Clin Oncol. 2019 Jun;16(6):356-371. doi: 10.1038/s41571-019-0175-7. PMID: 30705439.
148. Curiel TJ, Coukos G, Zou L, Alvarez X, Cheng P, Mottram P, Evdemon-Hogan M, Conejo-Garcia JR, Zhang L, Burow M, Zhu Y, Wei S, Kryczek I, Daniel B, Gordon A, Myers L, Lackner A, Disis ML, Knutson KL, Chen L, Zou W. Specific recruitment of regulatory T cells in ovarian carcinoma fosters immune privilege and predicts reduced survival. Nat Med. 2004 Sep;10(9):942-9. doi: 10.1038/nm1093. Epub 2004 Aug 22. PMID: 15322536.
149. Gobert M, Treilleux I, Bendriss-Vermare N, Bachelot T, Goddard-Leon S, Arfi V, Biota C, Doffin AC, Durand I, Olive D, Perez S, Pasqual N, Faure C, Ray-Coquard I, Puisieux A, Caux C, Blay JY, Ménétrier-Caux C. Regulatory T cells recruited through CCL22/CCR4 are selectively activated in lymphoid infiltrates surrounding primary breast tumors and lead to an adverse clinical outcome. Cancer Res. 2009 Mar 1;69(5):2000-9. doi: 10.1158/0008-5472.CAN-08-2360. Epub 2009 Feb 24. PMID: 19244125.
150. Grossman WJ, Verbsky JW, Barchet W, Colonna M, Atkinson JP, Ley TJ. Human T regulatory cells can use the perforin pathway to cause autologous target cell death.

Immunity. 2004 Oct;21(4):589-601. doi: 10.1016/j.immuni.2004.09.002. PMID: 15485635.

151. Thornton AM, Shevach EM. CD4+CD25+ immunoregulatory T cells suppress polyclonal T cell activation in vitro by inhibiting interleukin 2 production. J Exp Med. 1998 Jul 20;188(2):287-96. doi: 10.1084/jem.188.2.287. PMID: 9670041; PMCID: PMC2212461
152. Jarnicki AG, Lysaght J, Todryk S, Mills KH. Suppression of antitumor immunity by IL-10 and TGF-beta-producing T cells infiltrating the growing tumor: influence of tumor environment on the induction of CD4+ and CD8+ regulatory T cells. J Immunol. 2006 Jul 15;177(2):896-904. doi: 10.4049/jimmunol.177.2.896. PMID: 16818744.
153. Zhang W, Borcherding N, Kolb R. IL-1 Signaling in Tumor Microenvironment. Adv Exp Med Biol. 2020;1240:1-23. doi: 10.1007/978-3-030-38315-2_1. PMID: 32060884.
154. Gilmore TD. The Re1/NF-kappa B/I kappa B signal transduction pathway and cancer. Cancer Treat Res. 2003;115:241-65.
155. Stratton MR, Campbell PJ, Futreal PA. The cancer genome. Nature. 2009 Apr 9;458(7239):719-24.
156. Salazar L, Kashiwada T, Krejci P, Meyer AN, Casale M, Hallowell M, Wilcox WR, Donoghue DJ, Thompson LM. Fibroblast growth factor receptor 3 interacts with and activates TGFβ-activated kinase 1 tyrosine phosphorylation and NFκB signaling in multiple myeloma and bladder cancer. PLoS One. 2014 Jan 23;9(1):e86470.
157. Kim SH, Ezhilarasan R, Phillips E, Gallego-Perez D, Sparks A, Taylor D, Ladner K, Furuta T, Sabit H, Chhipa R, Cho JH, Mohyeldin A, Beck S, Kurozumi K, Kuroiwa T, Iwata R, Asai A, Kim J, Sulman EP, Cheng SY, Lee LJ, Nakada M, Guttridge D, DasGupta B, Goidts V, Bhat KP, Nakano I. Serine/Threonine Kinase MLK4 Determines Mesenchymal Identity in Glioma Stem Cells in an NF-κB-dependent Manner. Cancer Cell. 2016 Feb 8;29(2):201-13.
158. Köntgen F, Grumont RJ, Strasser A, Metcalf D, Li R, Tarlinton D, Gerondakis S. Mice lacking the c-rel proto-oncogene exhibit defects in lymphocyte proliferation, humoral immunity, and interleukin-2 expression. Genes Dev. 1995 Aug 15;9(16):1965-77.
159. Amato CM, Hintzsche JD, Wells K, Applegate A, Gorden NT, Vorwald VM, Tobin RP, Nassar K, Shellman YG, Kim J, Medina TM, Rioth M, Lewis KD, McCarter MD, Gonzalez R, Tan AC, Robinson WA. Pre-Treatment Mutational and Transcriptomic Landscape of Responding Metastatic Melanoma Patients to Anti-PD1 Immunotherapy. Cancers (Basel). 2020 Jul 17;12(7):1943.
160. Volanti C, Matroule JY, Piette J. Involvement of oxidative stress in NF-kappaB activation in endothelial cells treated by photodynamic therapy. Photochem Photobiol. 2002 Jan;75(1):36-45.

161. Brasier AR. The nuclear factor-kappaB-interleukin-6 signalling pathway mediating vascular inflammation. Cardiovasc Res. 2010 May 1;86(2):211-8.
162. Fukano R, Matsubara T, Inoue T, Gondo T, Ichiyama T, Furukawa S. Time lag between the increase of IL-6 with fever and NF-kappaB activation in the peripheral blood in inflammatory myofibroblastic tumor. Cytokine. 2008 Nov;44(2):293-7.
163. Jain RK. Therapeutic implications of tumor physiology. Curr Opin Oncol. 1991 Dec;3(6):1105-8. doi: 10.1097/00001622-199112000-00020. PMID: 1843113
164. Lamplugh Z, Fan Y. Vascular Microenvironment, Tumor Immunity and Immunotherapy. Front Immunol. 2021 Dec 20;12:811485. doi: 10.3389/fimmu.2021.811485. PMID: 34987525; PMCID: PMC8720970.
165. Goel S, Duda DG, Xu L, Munn LL, Boucher Y, Fukumura D, Jain RK. Normalization of the vasculature for treatment of cancer and other diseases. Physiol Rev. 2011 Jul;91(3):1071-121. doi: 10.1152/physrev.00038.2010. Erratum in: Physiol Rev. 2014 Apr;94(2):707. PMID: 21742796; PMCID: PMC3258432.
166. Kozin SV, Boucher Y, Hicklin DJ, Bohlen P, Jain RK, Suit HD. Vascular endothelial growth factor receptor-2-blocking antibody potentiates radiation-induced long-term control of human tumor xenografts. Cancer Res. 2001 Jan 1;61(1):39-44. PMID: 11196192.
167. Tvorogov D, Anisimov A, Zheng W, Leppänen VM, Tammela T, Laurinavicius S, Holnthoner W, Heloterä H, Holopainen T, Jeltsch M, Kalkkinen N, Lankinen H, Ojala PM, Alitalo K. Effective suppression of vascular network formation by combination of antibodies blocking VEGFR ligand binding and receptor dimerization. Cancer Cell. 2010 Dec 14;18(6):630-40. doi: 10.1016/j.ccr.2010.11.001. Epub 2010 Dec 2. PMID: 21130043.
168. Juan TY, Roffler SR, Hou HS, Huang SM, Chen KC, Leu YL, Prijovich ZM, Yu CP, Wu CC, Sun GH, Cha TL. Antiangiogenesis targeting tumor microenvironment synergizes glucuronide prodrug antitumor activity. Clin Cancer Res. 2009 Jul 15;15(14):4600-11. doi: 10.1158/1078-0432.CCR-09-0090. Epub 2009 Jul 7. PMID: 19584154.
169. Hamzah J, Jugold M, Kiessling F, Rigby P, Manzur M, Marti HH, Rabie T, Kaden S, Gröne HJ, Hämmerling GJ, Arnold B, Ganss R. Vascular normalization in Rgs5-deficient tumours promotes immune destruction. Nature. 2008 May 15;453(7193):410-4. doi: 10.1038/nature06868. Epub 2008 Apr 16. PMID: 18418378.
170. Ma W, Wang Y, Zhang R, Yang F, Zhang D, Huang M, Zhang L, Dorsey JF, Binder ZA, O'Rourke DM, Fraietta JA, Gong Y, Fan Y. Targeting PAK4 to reprogram the vascular microenvironment and improve CAR-T immunotherapy for glioblastoma. Nat Cancer. 2021 Jan;2(1):83-97. doi: 10.1038/s43018-020-00147-8. Epub 2020 Nov 30. PMID: 35121889; PMCID: PMC10097424.

171. Greenberg JI, Shields DJ, Barillas SG, Acevedo LM, Murphy E, Huang J, Scheppke L, Stockmann C, Johnson RS, Angle N, Cheresh DA. A role for VEGF as a negative regulator of pericyte function and vessel maturation. Nature. 2008 Dec 11;456(7223):809-13. doi: 10.1038/nature07424. Epub 2008 Nov 9. Erratum in: Nature. 2009 Feb 26;457(7233):1168. PMID: 18997771; PMCID: PMC2605188.
172. Lingappan K. NF-κB in Oxidative Stress. Curr Opin Toxicol. 2018 Feb;7:81-86.
173. Shih VF, Tsui R, Caldwell A, Hoffmann A. A single NFκB system for both canonical and non-canonical signaling. Cell Res. 2011 Jan;21(1):86-102.
174. Kreuger J, Phillipson M. Targeting vascular and leukocyte communication in angiogenesis, inflammation and fibrosis. Nat Rev Drug Discov. 2016 Feb;15(2):125-42. doi: 10.1038/nrd.2015.2. Epub 2015 Nov 27. PMID: 26612664.
175. Moreira MB, G.-C. G. (2018). Endothelium: A Coordinator of Acute and Chronic Inflammation, in Endothelium and Cardiovascular Diseases. Elsevier, 485–491.
176. Witz IP. The selectin-selectin ligand axis in tumor progression. Cancer Metastasis Rev. 2008 Mar;27(1):19-30. doi: 10.1007/s10555-007-9101-z. PMID: 18180878
177. Ghislin S, Obino D, Middendorp S, Boggetto N, Alcaide-Loridan C, Deshayes F. LFA-1 and ICAM-1 expression induced during melanoma-endothelial cell co-culture favors the transendothelial migration of melanoma cell lines in vitro. BMC Cancer. 2012 Oct 5;12:455. doi: 10.1186/1471-2407-12-455. PMID: 23039186; PMCID: PMC3495854.
178. Yang B, Yin S, Zhou Z, Huang L, Xi M. Inflammation Control and Tumor Growth Inhibition of Ovarian Cancer by Targeting Adhesion Molecules of E-Selectin. Cancers (Basel). 2023 Apr 4;15(7):2136. doi: 10.3390/cancers15072136. PMID: 37046797; PMCID: PMC10093113.
179. McCarthy JB, Skubitz AP, Iida J, Mooradian DL, Wilke MS, Furcht LT. Tumor cell adhesive mechanisms and their relationship to metastasis. Semin Cancer Biol. 1991 Jun;2(3):155-67. PMID: 1912525.
180. Dianzani C, Brucato L, Gallicchio M, Rosa AC, Collino M, Fantozzi R. Celecoxib modulates adhesion of HT29 colon cancer cells to vascular endothelial cells by inhibiting ICAM-1 and VCAM-1 expression. Br J Pharmacol. 2008 Mar;153(6):1153-61. doi: 10.1038/sj.bjp.0707636. Epub 2007 Dec 17. PMID: 18084316; PMCID: PMC2275462.
181. Chen M, Wu C, Fu Z, Liu S. ICAM1 promotes bone metastasis via integrin-mediated TGF-β/EMT signaling in triple-negative breast cancer. Cancer Sci. 2022 Nov;113(11):3751-3765. doi: 10.1111/cas.15532. Epub 2022 Aug 26. PMID: 35969372; PMCID: PMC9633300.
182. Taftaf R, Liu X, Singh S, Jia Y, Dashzeveg NK, Hoffmann AD, El-Shennawy L, Ramos EK, Adorno-Cruz V, Schuster EJ, Scholten D, Patel D, Zhang Y, Davis AA, Reduzzi C, Cao Y,

D'Amico P, Shen Y, Cristofanilli M, Muller WA, Varadan V, Liu H. ICAM1 initiates CTC cluster formation and trans-endothelial migration in lung metastasis of breast cancer. Nat Commun. 2021 Aug 11;12(1):4867. doi: 10.1038/s41467-021-25189-z. PMID: 34381029; PMCID: PMC8358026.

183. Figenschau SL, Knutsen E, Urbarova I, Fenton C, Elston B, Perander M, Mortensen ES, Fenton KA. ICAM1 expression is induced by proinflammatory cytokines and associated with TLS formation in aggressive breast cancer subtypes. Sci Rep. 2018 Aug 6;8(1):11720. doi: 10.1038/s41598-018-29604-2. PMID: 30082828; PMCID: PMC6079003.
184. Regev O, Kizner M, Roncato F, Dadiani M, Saini M, Castro-Giner F, Yajuk O, Kozlovski S, Levi N, Addadi Y, Golani O, Ben-Dor S, Granot Z, Aceto N, Alon R. ICAM-1 on Breast Cancer Cells Suppresses Lung Metastasis but Is Dispensable for Tumor Growth and Killing by Cytotoxic T Cells. Front Immunol. 2022 Jul 11;13:849701. doi: 10.3389/fimmu.2022.849701. PMID: 35911772; PMCID: PMC9328178.
185. Yamada M, Yanaba K, Hasegawa M, Matsushita Y, Horikawa M, Komura K, Matsushita T, Kawasuji A, Fujita T, Takehara K, Steeber DA, Tedder TF, Sato S. Regulation of local and metastatic host-mediated anti-tumour mechanisms by L-selectin and intercellular adhesion molecule-1. Clin Exp Immunol. 2006 Feb;143(2):216-27. doi: 10.1111/j.1365-2249.2005.02989.x. PMID: 16412045; PMCID: PMC1809598.
186. Klemke M, Weschenfelder T, Konstandin MH, Samstag Y. High affinity interaction of integrin alpha4beta1 (VLA-4) and vascular cell adhesion molecule 1 (VCAM-1) enhances migration of human melanoma cells across activated endothelial cell layers. J Cell Physiol. 2007 Aug;212(2):368-74. doi: 10.1002/jcp.21029. PMID: 17352405
187. Sikpa D, Whittingstall L, Fouquet JP, Radulska A, Tremblay L, Lebel R, Paquette B, Lepage M. Cerebrovascular inflammation promotes the formation of brain metastases. Int J Cancer. 2020 Jul 1;147(1):244-255. doi: 10.1002/ijc.32902. Epub 2020 Feb 25. PMID: 32011730.
188. Nakajima K, Ino Y, Yamazaki-Itoh R, Naito C, Shimasaki M, Takahashi M, Esaki M, Nara S, Kishi Y, Shimada K, Hiraoka N. IAP inhibitor, Embelin increases VCAM-1 levels on the endothelium, producing lymphocytic infiltration and antitumor immunity. Oncoimmunology. 2020 Oct 27;9(1):1838812. doi: 10.1080/2162402X.2020.1838812. PMID: 33178497; PMCID: PMC7595596.
189. Bose A, Taylor JL, Alber S, Watkins SC, Garcia JA, Rini BI, Ko JS, Cohen PA, Finke JH, Storkus WJ. Sunitinib facilitates the activation and recruitment of therapeutic anti-tumor immunity in concert with specific vaccination. Int J Cancer. 2011 Nov 1;129(9):2158-70. doi: 10.1002/ijc.25863. Epub 2011 May 25. PMID: 21170961; PMCID: PMC3110980.

190. Garbi N, Arnold B, Gordon S, Hämmerling GJ, Ganss R. CpG motifs as proinflammatory factors render autochthonous tumors permissive for infiltration and destruction. J Immunol. 2004 May 15;172(10):5861-9. doi: 10.4049/jimmunol.172.10.5861. PMID: 15128765.
191. Lange T, Valentiner U, Wicklein D, Maar H, Labitzky V, Ahlers AK, Starzonek S, Genduso S, Staffeldt L, Pahlow C, Dück AM, Stürken C, Baranowsky A, Bauer AT, Bulk E, Schwab A, Riecken K, Börnchen C, Kiefmann R, Abraham V, DeLisser HM, Gemoll T, Habermann JK, Block A, Pantel K, Schumacher U. Tumor cell E-selectin ligands determine partialefficacy of bortezomib on spontaneous lung metastasis formation of solid human tumors in vivo. Mol Ther. 2022 Apr 6;30(4):1536-1552. doi: 10.1016/j.ymthe.2022.01.017. Epub 2022 Jan 12. PMID: 35031433; PMCID: PMC9077315.
192. Khan SU, Xia Y, Goodale D, Schoettle G, Allan AL. Lung-Derived Selectins Enhance Metastatic Behavior of Triple Negative Breast Cancer Cells. Biomedicines. 2021 Oct 30;9(11):1580. doi: 10.3390/biomedicines9111580. PMID: 34829810; PMCID: PMC8615792.
193. Morita Y, Leslie M, Kameyama H, Lokesh GLR, Ichimura N, Davis R, Hills N, Hasan N, Zhang R, Kondo Y, Gorenstein DG, Volk DE, Chervoneva I, Rui H, Tanaka T. Functional Blockade of E-Selectin in Tumor-Associated Vessels Enhances Anti-Tumor Effect of Doxorubicin in Breast Cancer. Cancers (Basel). 2020 Mar 19;12(3):725. doi: 10.3390/cancers12030725. PMID: 32204492; PMCID: PMC7140021.
194. Sackstein R, Schatton T, Barthel SR. T-lymphocyte homing: an underappreciated yet critical hurdle for successful cancer immunotherapy. Lab Invest. 2017 Jun;97(6):669-697. doi: 10.1038/labinvest.2017.25. Epub 2017 Mar 27. PMID: 28346400; PMCID: PMC5446300
195. Sackstein R. The First Step in Adoptive Cell Immunotherapeutics: Assuring Cell Delivery via Glycoengineering. Front Immunol. 2019 Jan 11;9:3084. doi: 10.3389/fimmu.2018.03084. PMID: 30687313; PMCID: PMC6336727.
196. Aires DJ, Yoshida M, Richardson SK, Bai M, Liu L, Moreno R, Lazar AJF, Wick JA, Rich BE, Murphy G, Blumberg RS, Fuhlbrigge RC, Kupper TS. T-cell trafficking plays an essential role in tumor immunity. Lab Invest. 2019 Jan;99(1):85-92. doi: 10.1038/s41374-018-0124-6. Epub 2018 Oct 23. PMID: 30353131; PMCID: PMC6309214.
197. Ruco LP, de Laat PA, Matteucci C, Bernasconi S, Sciacca FM, van der Kwast TH, Hoogsteden HC, Uccini S, Mantovani A, Versnel MA. Expression of ICAM-1 and VCAM-1 in human malignant mesothelioma. J Pathol. 1996 Jul;179(3):266-71. doi: 10.1002/(SICI)1096 9896(199607)179:3<266::AID-PATH592>3.0.CO;2-Y. PMID: 8774481.

198. Morani F, Bisceglia L, Rosini G, Mutti L, Melaiu O, Landi S, Gemignani F. Identification of Overexpressed Genes in Malignant Pleural Mesothelioma. Int J Mol Sci. 2021 Mar 8;22(5):2738.
199. Tsagkouli S, Kyriakoulis IG, Kyriakoulis KG, Fyta E, Syrigos A, Bakakos P, Charpidou A, Kotteas E. Serum and Pleural Soluble Cell Adhesion Molecules in Mesothelioma Patients: A Retrospective Cohort Study. Cancers (Basel). 2022 Jun 8;14(12):2825.
200. Dick IM, Lee YCG, Cheah HM, Miranda A, Robinson BWS, Creaney J. Profile of soluble factors in pleural effusions predict prognosis in mesothelioma. Cancer Biomark. 2022;33(1):159-169.
201. Davis RW 4th, Klampatsa A, Cramer GM, Kim MM, Miller JM, Yuan M, Houser C, Snyder E, Putt M, Vinogradov SA, Albelda SM, Cengel KA, Busch TM. Surgical Inflammation Alters Immune Response to Intraoperative Photodynamic Therapy. Cancer Res Commun. 2023 Sep 11;3(9):1810-1822.